LA-13317-T
Thesis

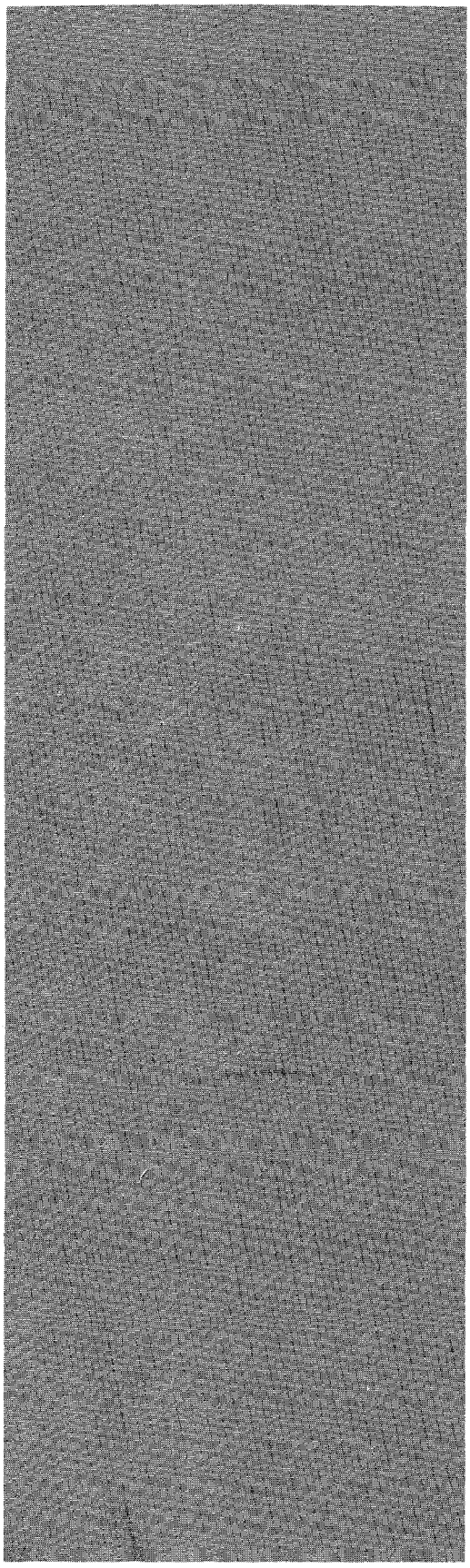

Measurements of Delayed Neutron Parameters for U-235 and Np-237

RECEIVED
JUL 28 1997
OSTI

Los Alamos
NATIONAL LABORATORY

Los Alamos National Laboratory is operated by the University of California for the United States Department of Energy under contract W-7405-ENG-36.

This thesis was accepted by the Department of Chemical and Nuclear Engineering, University of New Mexico, Albuquerque, New Mexico, in partial fulfillment of the requirements for the degree of Doctor of Philosophy in Nuclear Engineering. The text and illustrations are the independent work of the author and only the front matter has been edited by the CIC-1 Writing and Editing Staff to conform with Department of Energy and Los Alamos National Laboratory publication policies.

An Affirmative Action/Equal Opportunity Employer

This report was prepared as an account of work sponsored by an agency of the United States Government. Neither The Regents of the University of California, the United States Government nor any agency thereof, nor any of their employees, makes any warranty, express or implied, or assumes any legal liability or responsibility for the accuracy, completeness, or usefulness of any information, apparatus, product, or process disclosed, or represents that its use would not infringe privately owned rights. Reference herein to any specific commercial product, process, or service by trade name, trademark, manufacturer, or otherwise, does not necessarily constitute or imply its endorsement, recommendation, or favoring by The Regents of the University of California, the United States Government, or any agency thereof. The views and opinions of authors expressed herein do not necessarily state or reflect those of The Regents of the University of California, the United States Government, or any agency thereof. Los Alamos National Laboratory strongly supports academic freedom and a researcher's right to publish; as an institution, however, the Laboratory does not endorse the viewpoint of a publication or guarantee its technical correctness.

LA-13317-T
Thesis

UC-700
Issued: July 1997

Measurements of Delayed Neutron Parameters for U-235 and Np-237

David Loaiza

MASTER

DISTRIBUTION OF THIS DOCUMENT IS UNLIMITED

Los Alamos
NATIONAL LABORATORY
Los Alamos, New Mexico 87545

ACKNOWLEDGMENTS

First, I would like to express my gratitude to Glenn Brunson. I believe he derives pleasure from helping others, and I feel very fortunate to have collaborated and learned from him. He played a major role deciding what type of detection system and analysis that should be performed in this experiment. The many discussion I had with Glenn were both educational and enjoyable.

Many people provided time and helped operate Godiva IV. I would like to mention the great support provided by the Crew Chief Ken Butterfield. Ken was instrumental during the collection of data. He not only operated Godiva, but provided many stimulating discussions. He also helped fine-tune the retrieval system.

My thanks go to Rene Sanchez and Guy Arnone. It was Rene Sanchez who furnished the idea to measure the delayed neutrons for Np-237. Rene provided optimism and enthusiasm. Guy Arnone and Ray Hastings helped in many aspects of this experiment that are too numerous to mention.

Many thanks go to the design and shop teams led by Charlene Cappiello. Charlene has a great group of people and they were very supportive throughout the experiment.

My gratitude goes toward Rick Paternoster for his support and for providing me the opportunity to perform this experiment.

Finally, I would like to thank my advisors Dr. Eric Haskin and Dr. Robert Busch. I appreciate their hard work and dedication. They provided insightful suggestions for the improvement of my project and manuscript. It has been a great pleasure having them as advisors in both my master and doctorate studies.

There are many people who have contributed to this experiment. If I have failed to mention you, it is for lack of space and not lack of gratitude.

DISCLAIMER

Portions of this document may be illegible in electronic image products. Images are produced from the best available original document.

TABLE OF CONTENTS

LIST OF FIGURES

LIST OF TABLES

Measurements of Delayed Neutron Parameters for U-235 and Np-237

by

David Loaiza

ABSTRACT

The delayed neutron yields, decay constants, and the absolute yield for the six-group delayed neutrons have been measured for U-235 and Np-237. This experiment has been called for in the forecast of experiments needed to support operations in the United States.

The bare U-235 metal assembly "Godiva IV" at the Los Alamos Critical Experiment Facility (LACEF) provided the source of neutrons. Godiva IV generated about 10^7 total fissions in the samples for the "infinite" and "instantaneous" irradiation needed to accentuate the shorter and longer-lived groups of delayed neutrons. The detection system used in the experiment consisted of 20 He-3 tubes embedded in a polyethylene cylinder.

The delayed neutron activity resulting from the fast neutron-induced fission has been measured. The measured absolute yield for U-235 was determined to be 0.0163 ± 0.0009 neutrons/fission. This value compares very well with the well-established Keepin absolute yield of 0.0165 ± 0.0005. The newly measured absolute yield value for Np-237 was 0.0126 ± 0.0007, which compares well to the recently reported value of 0.0129 ± 0.0004 by Saleh and Parish. The measured values for U-235 are corroborated with period (e-folding time) versus reactivity calculations.

1. INTRODUCTION

Delayed neutrons are emitted by excited nuclei formed in beta decay of fission products called delayed neutron precursors. About 1% of the total neutrons released in fission are delayed neutrons; however, this small fraction plays an important role in nuclear reactor control (Anderson et al., 1947). The delayed neutrons determine the time-dependent behavior of reactors, and knowledge of parameters used to predict neutron emission rate is essential for establishing reactivity worths (Keepin, 1965).

Delayed neutrons have been recognized as a minor product of fission since 1939. Originally it was thought that delayed neutrons emission competed with beta decay from fission fragments (Szilard and Zinn, 1939). Later studies showed that a delayed neutron is emitted with a half-life equal to its precursor (Bohr and Wheeler, 1939). Precursors are usually studied in groups rather than individually. Keepin and Wimett (1957) showed that delayed neutron emission rates following irradiations can be modeled very well using six groups.

Each delayed neutron group has a characteristic yield and decay constant. Therefore, for a six-group representation, twelve parameters are needed to describe the delayed neutron emission rate of each fissioning nuclide. In most cases, this data is obtained by combining the data from fast and thermal neutron induced fission, since no significant difference in parameters has been conclusively demonstrated for incident neutron energies below the threshold for second chance fission (Krick and Evans, 1972). Some recent calculations of delayed neutron data for reactor physics suggest that the differences between measured delayed neutron yields from thermal fission and those from fast neutron induced fission are statistically significant (Tuttle, 1975), but this could be due to the shortage of recent measurements using thermal neutrons.

The use of six groups to describe delayed neutron parameters has followed from the work performed by Keepin and Wimett (1956). Other experimenters have reported data for four or five groups, but the only proper test for number of groups should be whether or not a significant

improvement in the fit to the data can be achieved by increasing the number of groups. This test yields different results for different experiments based on the statistical precision of the instruments used and on the time domain used. A practical difficulty arises when one wishes to make use of more than one measurement to obtain a recommended set of parameters, as it is not obvious how to compare parameters when the number of groups is different. Even for sets of results that are reported using the same number of groups, it is not clear that averaging the parameters is a justifiable procedure. Because of these problems, it has been the norm to use the recommended data obtained by Keepin and Wimett to describe the time dependence of delayed neutron emission.

Requirements to improve delayed neutron data exist for several significant nuclides. The quantity of data available and the accuracy with which it is known reflects the long-standing interest in U-235, U-238 and Pu-239. Many fissile and fissionable nuclides (Th-232, U-233, U-235, U-238 and Pu-239) have received considerable attention in the laboratory, but the data available are not totally adequate. Yields at high energies are somewhat speculative, except in the 14 MeV energy region. The yield values for all fissionable materials are almost nonexistent above 7 MeV. For the important cases of Th-232 and Pu-239, measurements do not appear to exist above 4 and 6 MeV (Tuttle, 1979).

The experiments performed for this dissertation measure the six-group decay constants, six-group yields, and the total delayed neutron fraction for both U-235 and Np-237. The six-group representation of Np-237 lacks experimental determination, which has been called for in a forecast of experiments needed to support operations in the United States (Rutherford, 1994). The U-235 measurements are performed for two reasons: 1) to validate the experimental method, which employs a high-efficiency detection system and state-of-the-art data acquisition system, and 2) to investigate differences that exist between alternative sets of U-235 group parameters in current use.

2. LITERATURE RESEARCH ON DELAYED NEUTRONS PARAMETERS.

A small fraction of the neutrons produced in a fission reactor are emitted following the beta decay of fission products having half-lives from 0.2 to 56 seconds. Because of their delayed emission times following fission, these neutrons are of fundamental importance to the control and kinetic behavior of fission reactors. This chapter provides a chronological description of delayed neutron research.

2.1 HISTORICAL BACKGROUND.

Delayed neutron emission after fission was first reported in 1939. The delayed neutrons were reported to have a half-lives of 12.5 seconds, and were thought to be either photoneutrons produced by the alpha decay of fission fragments or neutrons emitted by one of the fission fragments. Later measurements (Roberts et al., 1939) disproved the first hypothesis. Bohr and Wheeler (1939) provided a plausible mechanism for delayed neutron emission that was consistent with the second hypothesis. Following this, other researchers measured decay constants for 2, 5, and 6 groups of delayed neutrons.

The earliest measurements of delayed neutrons emission rates from U-235 fission were made at Chicago (Snell et al., 1947). A BF_3 counter surrounded by paraffin was utilized to count the decay of delayed neutrons from a block of U_3O_8 bombarded with Be-9(d,n)B-10 neutrons. Snell measured five delayed neutron groups. The two longer-lived groups were attributed to Br-87 and I-137. Later the delayed neutron decay was studied using a nuclear reactor, the Argone graphite pile (Redman and Saxon, 1947). This was the first time that a reactor was used to measure delayed neutron parameters, and these measurements showed disagreement only with the two shorter half-lives.

Taking advantage of the higher neutron flux available at the Argonne heavy water pile and with a newer and faster rapid transfer system, the delayed neutrons from U-235 fission were studied (Hughes et al., 1948).

The decays of delayed neutrons from the irradiated sample of U-235 were recorded and analyzed to determine the decay constants and abundances of six delayed neutron groups. The results became the standard of comparison for all other studies on U-235 and other fissionable isotopes. At Los Alamos, more measurements for U-235 delayed neutrons were made using a very short burst of prompt neutrons from the Dragon assembly with particular attention on the shorter-lived groups. The researchers obtained five group half-lives which agreed with those reported by Hughes et al., and a sixth shorter-lived group was reported (Hoffmann et al., 1948).

The first attempt to measure the short-lived delayed neutrons was made with a pulse neutron generated on U_3O_8 (Sun et al., 1950). This investigation found no short-lived delayed neutrons of appreciable abundance. However, the work at Argonne by Kunstadtter et al. (1953) revealed a new short delayed neutron group from U-235 with a half-life of 0.05 sec and a fractional yield 0.033 of delayed neutrons. These short half-life studies were made at the Argonne heavy water pile with a thermal neutron shutter to produce short irradiation. Bendt and Scott (1955) used a bare U-235 critical assembly pulsed at intervals with an 11 MeV betatron and measured a short-lived group with a half-life of 0.150 sec and an abundance of 2.7%. They indicated that this group follows the decay of Li-9 being formed as the light fragment in ternary fission.

Smith and Thorne, 1957 used a fast reactor as a neutron source. Irradiation intervals of 0.6, 6, and > 480 sec were performed to observe the decay constants of short and long-lived delayed neutron groups. The detector system consisted of six BF_3 counters embedded in paraffin arranged in an annular geometry. A 10 mg U-235 sample was used for the irradiation. Because of poor statistics, decay constants obtained by Hughes et al. (1948) were used, and the counting data was used to calculate relative yields of each group by the graphical or "peeling off" method. Because of the long transit time of 0.5 sec between the irradiation position and the detector, half-lives shorter than 0.5 sec could not be determined.

Delayed neutrons from fission of U-235, U-238, U-233, Pu-239, and Th-232 were investigated by Brunson et al. (1955) at the Reactor Testing

Station, Arco, Idaho. Fission samples were irradiated in the EBR reactor, which has a degraded fission spectrum near the center and an accessible thermal region in the graphite reflector. Because of the long irradiation times (3, 9, 30, and 360 sec) and the long transfer time (1.3 sec), it was only possible to separate the decay data into four delayed neutron groups. Corrections for energy response of the detector were not applied to the data. Relative total delayed neutron yields to U-235 were also measured at the EBR, but based only on the four groups.

The Los Alamos measurements conducted by Keepin and Wimett, 1956 are perhaps the most comprehensive experiment performed up to this point. These experiments measured the delayed neutrons from fast fission of six nuclides (U-235, U-238, U-233, Pu-239, Pu-240, and Th-232), and the thermal fission of three nuclides (U-235, U-233, and Pu-239). The bare U-235 Godiva assembly was used as the neutron source. The Godiva central spectrum, a slightly degraded fission spectrum, was used for fast irradiations. The thermal spectrum was obtained with an eight-inch cubic block of polyethylene which was cadmium shielded and mounted near Godiva, and the fissile samples were passed through it via the transfer system. Both the instantaneous and infinite irradiations consisted of $\sim 10^{16}$ total fissions, produced by a superprompt critical burst of 0.25 μsec for the instantaneous irradiation. A delayed critical approach was used for the infinite irradiation. Small amounts of fissile material were used to minimize multiplication within the sample while providing good counting statistics. Both instantaneous and saturation irradiations were performed to observe short and long-lived delayed neutrons (Keepin et al., 1956).

The Keepin studies of delayed neutrons are based on the assumption that delayed neutron activity as a function of time can be represented by a linear superposition of exponential functions that represent the decay. The initial delayed neutron activity is proportional to $a_i\lambda_i$ following an instantaneous irradiation and proportional to a_i for a saturated irradiation (a_i and λ_i are the abundance and decay constant for the i-th delayed neutron group). To fit the instantaneous irradiation data, A_i is set equal to $a_i\lambda_i$ and for the infinite or saturated irradiation A_i is set equal to a_i. This effective

weighting of initial activity by the factor λ_i for an instantaneous irradiation is advantageous in studying the short-lived delayed neutron groups. The relationship that describes the exponential decay is:

$$n(t) = \sum_{i=1}^{j} A_i e^{-\lambda_i t} \qquad (2.1)$$

Where n(t) is the delayed neutron activity as a function of time, j is the number of groups, and A_i and λ_i are the parameters identified by least square fits to the experimental data.

In Keepin's experiments, a pneumatic system transferred a 2 to 5g fissile material sample from Godiva to a 4π-shield counting geometry in about 50 msec. For the instantaneous irradiation experiments, the output from a scintillator detector was used to generate a trigger pulse which initiated sample transfer and counting. The delayed neutrons were counted by a BF_3 proportional counter in long geometry, modified to give a flat response within 5% over the energy range of 23 keV to 1.5 MeV (Keepin, 1956). The absolute counter efficiency was determined using four calibrated neutron sources. The decay of delayed neutron activity was monitored by a crystal-controlled multichannel time delayed analyzer with 0.001, 0.01, 0.1, 1, and 10 sec channel widths following in automatic sequence. The number of channels of each width was variable, thus allowing selection of the most suitable channel-width distribution for a given decay curve (Keepin, 1956).

Six exponential functions were determined to be necessary and sufficient for optimum least-square fits to the data. Satisfactory convergence was not obtained for five or fewer groups. For seven or more groups, the weighted variance was invariably larger (indicating poorer fit). Two approaches for the six-group analysis were used (Keepin et al., 1957). The first was a simultaneous solution for all decay constants and abundance (12x12 matrix) from prompt burst irradiation data. The second was a determination of the four long groups from the infinite irradiation data and the determination of the four shorter groups from burst irradiation data. The latter method provided more accurate values for a_i and λ_i (smaller

calculated errors). Standard deviations for both decay constants and abundance values were computed from the inverse of the matrix which occurs in the solution of the normal least square equation. These calculated errors indicated that the two longer-lived groups (groups 1 and 2) were determined more accurately from the long irradiation, while the short-lived groups (groups 3, 4, 5, and 6) were better determined from prompt burst irradiation (Keepin et al., 1957).

Cox et al. (1958) measured the delayed neutrons emitted from the spontaneous fission of Cf-252. The fission source was detected by a BF_3 counter in a moderating medium. The moderating medium was mineral oil. The neutron counter was calibrated with a Cf-252 neutron source; the efficiency was assumed to be the same for delayed neutrons as for fission neutrons. They reported three delayed groups and corresponding absolute group yields. Cox also published the delayed-neutron parameters for Pu-241 thermal fission. Parameters for delayed neutrons with short half-lives could not be measured due to limitations of the transfer system.

In the former Soviet Union, delayed neutron decay constants and yields from U-235, U-238, and Th-232 fission have been studied as a function of the energy of the neutron inducing fission using a 1 MeV cascade accelerator (Maksiutenko, 1958). The fissionable materials were covered by a cadmium disk and exposed to fast neutrons. The H-2(d,n)He-3 and the H-3(d,n)He-4 target reactions were used to produce neutrons of 2.4, 3.3, and 15 MeV. Thermal neutrons were produced by slowing down fast neutrons from the Be-9(d,n)B-10 reaction in a paraffin block which surrounded the target. The samples were irradiated for 30 sec and 300 sec, and dropped into a detector bank of four BF_3 counters in a paraffin geometry. The accelerator ion source and high voltage were gated off during the counting interval to give essentially no background counts. Five groups of delayed neutrons were resolved by Maksiutenko. He stated that a sixth group could not be detected due to its low intensity and short half-life. Using the same experimental setup, Maksiutenko also measured total delayed neutron yields from fast fission of U-235, U-238, and Th-232.

Delayed neutrons from Th-232 and Pu-239 were measured by Shpakov et al., in 1962. Samples were irradiated by 14.5 MeV neutrons. The delayed neutrons were detected after irradiation by boron counters in a paraffin block surrounding the sample. The counter was calibrated using different neutron sources. Fissions were determined using a fission counter.

The delayed neutrons from Th-232 and U-238 were measured in a paraffin box (Moscati and Goldemberg, 1962). The paraffin box contained BF_3 counters, and the samples were irradiated by bremmstrahlung pulses from a betatron. The delayed neutrons were measured by separately recording neutron counts during the pulses and between pulses. A correction was made for the (γ,n) and $(\gamma,2n)$ reactions. The energy dependence of the neutron detector response was not discussed.

Experimental measurements were performed on samples of Th-232, U-235, U-238, and Pu-239 by Nikotin and Petrzhak (1966). Samples were irradiated by bremsstrahlung from a betatron. The samples were transferred to a neutron detector for counting. The detector efficiency was measured by means of several photoneutron sources calibrated using a manganese sulfate bath. Fissions were measured by radiochemical determination of Ba-140 and by mica track recorders in conjunction with thin foils. The absolute delayed neutron yield of U-238 was found to be essentially independent of maximum photon energy from 10 to 15.5 MeV.

Delayed neutron yields for Th-232, U-233, U-235, Pu-239, Pu-240 and Pu-241 were measured by Keepin (1969). The samples were irradiated by neutrons produced from the H-3(d,n)He-4 reaction. These delayed neutrons were counted with a slab detector gated in anticoincidence with the source. The neutron counter efficiency was determined by means of a calibrated Pu-238/Li neutron source. Delayed neutron yields per incident neutron were determined for incident energies of 14.1 and 14.9 MeV. The accelerator neutron production was determined by counting alpha particles resulting from the H-3(d,n)He-4 reaction. The reported yields show good agreement with previous measurements.

Later experiments were conducted using 2-10 g samples of fissionable isotopes (Krick and Evans, 1970). The samples were U-233, U-235, U-238, Pu-239 and Pu-242. These samples were sandwiched between fission chambers containing active foils of the same isotope and irradiated with Li-7(p,n)Be-7 and H-2(d,n)He-3 neutrons with varying energies. The thickness of the foils and geometry of the chamber were such that it was possible to count fission in the foils with nearly 100% efficiency. The accuracy with which the fissions in the large sample were measured was dependent upon accurate mass determination of the foils. The neutron source was modulated, and the delayed neutrons emitted between pulses were counted with a slab detector consisting of He-3 counters in polyethylene. The polyethylene-moderated He-3 long counter used in the experiment had the same energy independence and gamma insensitivity as the BF_3 long counter, but the efficiency was considerably higher. The results from this experiment compared well with the traditional Keepin data measured in 1956.

Samples of U-235 and U-238 were irradiated in the copper reflector of VIPER during a prompt critical burst, then transferred outside the reactor cell in 130 msec (Clifford, 1972). Neutron emission was measured for 10-15 minutes by a detector calibrated by a Pu-240 spontaneous fission neutron source. The relative energy response was checked with several monoenergetic neutron sources. Calibrated foils in fission chambers were used to measure the number of fissions in each sample. The delayed neutron parameters measured agreed with previously published data.

Delayed neutron yields and decay constants were measured using foils of U-235 irradiated in a thermal column at the University of London reactor (Synetos and Williams, 1983). The samples were transferred pneumatically to and from the irradiation position where a constant thermal flux was maintained. After each irradiation the delayed neutron emission was measured in a detector consisting of a water cylinder containing a BF_3 detector. The geometry of the detector was selected to minimize the neutron energy dependence on its response, and the efficiency of the detector was measured using a calibrated Am/Li source. The delayed

neutron curve was fit to the sum of five exponentials by the least square method. No sixth group was observed because of the 380-msec transfer time. When the six-group parameters of Keepin and Wimett were used to analyze the data in this experiment, the obtained results compared very well.

Additional research has been done on the energy of delayed neutrons. Early estimates (Roberts et al., 1939) reported the mean energy of delayed neutrons from U-235 to be 0.5 MeV. Later investigations at Argonne and Oak Ridge measured the mean energies of the individual groups. In 1956, Los Alamos performed cloud chamber experiments to measure the group 4 spectrum. The most accurate and comprehensive of the early spectral measurements were reported by Batchelor and MckHyder in 1956. They used an He-3 spectrometer to measure energies of delayed neutrons from a slug of natural uranium. The counting and irradiation times were varied to observe the different group spectra in which they reported an average energy of 550 keV. The energy resolution and counting statistics were considered faulty; however, these spectra comprised the best delayed neutron spectra data until early 1970.

In 1972, measurements were reported of delayed neutron spectra from thermal and 14 MeV fission in U-235 and 15 MeV fission of U-238 and Pu-239 (Fiegs, 1972). These experiments used proton recoil proportional counters and measurements were made at different times to differentiate the group spectra for the first four groups. The experiment produced results in agreement with the Batchelor data within the error limits. The aggregate results from thermal and 14 MeV fission in U-235 were also compared and showed that the same precursors were responsible for the different neutron groups.

A high pressure He-3 proportional counter with good energy resolution for fast neutron measurement was used to measure the delayed neutron energy distribution for samples of Th-232, U-233, U-235, U-238, and Pu-239 irradiated in the Israel Research Reactor (Shalev and Cuttler, 1973). Irradiation and counting times were optimized to accentuate delayed neutrons in groups 2 and 4. An approximate energy spectrum was obtained for group 1 and more precise spectra were obtained for group 2 delayed

neutrons. The He-3 counter had better resolution than Fiegs's proton recoil detector, but the measurements performed by Fiegs extended to much lower energies (80 keV) than did the He-3 counter (150 keV).

In 1975, the equilibrium delayed neutron spectra from fast fission of U-235, U-238, and Pu-239 were measured (Evans and Krick, 1976). For the experiment, an 80 to 420 keV spectrum of Li-7(p,n)Be-7 neutrons produced by the Van de Graaff accelerator was used. The accelerator was modulated in a 40 msec on, 60 msec off mode with a post acceleration electrostatic deflector and a mechanical beam shutter. The measured neutron on-to-off ratio in the target area was in excess of 10^{10}. The experiment used a pulse shape analysis to remove the He-3 recoil contribution from the Cuttler-Shalev ion chamber and to improve energy resolution. The experiment was done in open geometry over a deep pit with light steel covers and with walls at least 3 meters away. The obtained spectra show a maximum at 400-450 keV, which is in contradiction to other works published. It was suggested that this was due to a "leakage of the counting gate, which allowed primary neutrons into the spectra" (Evans and Krick, 1976).

A composite delayed neutron energy spectra from the thermal fission of U-235 has been measured for eight delay time intervals between 0.17 and 85.5 seconds (Tanczyn et al., 1986). This experiment combines a helium-pressure type transfer system with beta-neutron time-of-flight spectrometer. The neutron energy range of 0.01 to 2 MeV is spanned with Li-6 glass, plastic, and liquid scintillators. Spectra were compared to ENDF/B-V as well as to individual-precursor data. An equilibrium spectrum was also calculated and compared to ENDF/B-V and individual precursor measurements.

The most commonly used data on delayed neutrons is contained in the ENDF/B library (Pearlestein and Kinsey 1976). The six-group decay constants and relative abundances are included in the data files for the fissionable nuclides (Th-232, U-233, U-235, U-238, Pu-239, Pu-240, and Pu-241). The ENDF/B data files also include the average delayed neutron yield per fission (ν_d) as a function of time. The group decay constants and

their respective group spectra are not presented as a function of the incident neutron energy. The group spectra in the ENDF/B files include the seven nuclides reported above, but only the spectra for U-235, U-238, and Pu-239 are based on measurements. The spectra presented for Th-232 and U-233 are the same as for U-235, and those for Pu-240 and Pu-241 are the same as for Pu-239. In addition, the spectra of the measured nuclides do not include the group six spectra, and only U-238 has the measured spectrum for group five (Brady, 1989).

For Np-237 few experiments have been conducted to determine the delayed neutron parameters. Measurements of delayed neutron emission from 'thermal' neutron induced fission of Np-237 were published early this year (Saleh and Parish, 1997). These authors measured five delayed neutron groups for Np-237. They were unable to measure the sixth group for Np-237 because of a long transfer time (440 msec). They concluded that the results were reasonable for the five groups of delayed neutrons. One of their recommendations was that future work should attempt to measure the sixth group. Other recommendations were to measure the delayed neutrons of Np-237 for the fast neutron induced fission. This recommendation is unclear, as Np-237 is a threshold fissioner and the threshold occurs at (600 keV).

Tables 1 through 3 illustrate the six-group delayed neutron parameters from the three most commonly used sources. This data comprises the most current and complete six-group parameters.

Table 1. Keepin Recommended Delayed Neutron Parameters.

Nuclide	Group	Relative Abundances a_i	Decay Constant λ_i (sec^{-1})
U-235	1	0.038 ± 0.003	0.0127 ± 0.0002
(Fast)	2	0.213 ± 0.005	0.0317 ± 0.0008
	3	0.188 ± 0.016	0.1150 ± 0.0030
	4	0.407 ± 0.007	0.3110 ± 0.0080
	5	0.128 ± 0.008	1.4 ± 0.081
	6	0.026 ± 0.003	3.87 ± 0.369
U-238	1	0.013 ± 0.001	0.0132 ± 0.0003
(Fast)	2	0.137 ± 0.002	0.0321 ± 0.0060
	3	0.162 ± 0.020	0.139 ± 0.005
	4	0.388 ± 0.012	0.358 ± 0.014
	5	0.225 ± 0.013	1.41 ± 0.067
	6	0.075 ± 0.005	4.02 ± 0.214
U-233	1	0.086 ± 0.003	0.0126 ± 0.0004
(Fast)	2	0.274 ± 0.005	0.0334 ± 0.0014
	3	0.227 ± 0.035	0.131 ± 0.005
	4	0.317 ± 0.011	0.302 ± 0.024
	5	0.073 ± 0.014	1.27 ± 0.266
	6	0.023 ± 0.007	3.13 ± 0.675
Pu-239	1	0.038 ± 0.003	0.0129 ± 0.0002
(Fast)	2	0.280 ± 0.004	0.0311 ± 0.0005
	3	0.216 ± 0.018	0.134 ± 0.003
	4	0.328 ± 0.01	0.331 ± 0.012
	5	0.103 ± 0.009	1.26 ± 0.115
	6	0.035 ± 0.005	3.21 ± 0.255
Pu-240	1	0.028 ± 0.003	0.0129 ± 0.0004
(Fast)	2	0.273 ± 0.004	0.0313 ± 0.0005
	3	0.192 ± 0.053	0.135 ± 0.011
	4	0.350 ± 0.020	0.333 ± 0.031
	5	0.128 ± 0.018	1.36 ± 0.205
	6	0.029 ± 0.006	4.04 ± 0.782

Th-232 (Fast)	1	0.034 ± 0.002	0.0124 ± 0.0003
	2	0.150 ± 0.005	0.0334 ± 0.0011
	3	0.155 ± 0.021	0.121 ± 0.005
	4	0.446 ± 0.015	0.321 ± 0.011
	5	0.172 ± 0.013	1.21 ± 0.090
	6	0.043 ± 0.006	3.29 ± 0.297
U-235 (Thermal)	1	0.033 ± 0.003	0.0124 ± 0.0003
	2	0.219 ± 0.009	0.0305 ± 0.0010
	3	0 196 ± 0.022	0.111 ± 0.004
	4	0.395 ± 0.011	0.301 ± 0.011
	5	0.115 ± 0.009	1.14 ± 0.15
	6	0.042 ± 0.008	3.01 ± 0.29
Pu-239 (Thermal)	1	0.035 ± 0.009	0.0128 ± 0.0005
	2	0.298 ± 0.035	0.0301 ± 0.0022
	3	0.211 ± 0.048	0.124 ± 0.009
	4	0.326 ± 0.033	0.325 ± 0.036
	5	0.086 ± 0.029	1.12 ± 0.39
	6	0.044 ± 0.016	2.69 ± 0.48
U-233 (Thermal)	1	0.086 ± 0.003	0.0126 ± 0.0003
	2	0.299 ± 0.004	0.0337 ± 0.0006
	3	0.252 ± 0.040	0.139 ± 0.006
	4	0.278 ± 0.020	0.325 ± 0.030
	5	0.051 ± 0.024	1.13 ± 0.40
	6	0.034 ± 0.014	2.50 ± 0.42

Table 2. Tuttle Recommended Delayed Neutron Parameters.

Nuclide	Group	Relative Abundances a_i	Decay Constant λ_i (sec^{-1})
U-235	1	0.038 ± 0.004	0.0126 ± 0.0003
	2	0.213 ± 0.007	0.0317 ± 0.0012
	3	0.188 ± 0.024	0.1150 ± 0.004
	4	0.407 ± 0.010	0.3110 ± 0.0080
	5	0.128 ± 0.012	1.4 ± 0.12
	6	0.026 ± 0.004	3.87 ± 0.55
U-238	1	0.013 ± 0.001	0.0132 ± 0.0004
	2	0.137 ± 0.003	0.0321 ± 0.0009
	3	0.162 ± 0.030	0.139 ± 0.007
	4	0.388 ± 0.018	0.358 ± 0.021
	5	0.225 ± 0.019	1.41 ± 0.1
	6	0.075 ± 0.007	4.02 ± 0.32
U-233	1	0.086 ± 0.004	0.0126 ± 0.0006
	2	0.274 ± 0.007	0.0334 ± 0.0021
	3	0.227 ± 0.052	0.131 ± 0.007
	4	0.317 ± 0.016	0.302 ± 0.036
	5	0.073 ± 0.021	1.27 ± 0.390
	6	0.023 ± 0.010	3.13 ± 1.00
Pu-239	1	0.038 ± 0.004	0.0129 ± 0.0007
	2	0.280 ± 0.006	0.0311 ± 0.0005
	3	0.216 ± 0.027	0.134 ± 0.004
	4	0.328 ± 0.015	0.331 ± 0.018
	5	0.103 ± 0.013	1.26 ± 0.170
	6	0.035 ± 0.007	3.21 ± 0.380
Pu-240	1	0.028 ± 0.004	0.0129 ± 0.0006
	2	0.273 ± 0.006	0.0313 ± 0.0007
	3	0.192 ± 0.078	0.135 ± 0.0116
	4	0.350 ± 0.030	0.333 ± 0.046
	5	0.128 ± 0.027	1.36 ± 0.30
	6	0.029 ± 0.009	4.04 ± 1.16

Pu-241	1	0.010 ± 0.003	0.0128 ± 0.0002
	2	0.229 ± 0.006	0.0299 ± 0.0006
	3	0.173 ± 0.025	0.124 ± 0.013
	4	0.390 ± 0.050	0.352 ± 0.018
	5	0.182 ± 0.019	1.61 ± 0.15
	6	0.016 ± 0.005	3.47 ± 1.7
Pu-242	1	0.004 ± 0.001	0.0128 ± 0.0003
	2	0.195 ± 0.032	0.0314 ± 0.0013
	3	0.161 ± 0.048	0.128 ± 0.009
	4	0.412 ± 0.153	0.325 ± 0.020
	5	0.218 ± 0.087	1.35 ± 0.09
	6	0.010 ± 0.003	3.70 ± 0.44
Th-232	1	0.034 ± 0.003	0.0124 ± 0.0003
	2	0.150 ± 0.007	0.0334 ± 0.0016
	3	0.155 ± 0.031	0.121 ± 0.007
	4	0.446 ± 0.022	0.321 ± 0.016
	5	0.172 ± 0.019	1.21 ± 0.13
	6	0.043 ± 0.009	3.29 ± 0.440

Table 3. ENDF/B-V Recommended Delayed Neutron Parameters.

Nuclide	Group	Relative Abundances a_i	Decay Constant λ_i (sec^{-1})
U-235	1	0.038	0.01272
	2	0.213	0.03174
	3	0.188	0.1160
	4	0.407	0.3110
	5	0.128	1.4
	6	0.026	3.87
U-238	1	0.013	0.01323
	2	0.127	0.03212
	3	0.162	0.139
	4	0.388	0.359
	5	0.225	1.41
	6	0.075	4.03
Pu-239	1	0.038	0.0129
	2	0.280	0.0311
	3	0.216	0.134
	4	0.328	0.332
	5	0.103	1.26
	6	0.035	3.21
Pu-240	1	0.028	0.01294
	2	0.273	0.03131
	3	0.192	0.135
	4	0.350	0.333
	5	0.128	1.36
	6	0.029	4.03
Pu-241	1	0.010	0.0128
	2	0.229	0.0299
	3	0.173	0.124
	4	0.390	0.352
	5	0.182	1.61
	6	0.016	3.47

Th-232	1	0.034	0.0123
	2	0.150	0.0334
	3	0.155	0.121
	4	0.446	0.321
	5	0.172	1.21
	6	0.043	3.29

2.2 REVIEW OF DELAYED NEUTRON EMISSION

Many excellent studies and reviews of the theory of delayed neutron emission have appeared in the past years, and these describe the topic with great detail. The object of this section is merely to outline the present knowledge and understanding of the subject.

It is well known that approximately 1300 isotopes are produced during the fission process. 271 of these isotopes have the property of delayed neutron emission (Appendix A). The delayed neutron curve obtained when any fissile material undergoes fission is simply the sum of the decay curves of the individual delayed neutron precursors. A comprehensive review of the theory of delayed neutron emission should mention: i) the existence of delayed neutrons precursors and ii) the delayed neutron emission probability.

2.3 DELAYED NEUTRON PRECURSORS

Figure 1 presents a schematic representation of the process of delayed neutron emission. As noted before, some of the fission products are beta unstable, and they are known as delayed neutron precursors (Z,N). These delayed neutron precursors have a characteristic maximum beta decay energy, Q_β This beta decay energy is the difference between the ground state of the precursor nuclide and the ground state of its (Z+1, N-1) beta

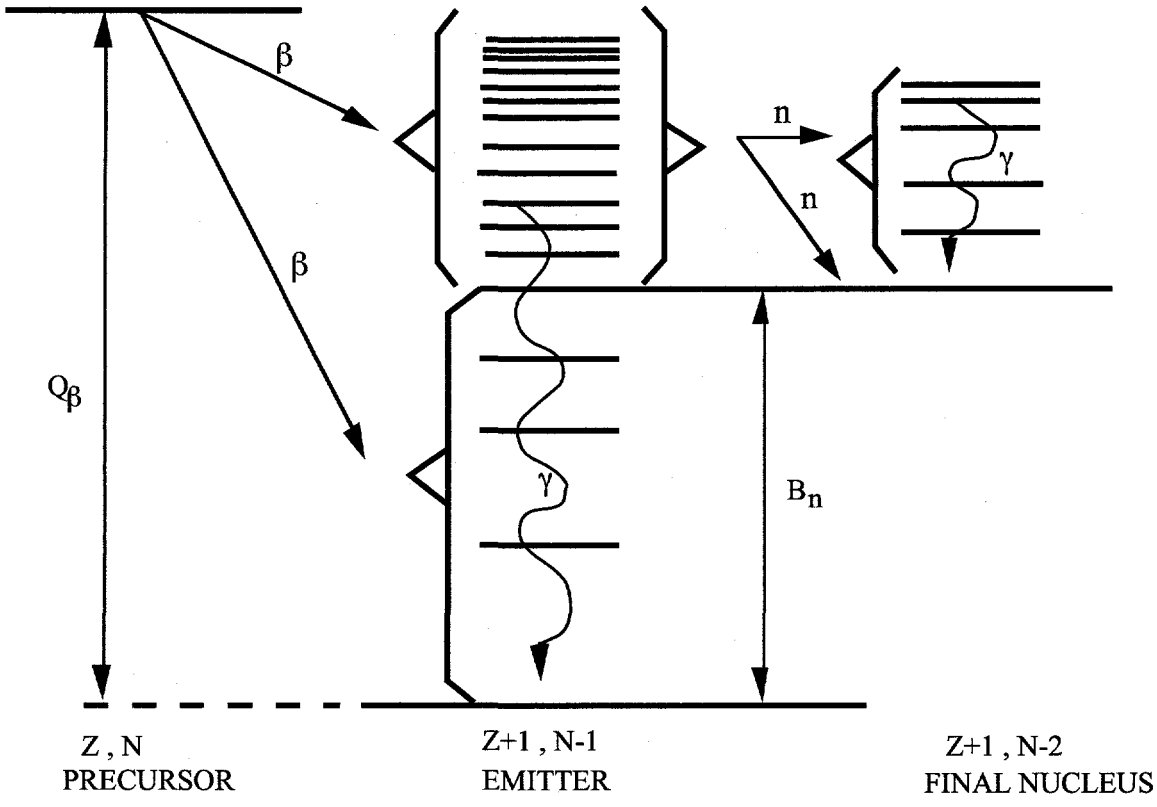

Figure 1. Schematic representation of delayed neutron emission.

decay daughter. This daughter nuclide is the one that actually decays by neutron emission and is known as the delayed neutron emitter. This emitter nucleus is often formed in an excited state occupying any one of the energy levels above the ground state as shown in Figure 1. The daughter nucleus decays by emitting a neutron when the excitation energy of the nucleus is greater than its characteristic neutron binding energy, B(n); then a neutron might be emitted producing a granddaughter (Z+1, N-2). Experimental evidence has also shown that in some cases the excitation energy exceeds not only the binding energy of the first neutron, B(n), but also that of the second neutron, B(2n). If that is the case, then the emission of two delayed neutrons is possible. This specific process (β-, 2n) has been experimentally observed in light nuclei and in nuclei that have an A>50 (Lyutostankii et al., 1983). Figure 1 shows another competing decay process for the daughter nucleus, namely, decay by gamma emission to its ground state.

The de-excitation of the emitter nucleus is instantaneous, consequently, the probability of delayed neutron emission and the time constant associated with delayed neutron production are attributed to the precursor nuclide instead of the emitter. Therefore, the production rate of delayed neutrons from a particular precursor nuclide is proportional to its rate of decay.

2.4 DELAYED NEUTRON EMISSION PROBABILITIES

The theory of delayed neutron emission is based on arguments developed by Bohr and Wheeler in 1939. The probability of delayed neutron emission, P_n, can in principle be calculated from the decay scheme shown in Figure 1. To calculate the probability P_n, it is necessary to know the level density in the emitter, the number of beta decays going to each level, the mode of decay (γ or n) of each level, and whether or not any neutron decay goes to an excited state rather than to the ground state in the final nucleus. Thus, the prediction of neutron emission probability based on theoretical calculations is difficult because of the lack of knowledge on level densities, spins, parities, and nuclear spectroscopy data.

Some semi-empirical relationships for neutron emission probability relate the P_n value to the energy window, Q_β - B(n), for neutron emission. Aniel and Feldestein (1970) have developed the following expression:

$$P_n = C(Q_\beta - B_n)^m \tag{2.2}$$

where C and m are free parameters determined from a fit to experimental data. The reported value for m is 1.65. This expression assumes that level density is a function of Q_β - B(n) and that gamma-ray competition due to spin and parity effects can be ignored. This assumption gains validity at higher excitation energies. Analysis of delayed proton spectra support the assumption of a uniform beta strength function for positron emission.

Other researchers have studied the theory of delayed neutron emission probabilities in an effort to relate the P_n value not only to the magnitude of the energy window but also to its position in the energy scale

(Kratz and Herrmann, 1984). The first attempts to calculate the delayed neutron emission probability were performed by Pappas and Rudstam in 1960. After some simplification, they developed the following expression:

$$P_n = \frac{\int_{B_n}^{Q_\beta} \frac{\Gamma_n}{\Gamma_n + \Gamma_\gamma} (Q_\beta - E)^5 \omega \, dE}{\int_0^{Q_\beta} (Q_\beta - E)^5 \omega \, dE} \qquad (2.3)$$

where w is the level density at energy E in the emitter, and Γ_n and Γ_γ are the partial widths for neutron and gamma decay. This expression can be evaluated by using mass formulae to give Q_β and B(n) values.

Based on this theory, Brady (1989) generated a set of precursor data to obtain the six-group parameters. To generate the activities of all precursor nuclides a fission depletion code, CINDER-10 was used. The CINDER-10 code generated activities for various cooling times following a prompt irradiation in 43 fissioning systems. The nuclide activities were combined with the evaluated emission probabilities to produce aggregate delayed neutron activities at different cooling times. The analysis of the calculated data is performed in a similar manner as Keepin analyzed his experimental data. A major exception is that current computational capabilities allow the derivation of all delayed neutron parameters from the pulse irradiation data rather than using the simultaneous saturated irradiation data. To determine the parameters A_i and λ_i, a non-linear least square routine, STEPIT was used. The results obtained from this analysis are shown later in this work.

3. EXPERIMENT AND EQUIPMENT DESCRIPTION

The objective of this experiment is to measure the absolute delayed neutron yield, the decay constants, and fractional yields of six delayed neutron groups for U-235 and Np-237. This experiment is included in the forecast of experiments needed to support nuclear operations in the United States (Rutherford, 1994).

The measurement of delayed neutrons is accomplished by irradiating a small sample of U-235 or Np-237 with neutrons. The bare U-235 metal assembly at the Los Alamos Critical Experiment Facility (LACEF) "Godiva IV" provides the source of neutrons. Godiva IV will generate about 10^7 total fissions in the sample for the "instantaneous" and "infinite" irradiations. The instantaneous irradiation is achieved by producing a burst of radiation with Godiva. The burst from Godiva is used to accentuate the shorter-lived delayed neutrons. The infinite irradiation is accomplished by operating Godiva at steady state (delayed critical operation). During steady state operation the sample is irradiated for 8 minutes. This operation accentuates the long-lived delayed neutrons. After irradiation, the sample is transferred into a fixed position in a well-shielded area where the decay of delayed neutrons is recorded as a function of time. The transfer of the sample should be less than 180 msec if the experiment is to measure group six, which has a half-life of about 179 msec. The decay of delayed neutrons is counted for 460 sec. The decay data are fit with a sum of exponentials to obtain the yields and decay constants of six delayed neutron groups. This chapter describes in some detail the equipment used in performing the measurements.

3.1 THE NEUTRON DETECTOR SYSTEM

The neutron detector has to meet a number of requirements. First, it has been shown that the count rate decreases by three orders of magnitude in about 100 seconds (Keepin et al., 1956); therefore, a detector with adequate neutron efficiency but with low dead-time is needed. The detector must also be insensitive to gamma rays. The detector efficiency should also be

insensitive to small sample displacement. A detector that meets these requirements is the well counter described by Anderson et al. (1991). The well counter consists of 20 He-3 tubes embedded in a cylindrical configuration inside polyethylene. This well counter has the qualities desired for the detection of delayed neutrons. The entire arrangement of the well counter is shown in Figure 2. This device is 58 cm by 59 cm by 72 cm high. The counter has a central cavity which is 17.78 cm in diameter and has an active depth of 40 cm. The counter is surrounded by 10 cm of polyethylene lined with a sheet of cadmium about 1.5 mm thick. The layer of cadmium absorbs background thermal neutrons that originate outside the cavity. To further reduce the high-neutron background from Godiva IV, two additional neutron-absorber layers have been placed around the well counter. The first layer is a 2-cm thick sheet of Boral. Boral is a uniform dispersion of boron carbide in aluminum. This sintered composite is clad with aluminum on both sides. Because of its high boron content, Boral has an exceptionally high cross section for thermal neutrons. The second layer consists of 7.62-cm thick borated polyethylene. The shielding was sufficient to reduce background neutrons from Godiva to negligible levels.

The He-3 tubes have an active length of 25 cm and an outside diameter of 2.54 cm. The tubes are filled with 98% He-3 at a pressure of 4 atm. The 20 He-3 detector tubes are arranged in 5 banks of 4, making the counter a segmented device consisting of 5 segments. The tubes are connected to one preamp with a T-type connection called an SHV connector. This type of connection can be used because the High-voltage (HV) cable coming from the preamp has a higher capacitance than the sum of the capacitance of the four tubes. The HV cable from the preamp has a capacitance of 69 Farads/m while each tube has a capacitance of 15 picoFarads. This arrangement was used to eliminate spurious data that might occur as a result of the failure of one tube or one tube bank. Four of the counter segments (A, B, C, and D) are composed of four tubes in a row and correspond to each of the four sides of the counter. The E segment consists of the remaining tubes, each separated by four tubes of the A, B, C, and D sections in a way that corresponds to the four corners of the counter (Anderson et al., 1991).

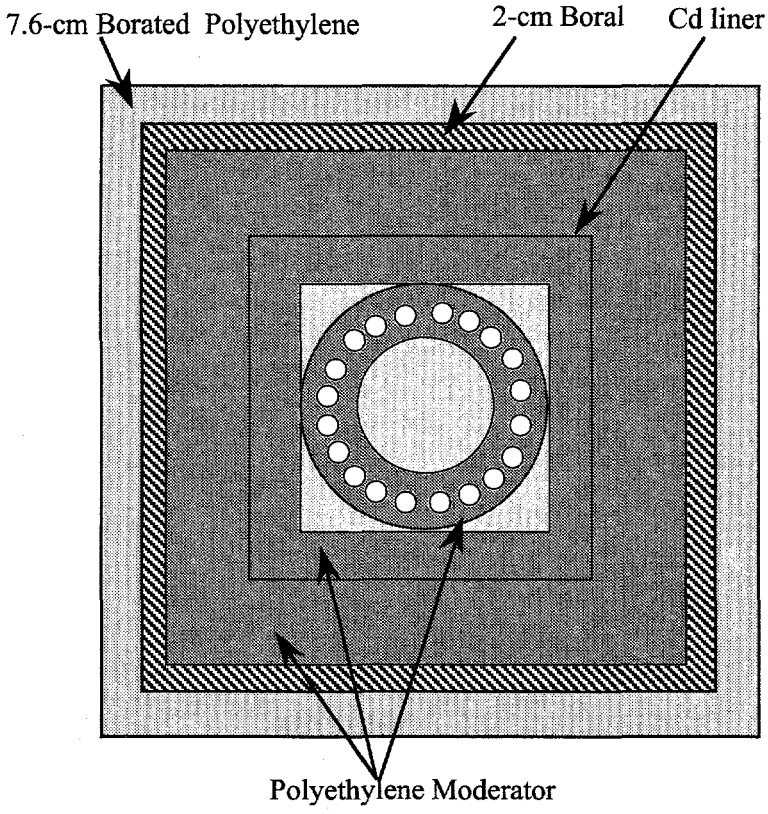

Figure 2. Cross sectional view of the well counter.

This system has occasionally shown erratic behavior due to significant change in the ambient temperature or humidity, although no problems were seen in the present configuration. Detection systems of this type are also known to have microphonic sensitivity, but this phenomena has not been observed in this well counter.

The electronic system for the measurement of delayed neutrons is shown in Figure 3. The four detectors in each counter bank are summed by Tennelec TC-175 preamps, and the output from the preamps is processed by Tennelec 202BLR amplifiers and LeCroy 623B discriminators. The processing module, a LeCroy 429A Fan in/Fan out, records the total neutron counts per counting interval and stores the total number of neutron counts detected by each of the five detector banks in an Ortec 772 Scaler. The output signals from the neutron detector discriminators are also fed into the input synchronizer of the Pulse Arrival-Time Recording Module (PATRM). The PATRM, with accompanying software, records the arrival times of

pulses from the detectors in a sequential manner. Other techniques convert the raw time history data into other data domains, such as a) the number of pulses in a gated window or b) the number of pulses in a shift register after a pulse exits. Because the original pulse arrival-time history is converted into other data domains, the raw data is completely lost and the analysis is limited to one or two algorithms. These other methods have their parameters (such as gate width, clocks, shift-register lengths, etc.) fixed in the hardware or software before the data collection begins. Therefore, once the data is taken, any change in the parameters requires running the experiment again. By using the PATRM, the original pulse arrival-time history can be recorded and saved. Thus, one can apply many algorithms on the same data and also change the parameters (gate width, shift register length) used in the analyses. This method of recording the original data also allows the user to use newly developed algorithms to analyze data taken previously (Arnone et al., 1991). The PATRM is read at a rate of 200 kbytes/sec by a PC with parallel CAMAC control card. It should also be noted that "the PATRM can record 4 million 32-bit time events at a continuous rate of 10 MHz and a burst rate of 150 MHz for 1.7 μs without any losses. When used in a typical thermal neutron counter application, the only dead time associated with the system is that due to losses caused by resolution time of the linear amplifiers." (Arnone et al., 1991).

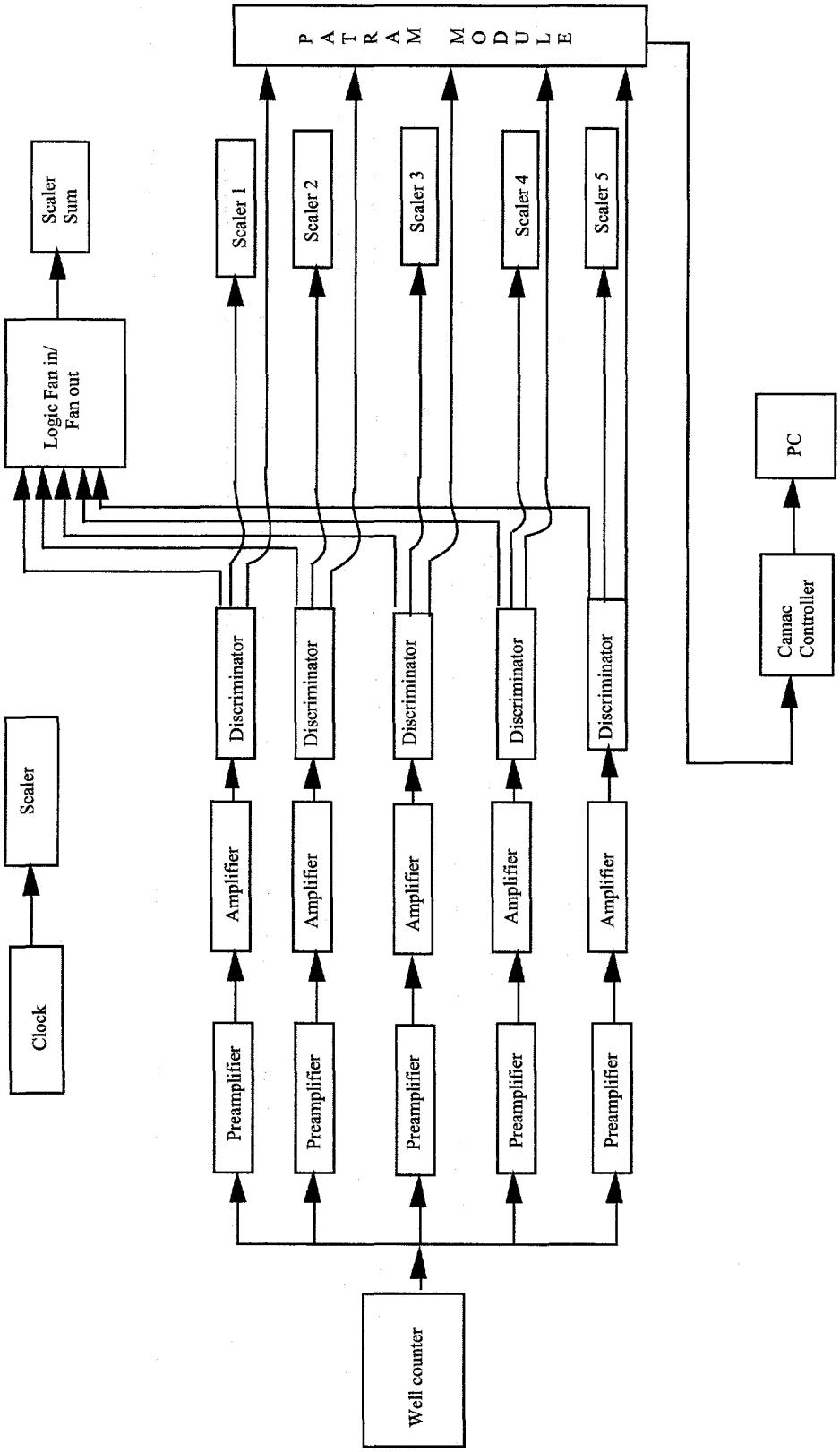

Figure 3. Electronic system for delayed neutron measurements.

The well counter was studied in detail to establish its operating parameters such as high-voltage plateau, pulse height spectrum, and source position. The characteristics of the well counter such as efficiency and dead time were also determined.

3.1.1 CALIBRATION OF THE WELL COUNTER

The measurement of delayed neutrons requires a detector with a high absolute efficiency. The absolute efficiency of the well counter was determined using a calibrated Am/Li neutron source. The absolute neutron emission rate of this source was determined to an accuracy of 3% relative to a standard source in a graphite pile and relative emission rates of the source were known to an accuracy of approximately 2%. The reported source strength was 1.70×10^3 neutrons per second. This source was calibrated on August 1996 by the Health Physics Measurements group (Clement, 1996). The Am/Li source is encapsulated in stainless steel, and has dimensions of 15 mm in diameter and 25 mm in height. This type of source was selected because its neutron energy spectrum is very similar to that of delayed neutrons (Synetos and Williams, 1979). Figure 4 shows the aggregate delayed neutron spectrum for U-235 and the neutron spectrum from an Am/Li source. Both curves have about the same average and maximum energy.

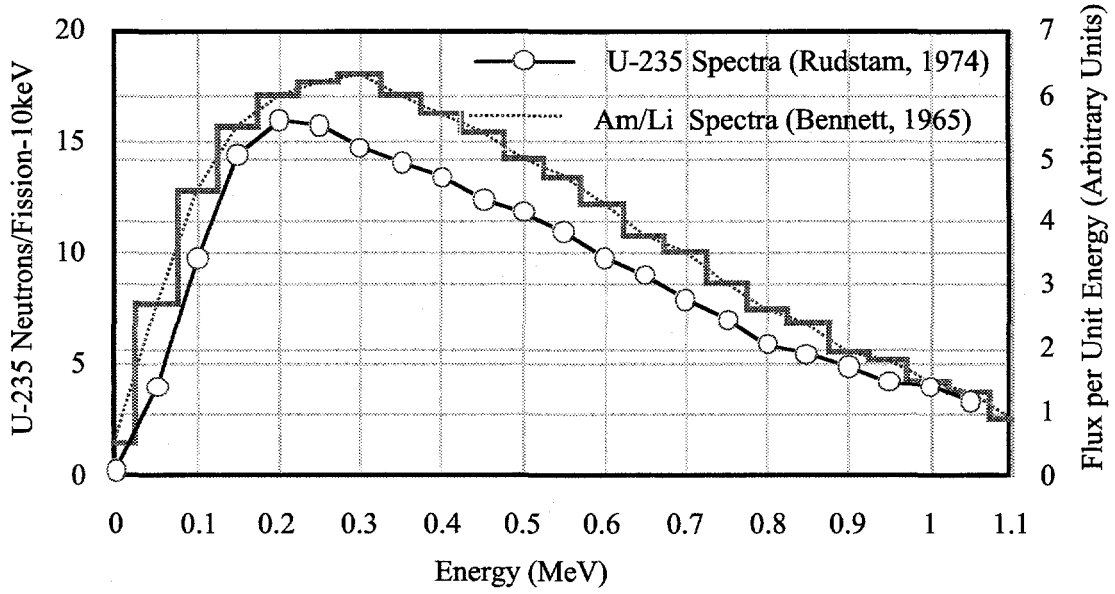

Figure 4. Comparison of delayed neutron spectrum for U-235 and Am/Li source.

The Am/Li source was placed in the well counter at the same position where the irradiated sample would be placed. The counting rate for the Am/Li source was taken several times to obtain acceptable statistics. The absolute efficiency calculated for the well counter is 29.04% ± 0.6%. This value of the efficiency is used in all calculations of the absolute delayed neutron yield. The efficiency of the well counter has also been studied by Anderson et al., 1991, and his findings are included in Table 4 as an illustration of the energy dependence of the detector.

Table 4. Absolute Efficiencies for the Well Counter.

Source	Strength /s	Count/sec	En (MeV)	Efficiency	Stdev
Cf-252 #1*	93074	2216	2.12	0.238	0.004
Cf-252 #2*	6739	1507	2.12	0.224	0.006
Cf-252 #3*	3395	769	2.12	0.227	0.008
Am/F^{+}	2122	539	1.54	0.254	0.0015
Am/Li*	1679	511	0.65	0.304	0.002
Am/Li^{+}	1750	491	0.65	0.2904	0.006

* (Anderson et al., 1991) $^{+}$ (This study)

Anderson and coworkers used several calibrated sources to obtain the counter efficiency and to observe its dependency in neutron energy. The efficiency for an Am/F source was also measured as part of this study to show an intermediate measurement between the Cf-252 source and the Am/Li. All the measured efficiencies are shown in Table 4 and Figure 5. As shown in Figure 5, the efficiency of the detector decreases with increasing neutron energy. This effect is typical of He-3 neutron detectors because the capture cross section increases with decreasing neutron energy.

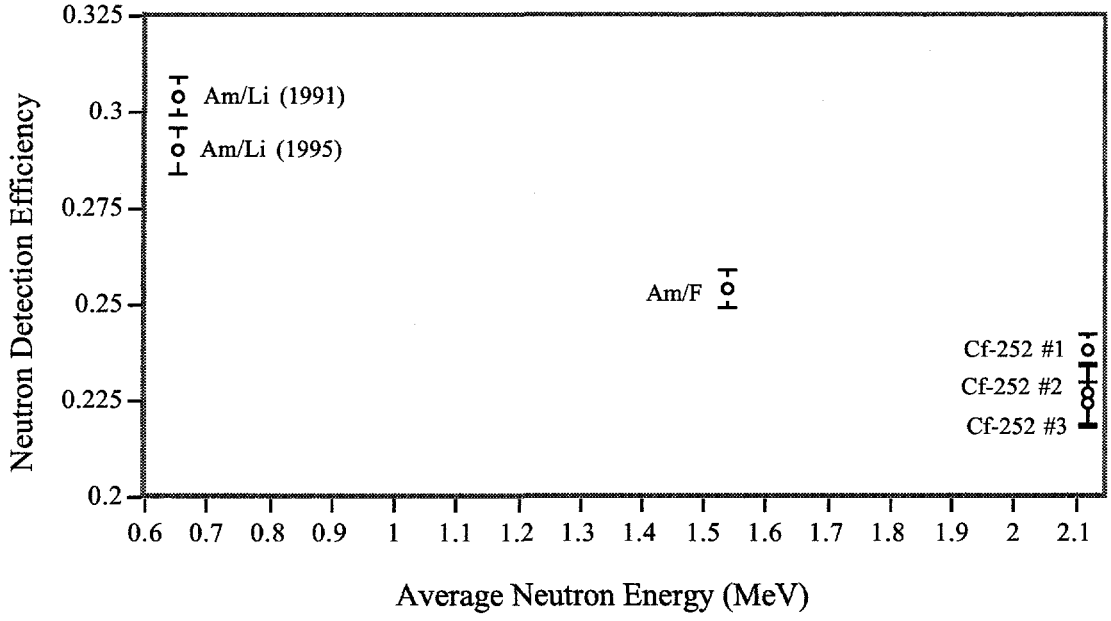

Figure 5. Efficiency of the well counter as a function of neutron energy.

Possible corrections were studied for the detector efficiency due to the use of the Am/Li source. The possible corrections are as follows: volume correction, self multiplication, and energy spectrum. The volume of the Am/Li source was about the same volume as the samples used in the irradiation. Because the difference in volume was less than 1%, no volume correction was necessary. When the neutron source is placed at the center of the delayed neutron detector, some of the neutrons scatter back into the source and are absorbed. Self-multiplication in the U-235 and Np-237 was estimated using TWODANT and was determined to be negligible, as shown in Figure 6. Because the detection efficiency is not independent of neutron energy, it is desirable to correct the measured detection efficiency to account for the difference between the spectra of neutrons from the Am/Li source and that of the delayed neutrons. Three uncertainties need to be considered: the uncertainty of the Am/Li neutron spectrum, the uncertainty of the delayed neutron spectrum, and the uncertainty of the detector-response function. This problem was extensively studied by Synetos and Williams (1979) who concluded that the combined uncertainties of the detector response and energy spectra cannot be quantified. In view of their conclusion, no corrections were applied to the Am/Li efficiency. Too many

combined uncertainties exist in the energy neutron spectrums to provide a reliable correction. The cited reference provides a more detailed explanation.

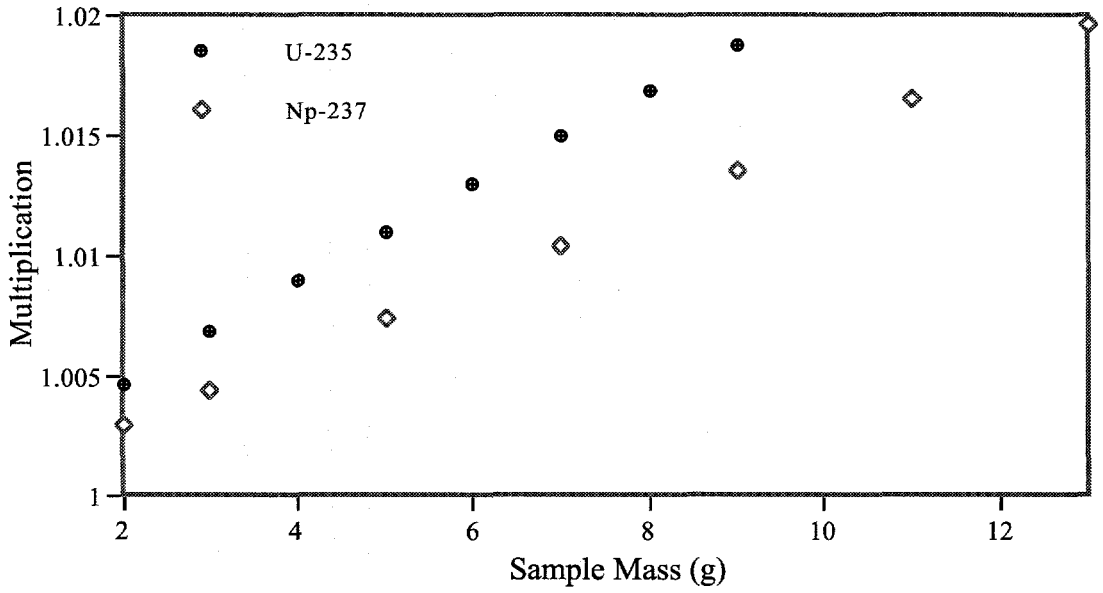

Figure 6. Multiplication vs sample mass.

3.1.2 THE HIGH-VOLTAGE PLATEAU

Because the well counter is used to detect delayed neutrons, it is desirable that changes in the counting rate be caused by changes in the neutron population and not by changes in the environment such as atmospheric pressure, temperature, humidity, or voltage. No significant changes were observed in atmospheric pressure, temperature, and humidity; therefore, for this experiment all these factors can be neglected except for voltage changes. Therefore, it is necessary to know by what fraction the counting rate will change when the HV changes by a certain amount. It is highly desirable to have a system for which a change in the counting rate is negligible when the HV changes for a reason beyond our control. These changes could be caused by change in the 110 V provided by the wall outlet, which in turn may cause a fluctuation in the output of the HV power supply. For this reason, the response of the well counter to variations in the voltage should be known. This information is provided by the HV plateau of the counter. The HV plateau is obtained by taking counts at various voltages.

The voltage is increased incrementally and a count rate is observed. Figure 7 shows the HV plateau curve obtained by varying the HV from 1100 V to 1600 V. From this figure, the operating voltage for the well counter was determined to be 1375 V. The slightly positive slope in the plateau at the operating point shown in Figure 7 is typical for detectors of this type.

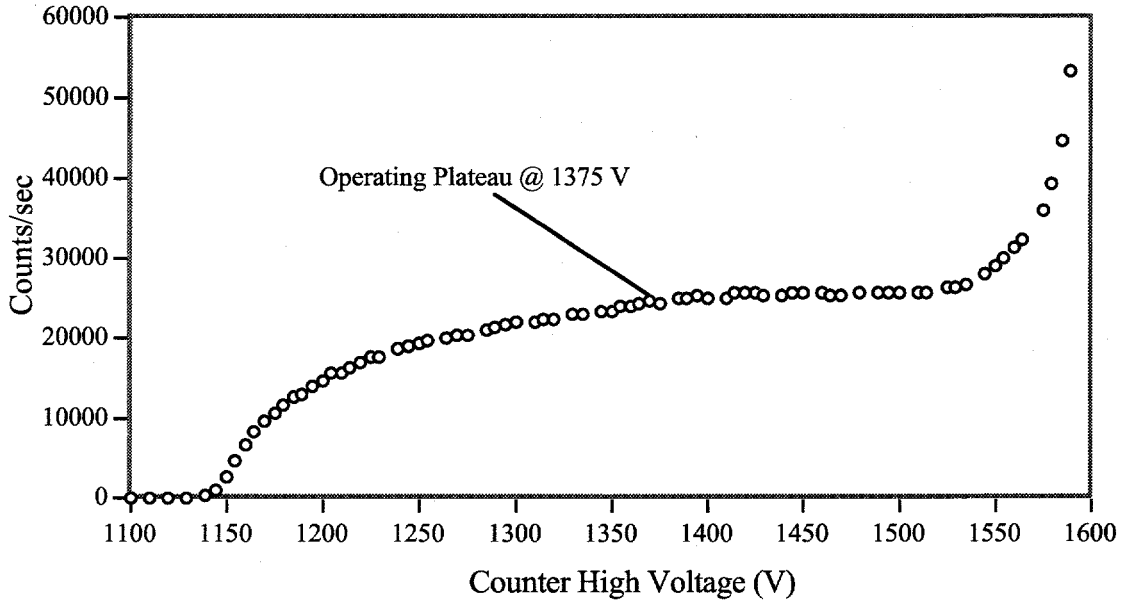

Figure 7. Plateau curve for He-3 well counter.

3.1.3 PULSE-HEIGHT SPECTRUM

When operating a counter in pulse mode, each individual pulse amplitude carries important information regarding the charge generated by the neutrons interacting in the detector. Figure 8 shows the pulse-height spectrum measured with the well counter. The multi-channel analyzer that obtained the data in Figure 8 was matched to the counts from the scaler to within 3%. The advantages of good resolution of the output pulse are efficient rejection of gamma-ray pile-up pulses and high stability of the overall counting system. Gamma-ray pile-up results from pulses not being randomly spaced in time. It should be noted that He-3 detectors are known to be gamma insensitive. This is because gamma rays interact very poorly with the gas, thus producing weak noise at the beginning of the spectrum. Most of the gamma pulses have been suppressed using the amplifier gain

and a discriminator. Figure 8 shows the pulse-shape spectrum in the well counter using the Am/Li source. This figure also shows the relative location at which the discriminator was set. Counts to the left of the discriminator level are produced by some gamma interaction with the gas and noise.

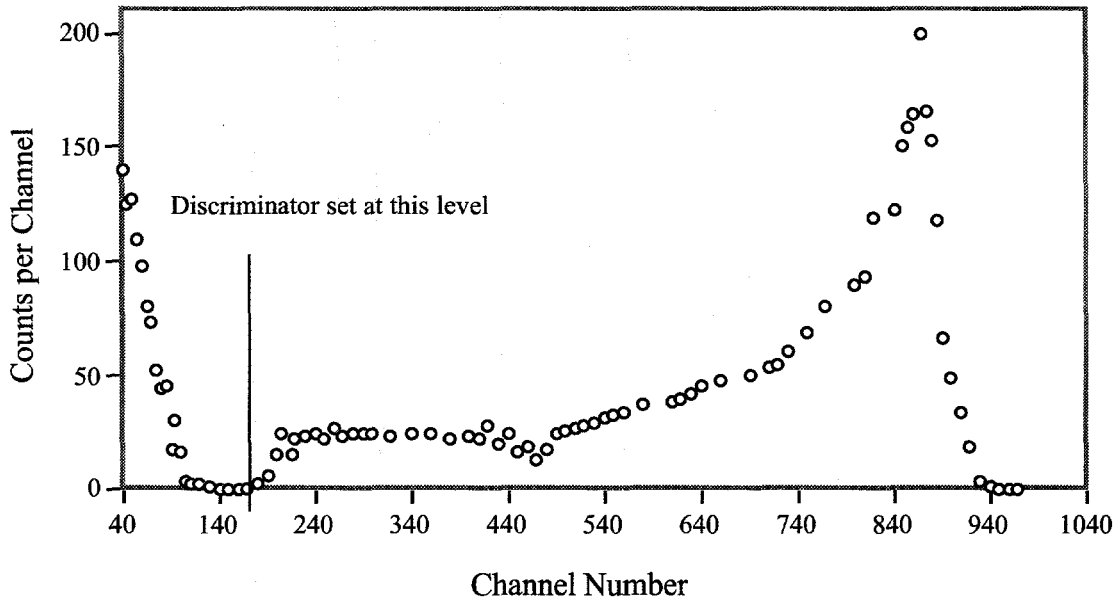

Figure 8. Pulse-height distribution in the He-3 counter

The pulse-height distribution for the thermal neutrons absorbed in the He-3 tube is a simple peak corresponding to the reaction

$$\text{He-3} + \text{n} \Rightarrow \text{p} + \text{H-3} + \text{Q} \qquad (\text{Q}=763.8\ \text{keV})$$

The peak in the pulse shape is produced when both the proton and the triton are ionized in the gas. The first hump in the pulse is produced when only the triton interacts with the gas while the second hump is produced by proton interaction with the gas. The relative high Q-value of 763.8 keV provides a bonus in that the gamma background signal will appear at a lower energy (< 763.8 keV) than the neutron signal. As seen in Figure 8, gamma interactions do not produce a pulse. To further test this concept, five gamma sources were used to calculate the gamma efficiency of the well counter. The gamma sources used for the test were: Am-241 with a strength of 12 μCi (E_γ = 0.060

MeV), Eu-152 with a strength of 55 μCi (E_γ = 0.344 MeV), Cs-137 with a strength of 7 μCi (E_γ = 0.662 MeV), Co-60 with a strength of 0.7 μCi (E_γ = 1.173 and 1.332 MeV), and Na-22 with a strength of 4 μCi (E_γ = 1.275 MeV). The counts produced by these sources could not be distinguished from the background counts.

3.1.4 DEAD TIME CALCULATION

As mentioned in the introduction, the detection of delayed neutrons requires a counter with a low dead time. The dead time of the counting system was measured using the two-source method. A 96.5 μCi Am/Be source and a 50 mCi Am/Li source were placed inside the cavity of the counter to provide counts without being too close to interfere with each other by scattering. The two-source method is based on observing the counting rate from two sources individually and in combination. Because the counting losses are nonlinear, the observed rate due to the combined sources will be less than the sum of the rates due to the two sources counted individually, and the dead time can be calculated from the discrepancy (Knoll, 1989). Since the measurement involves having two sources at one time, a dummy source with no activity was used to keep the scattering unchanged when one source alone was being counted. The counting rate of the source method was taken several times to obtain acceptable statistics. The dead time calculated by the two-source method was 0.46 ± 0.02 μsec.

3.1.5 SOURCE POSITION

Another requirement is that the counter be insensitive to sample displacement. The energy response of the detector depends upon the source distance from the effective center of the detector. The delayed neutron measurement requires the sample be stopped at the same position after each shot. Therefore, one must know over what positional range the counter has a flat response. To investigate this effect, the efficiency of the detector was measured as a function of axial distance from the bottom of the cavity. The source was placed at the bottom of the detector cavity (40-cm long) and moved axially upwards with the detector system in the vertical position. The efficiency was observed as a function of neutron-source position. Figure 9

shows this relationship. The irradiated sample can be stopped at any point within the first 10 cm of the cavity, and the response will be fairly constant. The center of the 25 cm active length of the detector is at about 7 cm on the figure. The active length of the detector ends at about 20 cm in the graph and the efficiency decreases rapidly. In the actual measurements, the sample was stopped at about the 7 cm mark. Note that the highest efficiency in this measurement is about 28% and not the 29.04% efficiency reported earlier. This is because the Am/Li source was being lifted by a string which was able to swing from side to side. This caused an efficiency change of 1%. During the measurement of delayed neutrons, the detector system lies horizontally and the transfer tube assures that the sample will not move from side to side.

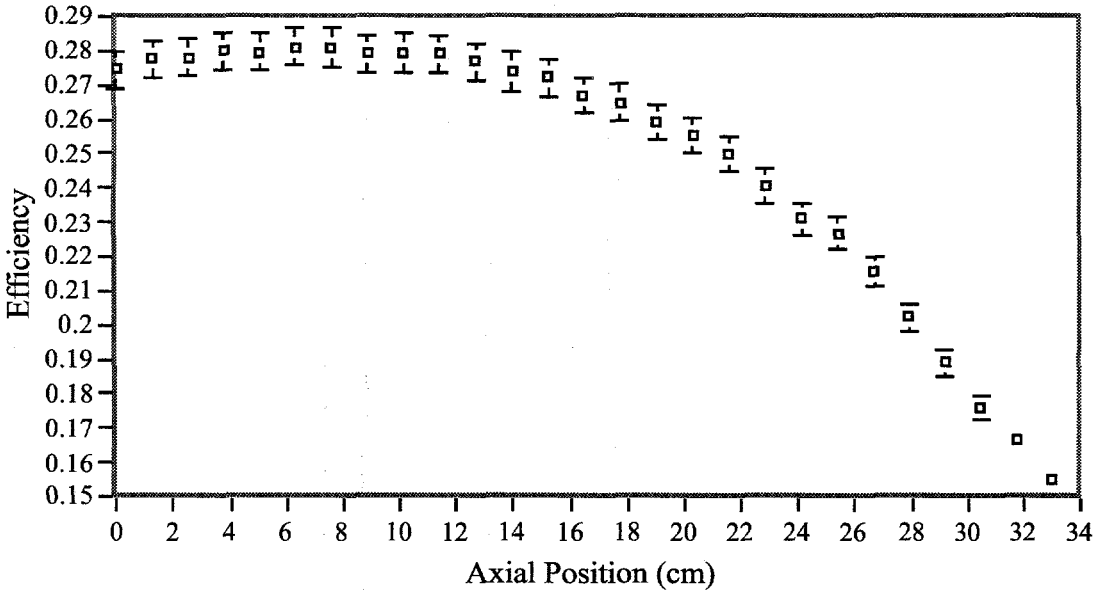

Figure 9. Dependency of efficiency on source position

3.1.6 DETECTOR SHIELDING OF GAMMA RAYS

He-3 detectors are known to be gamma ray insensitive, and that was one of the reasons for selecting the well counter. Gammas interact poorly with He-3; however, gamma pile-up is a concern. To reduce the gamma pile-up, a shield was installed between the sample and the He-3 tubes. The shield is a hollow cylinder made of bismuth with an outside diameter of 17 cm, inside diameter of 14 cm, and a height of 18 cm. The hollow bismuth

cylinder has a wall thickness of 3 cm. The size of the bismuth cylinder was chosen based on the limited space available inside the detector cavity and the materials available on-site. Accounting for build-up, mass attenuation calculations show that the bismuth shield reduces the gamma flux by about a factor of two.

3.2 EXPERIMENTAL SETUP

To analyze the delayed neutron decay, it is necessary to transfer the samples from a region of high flux to a well-shielded counting area. The transfer of the samples must be accomplished in a fraction of a second (< 180 msec. Then the rapidly changing counting rate as a function of time needs to be measured. The transfer system or "rabbit" meets these requirements. The rabbit system is an electronically controlled pneumatic transfer device which moves the sample from the irradiation position near Godiva IV to the counting room where the well counter is located. The total traveled distance is about 4.52 meters. The general experimental setup is shown in Figure 10.

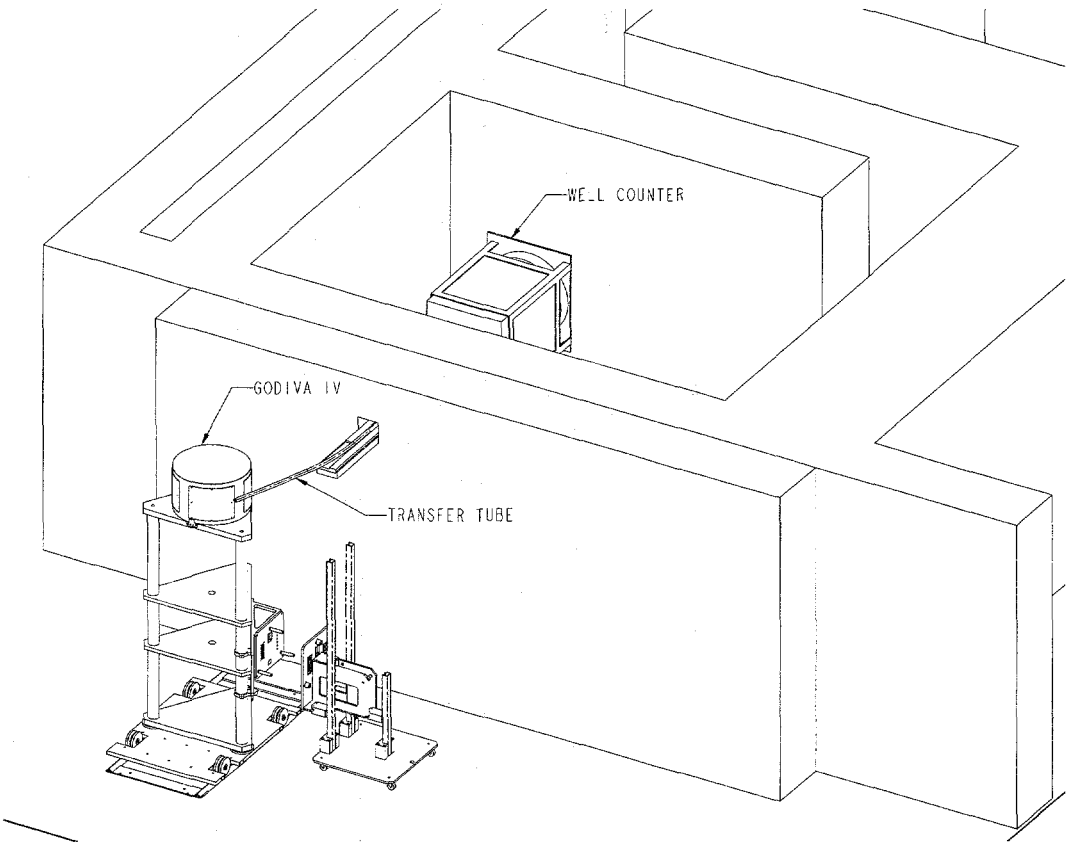

Figure 10. Schematic diagram of experimental setup with Godiva and the counter

3.3 GODIVA IV ASSEMBLY

As shown in Figure 10, the bare U-235 metal assembly of Godiva IV is used as the source of neutrons. Godiva IV is a burst assembly. The fuel composition is 93% enriched U-235 alloyed with 1.5% molybdenum by weight. The fuel components are all aluminum ion plated, and have a total mass of about 65 kg. The core of Godiva IV, when assembled, is 17.78 cm in diameter and 15.24 cm in height. The general configuration of this assembly is similar to that of Godiva II and III. Experimental measurements have shown that Godiva IV has a fast spectrum with an average energy of 1.4 MeV (LACEF, 1994).

3.4 TRANSFER SYSTEM AND EQUIPMENT

The description of the transfer equipment is separated into sections to provide a detailed explanation of each part of the transfer system. The

pneumatic transfer system transports the sample materials from the irradiation area into the well counter in less than 120 msec. The timing of the sample is explained in more detail in a later section. The transfer system consists of the following pieces of equipment: compressed air supply, solid state relay circuit, solenoid valve, photomultiplier circuit to open and close the valves, light emitting diode to detect arrival and departure of samples with appropriate circuits, and the necessary piping.

The U-235 and Np-237 samples are placed inside a capsule to facilitate the transfer of samples. The capsule is made out of polycarbonate (Lexan®). The capsule was made out of Lexan to reduce its mass. Decreasing the weight of the capsule reduces deformation to the capsule when it is stopped. The total mass of the capsule is 5.2 grams. A sketch of the capsule is shown in Figure 11. The capsule contains a cylindrical cavity where the samples are placed.

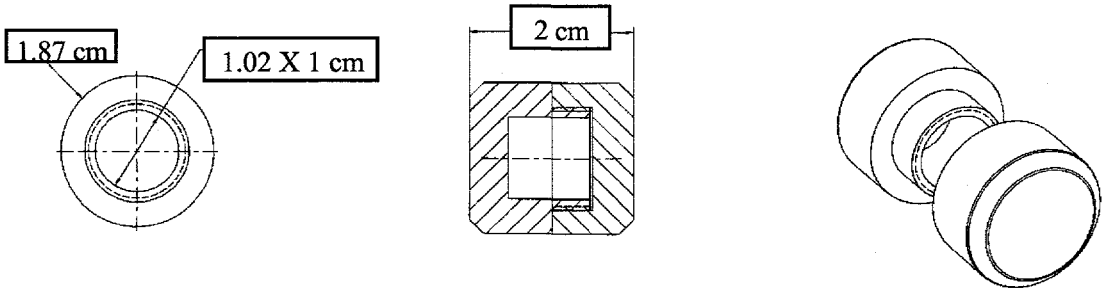

Figure 11. Schematic of the capsule.

The Np-237 sample will have an additional inner container. This inner container is placed inside the cavity of the capsule shown in Figure 11. Site procedures require that Np-237 samples be double encapsulated for routine handling. This inner container is shown in Figure 12. The inner container is made out of stainless steel and has a mass of 1 gram. The Np-237 is placed inside the inner container and is TIG welded to eliminate possible contamination when the capsule is stopped. MCNP calculations showed no neutronic perturbation from the stainless-steel container. The composition and mass of the U-235 and Np-237 samples are presented in Table 5.

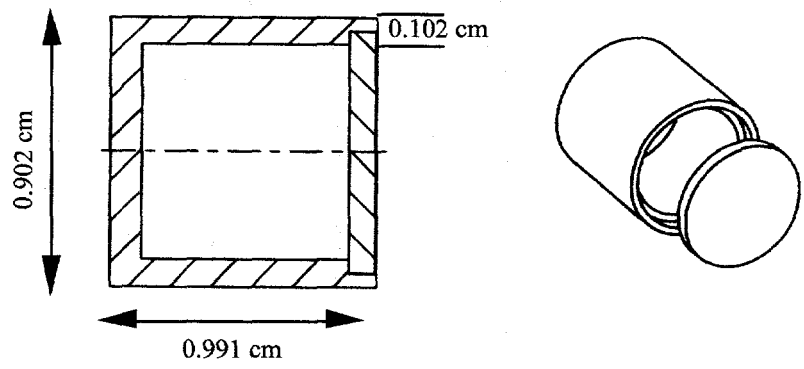

Figure 12. Inner capsule for Np-237 sample.

Table 5. Delayed neutron sample materials

Sample #	Weight (grams)	Composition (%)	Form of Mat.
1	3	U-235 93.5 U-238 5.3 U-234 1.2	Metal
2	4	Np-237 99.19 Others 0.81	Metal

Sample masses were selected as a compromise between low counting rates for small masses and excessive multiplication effects for the larger masses. Calculations presented in Figure 6 indicate that for the elements under study, yield enhancement due to multiplication effects is less than 5% for masses less than 6 grams. An analysis was also performed to determine the number of delayed neutron precursors per sample mass produced during an irradiation. It is desirable to have a large neutron count rate with minimum mass to reduce self-multiplication. The number of delayed neutron precursors was calculated based on a burst irradiation by Godiva IV and the number of atoms in a given sample mass. The fluence at the point of

irradiation produced by a burst irradiation is about $3x10^{11}$ neutrons/cm^2. Figure 13 shows the number of delayed neutron precursors produced as a function of sample mass. Figure 13 and Figure 6 show that the sample mass selected is acceptable for the experiment. These calculations served as a guideline to set upper limits for the sample masses.

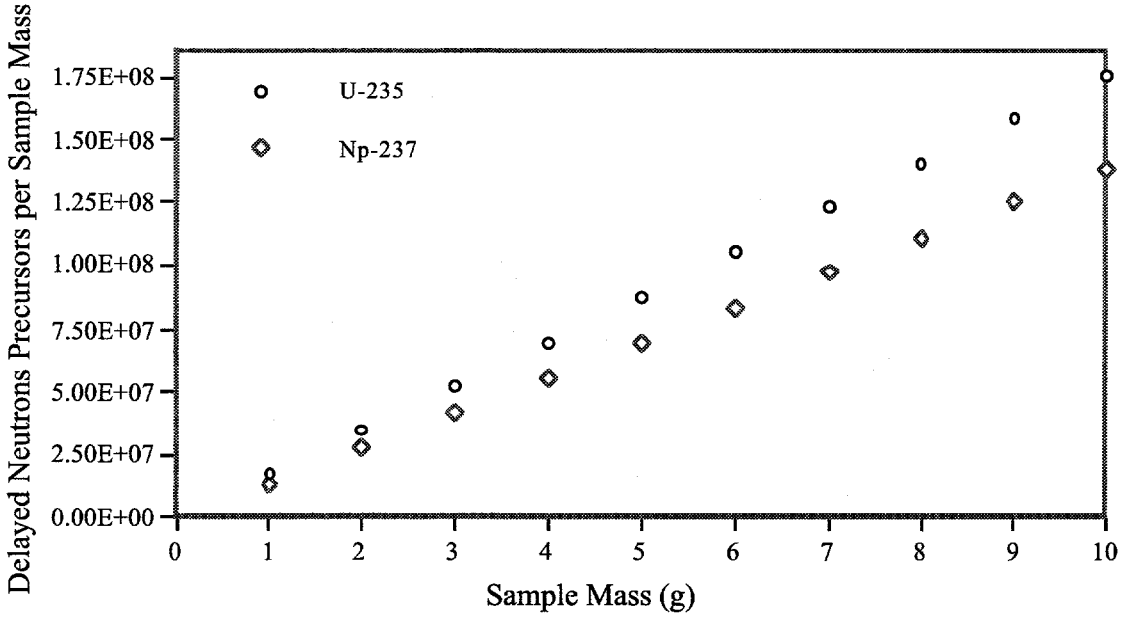

Figure 13. Delayed neutron precursors emitted per sample mass.

3.5 STOPPING MECHANISM AND TRANSFER TIME

To minimize perturbation of the decay rate, the capsule must be stopped with minimal bounce-back at the same position in the well counter after each shot. It should be noted that the capsule does not need to stop in exactly the same position after each shot because the efficiency of the detector is essentially constant within a 10 cm range as shown in Figure 9. Another requirement is that the transfer time of the capsule be less than 180 msec. The goal is to achieve short transit times without damaging the capsule on arrest. Several types of dash pots were tried in an effort to stop the capsule. Ultimately, a piece of nylon rope was used to absorb the impact. This rope absorbed and reduced the bounce to less than 0.5 cm.

The transfer time was investigated by varying the compressed-air pressure and by observing the transfer time and damage to the capsule. The goal was to achieve the desired transfer time without permanently damaging the capsule. Figure 14 shows the trial runs performed by increasing the pressure as a function of time for two different capsules. One capsule contains a depleted uranium sample while the other capsule is empty. The operating pressure in the experiment was 45 psi, which provided a transfer time of 110 msec.

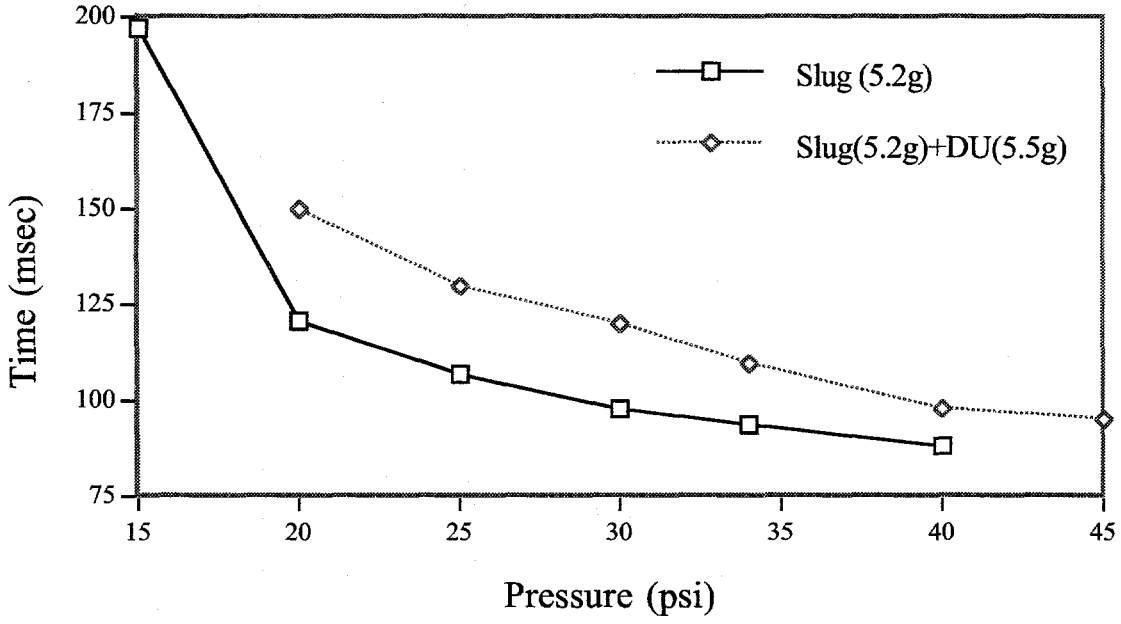

Figure 14. Transfer time for sample container.

3.6 TIMING CIRCUIT AND TRIGGER SYSTEM

The timing circuit is used to provide the time of travel for the capsule and sample from the irradiation point to the counting area. The arrival time circuit uses an Infrared Light-Emitting Diode (IRED LED) to measure the time. When the capsule crosses the beam of light emitted by the LED, the infrared light is interrupted, signaling the timer to stop. The light in the infrared diode breaks for only 1 nsec. This timing circuit uses a pulse generator with a 1-MHz clock, an Ortec 974 Quad Counter/Timer that

provides the transfer time, and a dual gate generator. The schematic diagram of the timing circuit is shown in Figure 15.

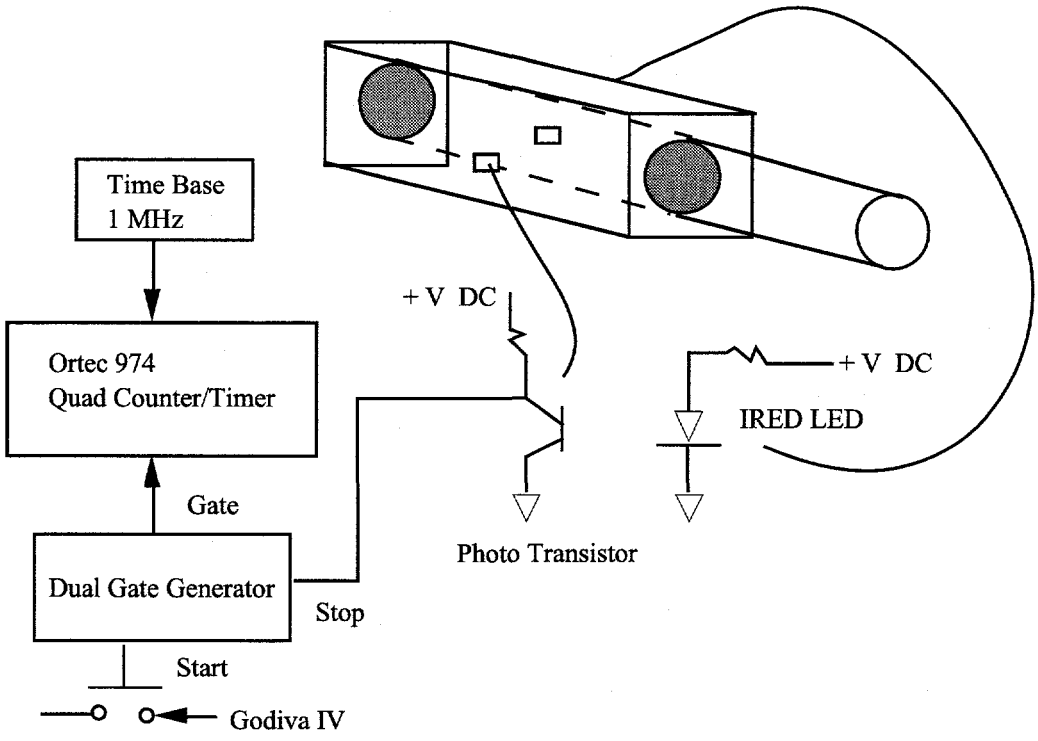

Figure 15. Timing circuit and NIM modules.

The trigger signal is obtained from a photomulitiplier placed close to Godiva. For the instantaneous irradiation, the output of a photomultiplier is used to generate (at a preset radiation level) a trigger pulse which initiates the sample transfer and the data-acquisition system. The trigger pulse from the photomultiplier is processed by the trigger module. This trigger module outputs two simultaneous signals. The first signal goes into the transfer module, which opens the solenoid valve, and the compressed air is released to initiate transfer of the capsule. The second signal is fed into the second channel of a Hex Scaler which is connected to a computer, and this signal is marked as the departure signal. When the capsule reaches the inside of the detector the infrared light emitting diode sends a signal to the Quad Timer to stop the clock and another signal to the computer acquisition system to begin collecting data. This signal is marked as the arrival signal. Figure 16 shows a global sketch of the trigger signal and its processes.

Timing on the infinite irradiation process is similar except that the photomultiplier signal is connected to the scram button of Godiva, so that the scram of Godiva and transfer of the sample occur simultaneously.

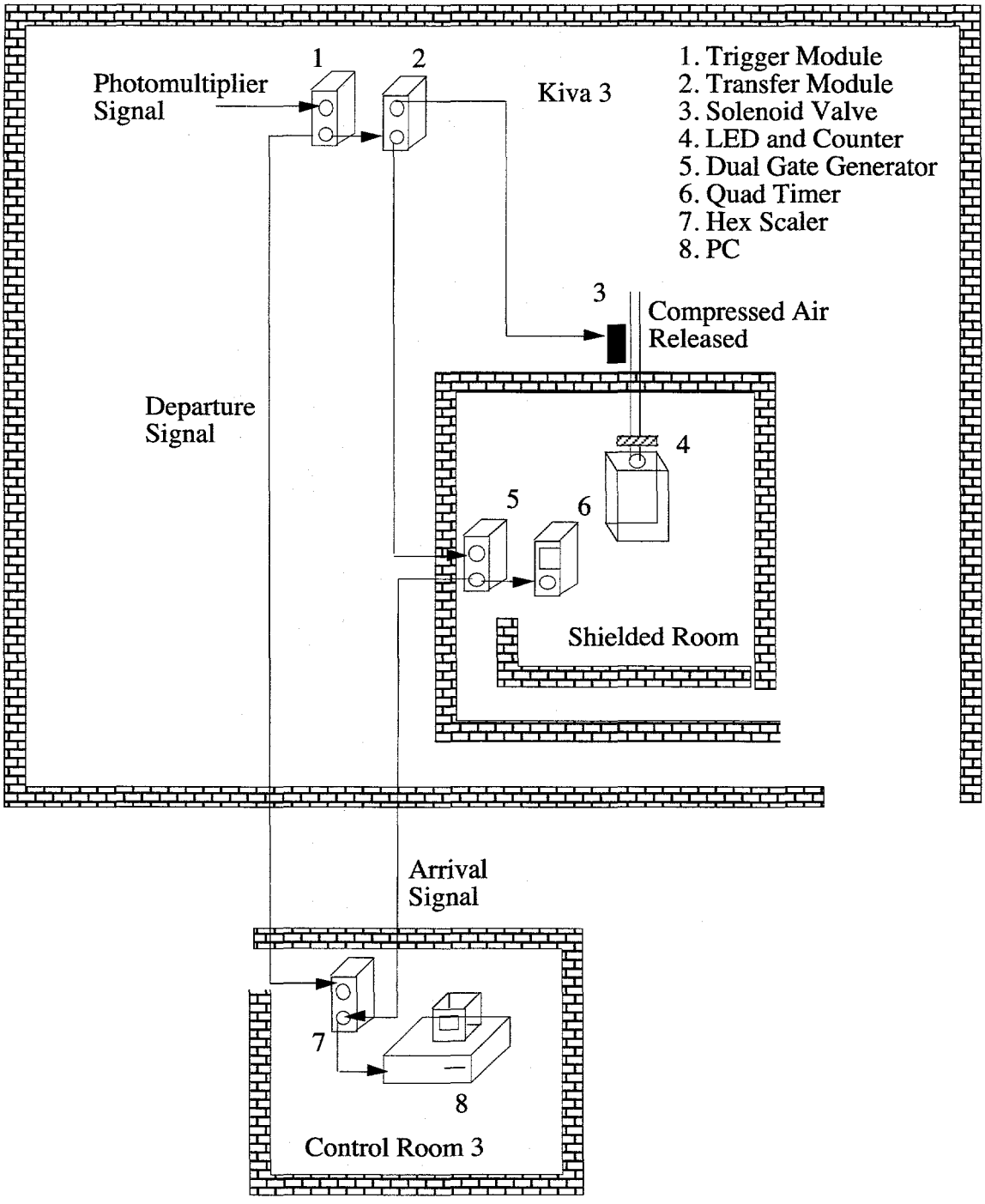

Figure 16. Diagram of the trigger signal and its process (not to scale).

3.7 RETRIEVAL SYSTEM

Initially, the transfer system was designed as a one-way rabbit system. This system was limited to only one run per day. Radiation fields were too high inside the kiva to allow access to reload. From past experiences it was known that most delayed neutron experimentalists used compressed air for retrieving the sample. However, using compressed air in this system was not feasible. There is limited space inside the detector, and by placing a valve at the end of the tube the transfer time would be increased considerably. A new idea was needed for a two-way system that fit the present design. During a brainstorming session a suggestion was made to attach a fishing line to the end of the capsule and use a fishing reel to retrieve it. The concept at first seemed absurd, but after initial testing it proved to be very promising. It was found out that the fishing line increased transfer time of the capsule by less than 5%. This was compensated for by increasing the compressed air pressure. The fishing reel proved to be very reliable for retrieving the capsule. Figure 17 shows a photograph of the retrieval system and its components.

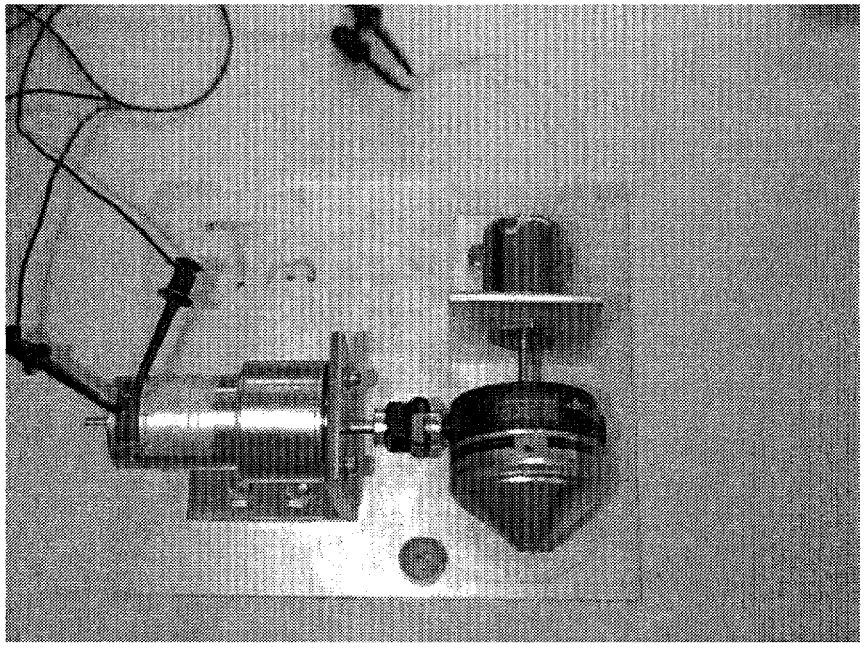

Figure 17. Retrieval system and components.

The retrieval system uses a Zebco-33 fishing reel, a 12-V motor to reel back the capsule, and a 24-V solenoid to reset the reel. Some minor alterations were made to the fishing reel to be able to reset it. The motor and solenoid are controlled by a PS503A Tektronix power supply located in control room 3.

4. DATA MODELING

This section discusses the method of analysis used to compute the delayed neutron parameters. A model is fit to the experimental data by finding the parameter values that provide the best agreement between the data and the model.

4.1 FITTING DATA TO SUM OF EXPONENTIALS

The complicated delayed neutron activity can be best measured when the irradiation time of the sample is a) instantaneous, short compared to the shortest delayed neutron period or b) infinite, long compared to the longest delayed neutron period. The infinite irradiation refers to delayed critical operation of Godiva IV, and the instantaneous irradiation refers to subprompt critical radiation bursts of 20 msec duration. Both types of irradiation produce about 10^7 total fissions in the sample. The decay constants and abundances of the longer-lived groups are calculated from infinite irradiation while the shorter-lived groups and their abundances are calculated from the instantaneous irradiations.

The analyses of the delayed neutron activity are modeled assuming that the activity as a function of time can be represented by a linear superposition of an exponential decay terms. Thus the decay of the delayed neutron activity for the saturation irradiation can be represented by:

$$y_S(t)=\sum_{i=1}^{M} \hat{a}_i e^{-\lambda_i t} \tag{4.1}$$

while the model for the instantaneous irradiation is represented by:

$$y_I(t)=\sum_{i=1}^{M} \hat{a}_i \lambda_i e^{-\lambda_i t} \tag{4.2}$$

here y is the counting rate, t is the decay time, $\hat{a}_i$ is proportional to the yield of the i-th group, and λ_i is the decay constant of the i-th group. The summation is taken over the number of groups required to achieve good fit.

The uncertainty σ_i associated with each measurement y_i is approximated by the square root of y_i. To determine how well the model agrees with the data, we use the well-known chi-square function, which in the case of the saturation irradiation becomes;

$$\chi_S^2(\hat{a},\lambda) = \sum_{j=1}^{N}\left(\frac{y_j - \sum_{i=1}^{M}\hat{a}_i e^{-\lambda_i t_j}}{\sigma_j}\right)^2 \tag{4.3}$$

The chi-square function for the instantaneous irradiation becomes;

$$\chi_I^2(\hat{a},\lambda) = \sum_{j=1}^{N}\left(\frac{y_j - \sum_{i=1}^{M}\hat{a}_i\lambda_i e^{-\lambda_i t_j}}{\sigma_j}\right)^2 \tag{4.4}$$

Equation (4.3) is minimized to determine the parameters $\hat{\mathbf{a}}$ and λ. At its minimum, derivatives of χ^2 ($\hat{\mathbf{a}}$, λ) with respect to $\hat{\mathbf{a}}$ and λ vanish.

$$\begin{aligned} 0 &= \frac{\partial\chi_S^2}{\partial\hat{a}} = -2\sum_{j=1}^{N}\frac{1}{\sigma_j^2}\left(y_j - \sum_{i=1}^{M}\hat{a}_i e^{-\lambda_i t_j}\right)\left(\sum_{i=1}^{M} e^{-\lambda_i t_j}\right) \\ 0 &= \frac{\partial\chi_S^2}{\partial\lambda} = -2\sum_{j=1}^{N}\frac{1}{\sigma_j^2}\left(y_j - \sum_{i=1}^{M}\hat{a}_i e^{-\lambda_i t_j}\right)\left(\sum_{i=1}^{M}\hat{a}_i t_j e^{-\lambda_i t_j}\right) \end{aligned} \tag{4.5}$$

Minimizing equation (4.4) we have;

$$\begin{aligned} 0 &= \frac{\partial\chi_I^2}{\partial\hat{a}} = -2\sum_{j=1}^{N}\frac{1}{\sigma_j^2}\left(y_j - \sum_{i=1}^{M}\hat{a}_i\lambda_i e^{-\lambda_i t_j}\right)\left(\sum_{i=1}^{M}\lambda_i e^{-\lambda_i t_j}\right) \\ 0 &= \frac{\partial\chi_I^2}{\partial\lambda} = -2\sum_{j=1}^{N}\frac{1}{\sigma_j^2}\left(y_j - \sum_{i=1}^{M}\hat{a}_i\lambda_i e^{-\lambda_i t_j}\right)\left(\sum_{i=1}^{M}\hat{a}_i e^{-\lambda_i t_j}\left(1+t_j\lambda_i\right)\right) \end{aligned} \tag{4.6}$$

Assuming that $\hat{a}_{io}$ and λ_{io} are the initial estimates of the real parameters $\hat{a}_i$ and λ_i, we can then proceed to use an iterative nonlinear least square method to find the final values $\hat{a}_i$ and λ_i which will minimize equations (4.5) and (4.6). The fractional group yields, a_i, are obtained by normalization of $a_i = \hat{a}_i / \Sigma\, \hat{a}_i$.

Most algorithms for the least squares estimation of nonlinear parameters have centered about either of two approaches, the Gauss-Newton method and the steepest-descent method (for a detailed description of these two methods refer to Numerical Recipes by Press et al., 1992). Marquardt (1963) introduced an algorithm that combines the two methods. His method is based on early work of Levenberg (1944). In the Gauss-Newton method, the model is expanded as a Taylor series, and corrections are made to the parameters calculated at each iteration. In the steepest-descent (or gradient) method the parameters are adjusted by small changes in the direction of the gradient. This technique provides slow convergence after the first iteration. The Levenberg-Marquardt technique performs an optimum interpolation between the two methods by introducing a constant that is varied to accelerate the convergence. Equation (4.7) shows a representative matrix equation to illustrate the Levenberg-Marquardt technique where a constant λ has been introduced.

$$\left(A^{(r)} + \lambda^{(r)} I\right)\delta a = b^{(r)} \tag{4.7}$$

δa is the step that is being taken to solve at the rth iteration, I is the unity matrix, and λ is a positive constant that is controlled during the iteration. When the constant $\lambda \rightarrow 0$, equation (4.7) approaches the steepest-descent method and when $\lambda \rightarrow \infty$, equation (4.7) approaches the Gauss-Newton method. This hybrid method works very well, and is used to solve for the unknown parameters in equations (4.5) and (4.6). The method is implemented in a Mathcad subroutine which uses the public domain MINPACK algorithms developed and published by the Argonne National Laboratory (More et al., 1980).

The least squares fit is applied in two ways. First, all decay constants and abundances are estimated from prompt burst irradiation data. Second, the four longer groups are estimated from infinite irradiation data. The results are combined to obtain a single estimate of the parameters for each group as described in the next chapter.

5. ANALYSIS AND RESULTS OF DELAYED NEUTRON DATA

The scheme for the analysis of delayed neutrons for the two isotopes (U-235 and Np-237) is described in this chapter. Delayed neutron precursors are created in the samples by fissions resulting from irradiations by neutrons generated from a Godiva pulse or steady-state operation. The Godiva pulse accentuates the short-lived precursors while the delayed critical operation or infinite irradiation accentuates the long-lived precursors. The decay data is collected by the well counter, processed by the PATRM module, and saved in a binary format. The recorded data is a list file where the arrival time of each delayed neutron pulse is recorded in the list. This binary list is read by an algorithm created for the analysis of delayed neutrons (Brunson, 1996). This algorithm reads the arrival time of each pulse and tallies it in a histogram of varying bin width. The bin width at first is set at 20 msec, then the time bin is doubled in size every 50 bins. The reason for varying the size of the time bins is to better observe the complicated decay of delayed neutrons. At the beginning of the decay, the delayed neutron precursors include those with short half-lives. To better fit this data, small time bins are applied. As the decay continues, the half-lives of the precursors are longer, and the bin width is adjusted accordingly (a sample binned list file is presented in Appendix B). Once the data has been binned at appropriate intervals, the following corrections are applied to the data: (a) correction for dead time losses and (b) correction for neutron background. If ct_0 is the initial count rate (before corrections) detected in a time bin, then the count rate corrected for dead-time is given by;

$$ct_n = \frac{ct_o}{(1 - DT \cdot ct_o)} \tag{5.1}$$

where ct_n is the corrected count rate and DT is the dead time for the system and equals 0.46 μsec as given in Chapter 3. The magnitude of the dead time correction was minimized by reducing the irradiation fluence, thus producing a lower counting rate. The worst-case dead time correction at

the time of arrival was less than 2%. Figure 18 shows the statistical distribution of the data before the dead-time was minimized.

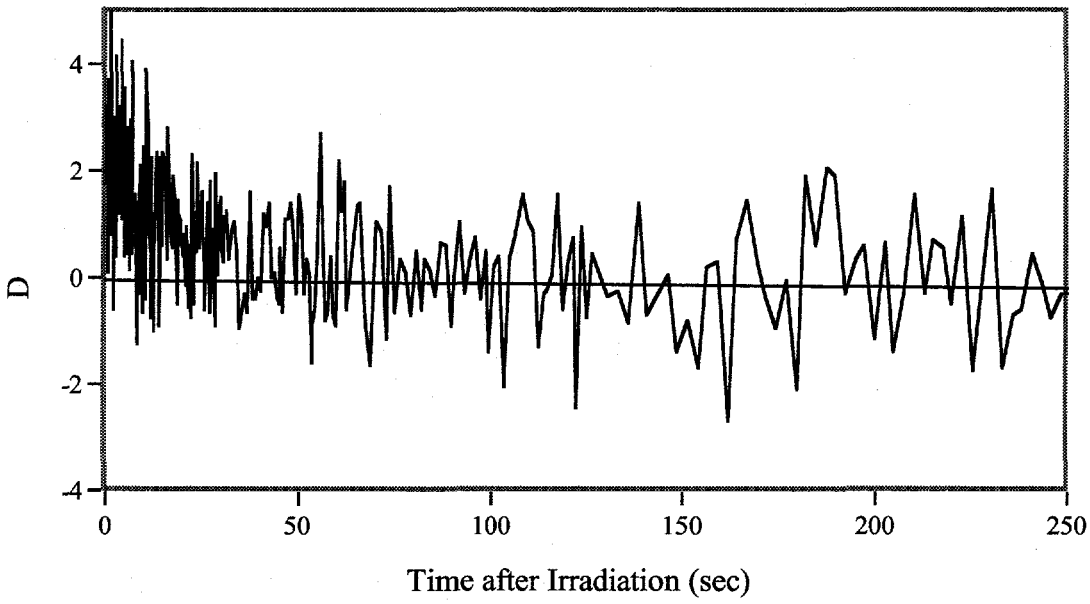

Figure 18. Statistical distribution for delayed neutrons with dead-time.

The normal distribution in Figure 18 was plotted using the following relationship.

$$D = \frac{(y_{cal} - y_{exp})}{\sqrt{y_{exp}}} \tag{5.2}$$

Where y_{cal} is the calculated count rate from the fitted parameters while y_{exp} is the measured data from the decay. From this figure can be inferred the biases in the collection of data. In the event of high dead time losses, the data set is shifted up in the early time interval and not distributed about zero. Figure 19 shows the statistical distribution after the dead time was minimized by reducing the fluence. It is apparent from this data set that the dead-time losses have been minimized.

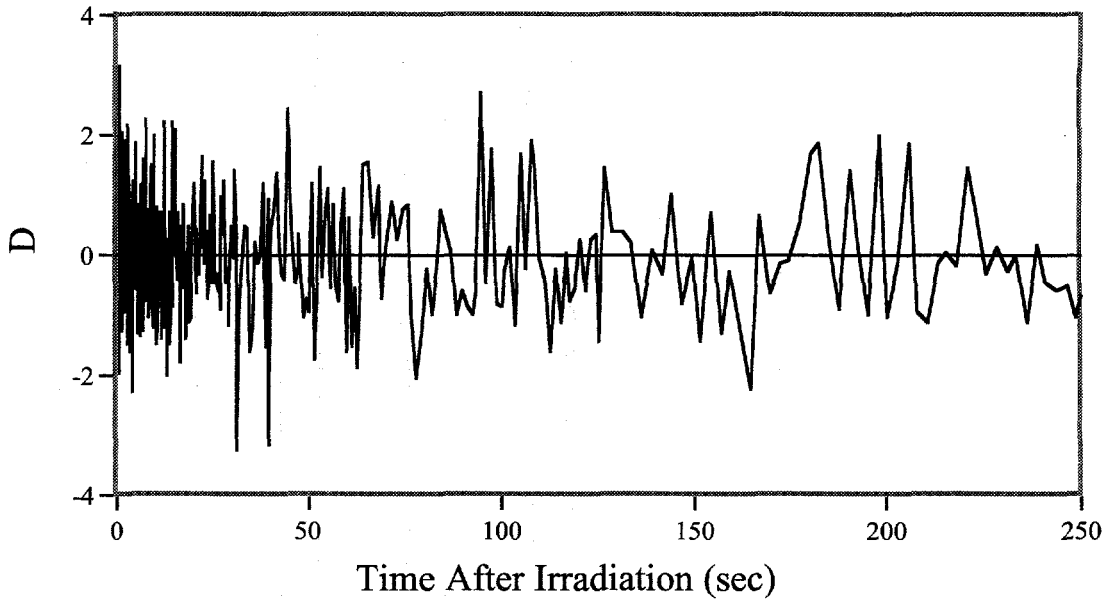

Figure 19. Statistical distribution for delayed neutron data after dead-time correction.

The second correction applied to the raw data is to compensate for the time-dependent neutron background. The neutron background was reduced by adding heavy shielding around the detector and also by reducing the size of the Godiva irradiations. The neutron background originating from Godiva was characterized by transporting an empty capsule after irradiation in Godiva. The maximum count rate observed under this conditions was 250 ct/sec. It drops to 5-4 ct/sec after less than 50 sec. The neutron background correction is less than 0.27% at the early time of arrival. Figure 20 shows the neutron background as a function of time after a Godiva irradiation.

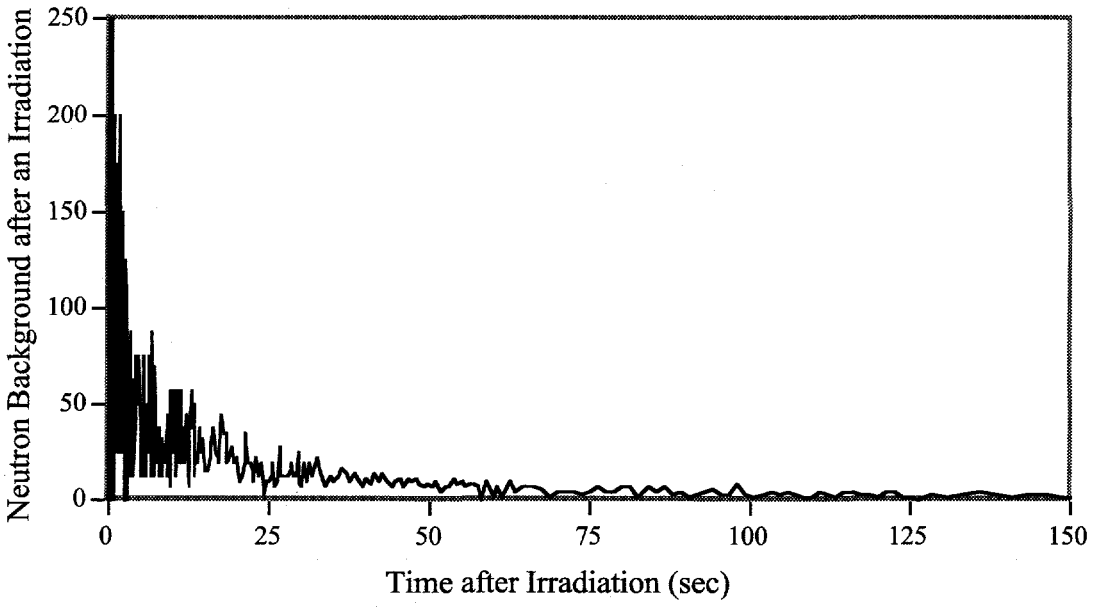

Figure 20. Background count rate after irradiation.

The complete decay data is then analyzed using the nonlinear least-squares Levenberg-Marquardt routine described in Chapter 4. All the delayed neutron parameters were required to be positive so that the optimization was constrained by physical considerations. The method and program for the analysis was also tested for accuracy and reliability using a set of simulated data. The results and technique for the testing of the nonlinear least squares Levenberg-Marquardt routine are given in Appendix C.

The true value of the delayed neutron parameters can never be determined; however, the deviation of the mean value can be calculated and reduced if the experiment is repeated many times. Consider that the experiment has been repeated N times, and that the mean value of a parameter is given by $\bar{n}$. The average $\bar{n}$ value for any particular parameter is calculated by:

$$\bar{n} = \frac{1}{N}\sum_{i=1}^{N} n_i \qquad (5.3)$$

where $\bar{n}$ represents the average value for any group parameter. The error in $\bar{n}$ depends on the way the individual measurements are distributed around $\bar{n}$. The larger the value of N, the smaller the error becomes. But with a finite number of runs, it can be shown that the best estimate of the standard error $\bar{n}$ is defined in terms of the standard deviation of the distribution (Tsoulfanidis, 1983). The standard deviation of the distribution of N measurements is given by.

$$\sigma_r^2 = \frac{1}{N-1}\sum_{i=1}^{N}(n_i - \bar{n})^2 \tag{5.4}$$

Where n_i is the delayed neutron parameter for an individual run. Equation (5.4) provides the raw standard error of a single measurement which is not the same as the standard error of an average $\bar{n}$ value. According to the definition of the standard error, if $\sigma_{\bar{n}}$ is the standard error of $\bar{n}$, it should have such a value that a new average $\bar{n}$ would have a 68.3 % chance of falling between $\bar{n} - \sigma_{\bar{n}}$ and $\bar{n} + \sigma_{\bar{n}}$. Therefore the standard deviation of $\bar{n}$ is (Jaech, 1973).

$$\sigma_{\bar{n}} = \frac{\sigma_r}{\sqrt{N-1}} \tag{5.5}$$

If the series of N measurements is repeated, the new calculated average value will probably be different from $\bar{n}$, but it has a 68.3 % chance of having a value between $\bar{n} - \sigma_{\bar{n}}$ and $\bar{n} + \sigma_{\bar{n}}$.

The parameters for groups 1 and 2 are computed from the infinite irradiations, and the parameters for groups 5 and 6 are computed from the pulse irradiations. However, the parameters for groups 3 and 4 are combined from instantaneous and infinite irradiations. The average values and standard deviations for groups 3 and 4 are calculated differently from the description given above, because these parameters are evaluated from two different type of irradiations. First, average values for groups 3 and 4 parameters are calculated based only on pulse irradiations using equation (5.3), and average values from infinite irradiations only are computed using

equation (5.3). The combined average values for groups 3 and 4 are then given by:

$$\bar{n}_3^c = \frac{B \cdot \bar{n}_3^b + D \cdot \bar{n}_3^d}{B + D} \tag{5.6}$$

where the c, b, and d superscripts signify combined, burst, and delayed operation; B is the number of pulse irradiations; and D is the number of delayed critical operations. The standard deviation for the combined average is then calculated by propagation of error.

$$\sigma_{\bar{n}} = \sqrt{\left(\frac{B}{B+D}\right)^2 \cdot \left(\sigma_{\bar{n}}^b\right)^2 + \left(\frac{D}{B+D}\right)^2 \cdot \left(\sigma_{\bar{n}}^d\right)^2} \tag{5.7}$$

where $\sigma^b{}_{\bar{n}}$ and $\sigma^d{}_{\bar{n}}$ are the standard deviation in the pulse irradiation only and in the delayed critical irradiation only, respectively.

As expected, infinite irradiation produced a smaller standard deviation in the decay constants for groups 1 and 2, and instantaneous irradiation produced a smaller standard deviation for groups 5 and 6. It should be noted that the quoted errors in the group parameters and the total yield values are mainly statistical in nature. As shown previously the parameters for groups 3 and 4 were obtained by combining data from the instantaneous and infinite irradiation. To illustrate the difficulty in accentuating groups 3 and 4 at any particular time, Figures 21 and 22 were created. Figure 21 shows the relative importance of the groups after an instantaneous irradiation. As can be seen from Figure 21, groups 5 and 6 dominate and are accentuated during the early decay times (t less than 1 second).

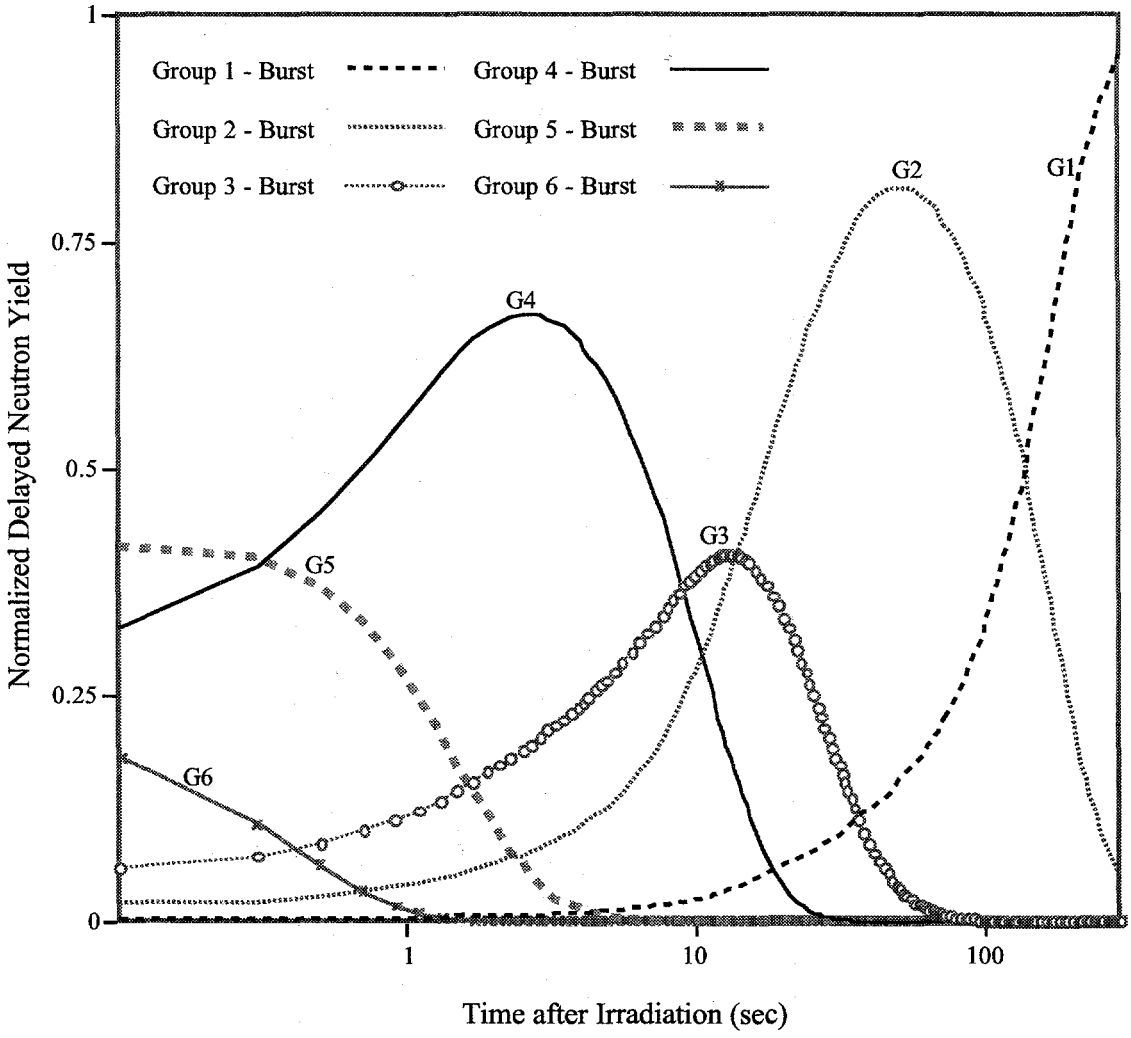

Figure 21. Accentuation of group parameters after an instantaneous irradiation.

In the same manner, Figure 22 shows the accentuation of groups 1 and 2 after an infinite irradiation. Groups 3 and 4 are accentuated during both types of irradiation, but their decays compete with the other groups at all times making their measurement more complicated.

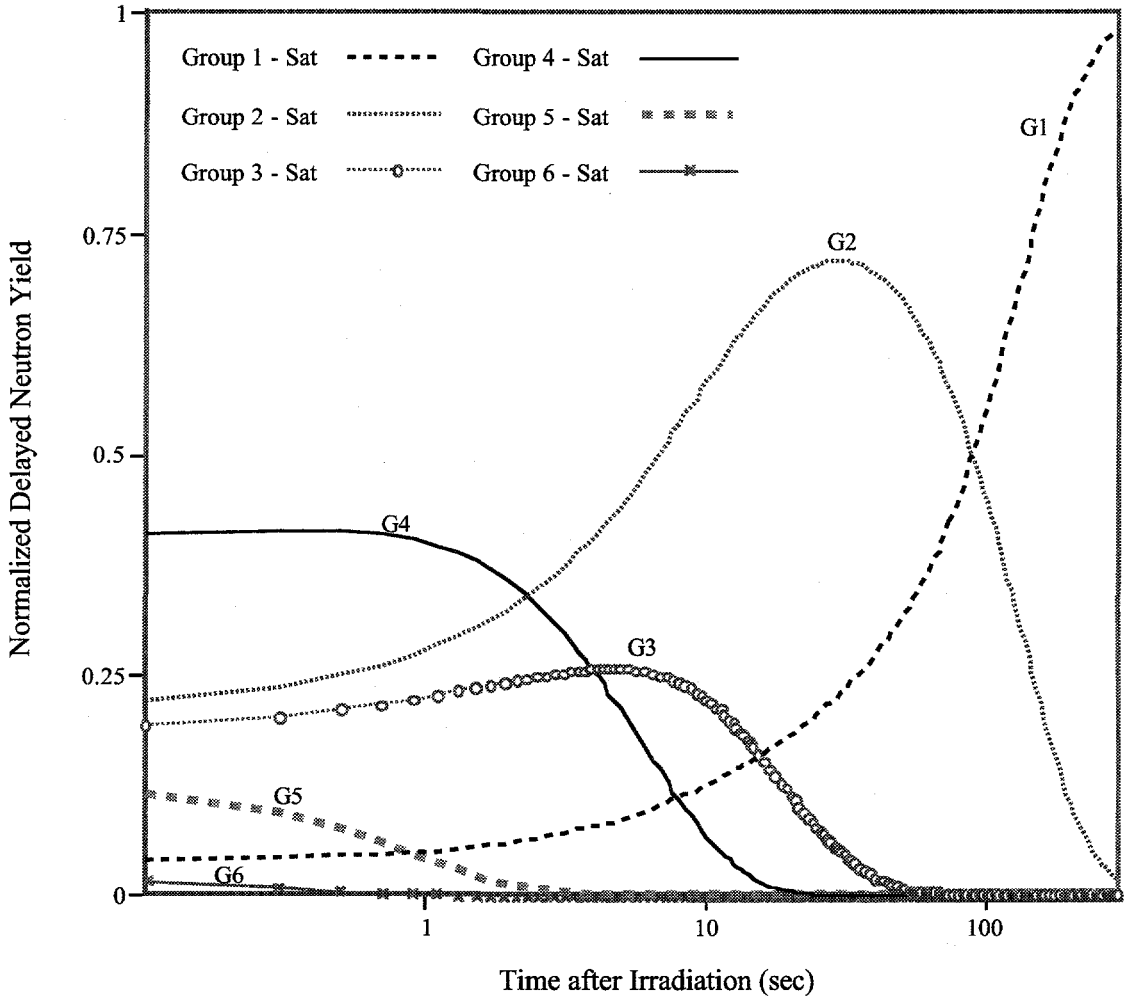

Figure 22. Accentuation of group parameters after an infinite irradiation.

5.1 URANIUM-235 MEASUREMENTS.

Table 6 summarizes the newly measured decay constants, relative yield, and absolute yield per fission for fast neutron-induced fission in U-235. In the last line, the measured absolute yield is also reported. The quoted uncertainties on abundances and decay constants were computed as described earlier in this chapter.

Table 6. Fast-fission delayed neutron data for ^{235}U.

Group #	Decay Constant $(sec)^{-1}$	Relative Yield (a_i/a)	Absolute Yield, $(fissions)^{-1}$
1	0.0127 ± 0.0001	0.0395 ± 0.001	0.000644
2	0.0315 ± 0.0004	0.235 ± 0.005	0.00383
3	0.117 ± 0.0064	0.207 ± 0.008	0.00337
4	0.314 ± 0.0107	0.381 ± 0.011	0.00621
5	1.37 ± 0.0514	0.114 ± 0.005	0.00186
6	3.83 ± 0.1138	0.0235 ± 0.001	0.000383
Absolute Yield (neutrons/fission)			
0.0163 ± 0.0009			

Figure 23 shows a typical decay of delayed neutrons measured during an instantaneous irradiation. The figure also illustrates the agreement between the experimental data and a curve calculated using the decay constants and abundances reported in Table 6. The reduced chi-square for this particular fit is 0.98, which means that there was good agreement between the experimental data and the fitted curve.

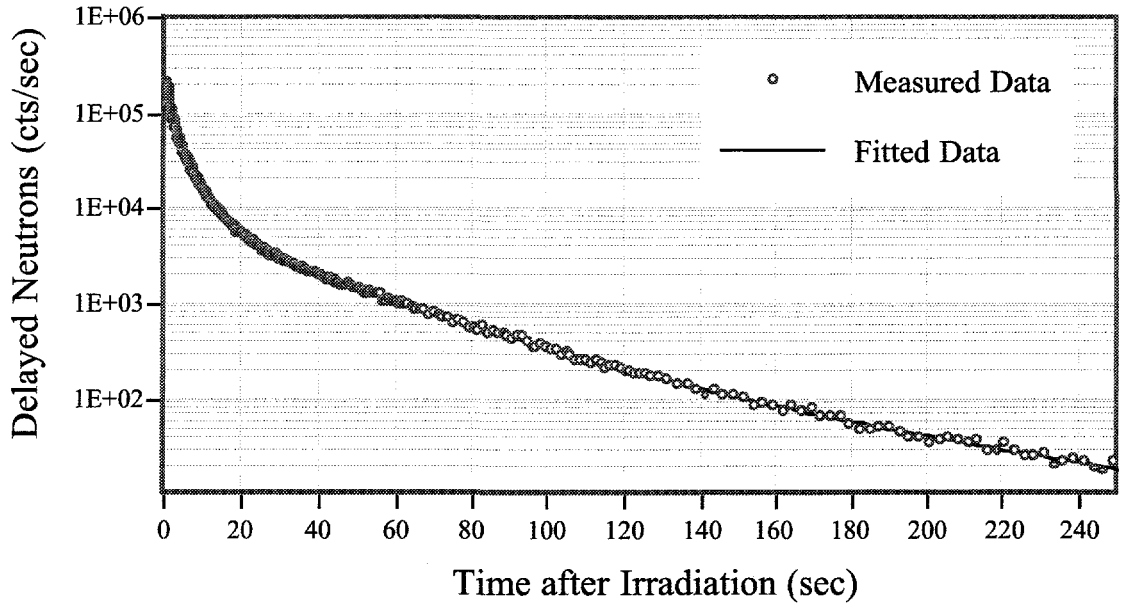

Figure 23. Measured delayed neutron decay for instantaneous irradiation shown with fitted data calculated from abundance and periods.

Figure 24 shows a representative delayed neutron decay for an infinite irradiation. This figure has a reduced chi-square of 1.02, indicating good agreement between experimental and fitted data from the measured parameters.

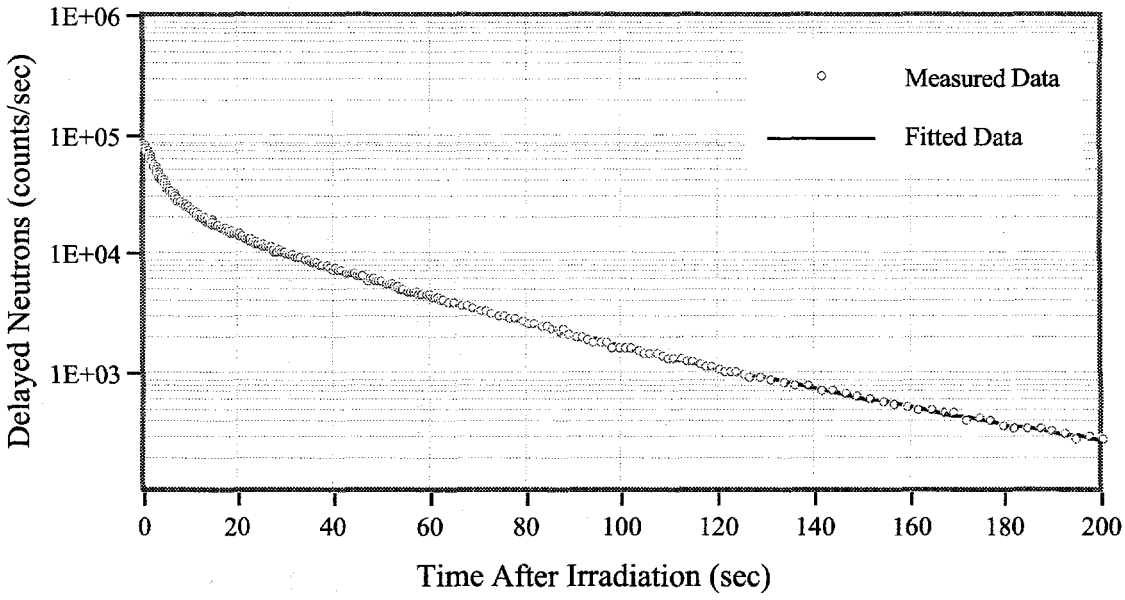

Figure 24. Measured delayed neutron decay after infinite irradiation shown with fitted data calculated from abundances and periods.

A comparison of the measured delayed neutron group constants with the values reported by Keepin et al. (1956) and Brady and England (1989) for U-235 is presented in Table 7. The parameters from this experiment are in good agreement with the reported values by Keepin. The total delayed neutron yield reported by Keepin is 0.0165 and the total delayed neutron yield in this experiment is 0.0163.

Table 7. Comparison of fast-fission delayed neutron data for ^{235}U.

Groups	Relative Yield, a_i/a			Decay Constant, λ_i		
	This Work	Keepin et al.	Brady et al.	This Work	Keepin et al.	Brady et al.
1	0.039±0.001	0.038±0.003	0.035	0.0127±1E-4	0.0127±2E-4	0.0133
2	0.235±0.005	0.213±0.005	0.1807	0.0315±4E-4	0.317±8E-4	0.0327
3	0.207±0.008	0.188±0.016	0.1725	0.117±0.006	0.115±0.003	0.1208
4	0.381±0.011	0.407±0.007	0.3868	0.314±0.010	0.311±0.008	0.3028
5	0.114±0.005	0.128±0.008	0.1586	1.37±0.051	1.40±0.081	0.8495
6	0.024±0.001	0.026±0.003	0.0664	3.83±0.114	3.87±0.369	2.853

Absolute Yield, n/f		
This Work	Keepin et al.	Brady et al.
0.0163 ± 0.0009	0.0165 ± 0.0005	0.0206 ± 0.002

Note that a sound comparison of the data is only possible for the absolute yield, since the group abundances and decay constants are in some degree arbitrary (fitting six groups to the 271 known delayed neutron precursors). However, the delayed neutron decay for ^{235}U and other fissionable isotopes can be satisfactorily fit with six exponential functions, which are in essence the same for all isotopes. It can be concluded that the six 'principal' groups each consist of either a single main precursor or a combination of precursors with similar half-lives that dominate the decay despite other perturbations. It also important to note that the reported uncertainty in the absolute yield for this experiment is larger than Keepin's. This is because Keepin used radio-chemistry to look at the number of fissions in a sample as opposed to using a High-purity Germanium detector. Keepin and Wimett also performed about 80 shots to collect their data. Radio-chemistry was not used in this experiment because of the cost and lack of facility and personnel to perform such analyses.

To better illustrate differences in the data of Table 7, Figures 25 and 26 were created. Figure 25 compares the group abundances for the

aforementioned references. As illustrated in Figure 25, Keepin's data and this experiment's data match very well except for group 2. The calculated values by Brady and England are higher than either those from this study or from Keepin for groups 5 and 6. Symbols without error bars (groups 1, 2, 5, and 6) signify that the error bar is smaller than the symbol plotted. Brady and England's data do not have errors bars because their data is based on computational methodologies.

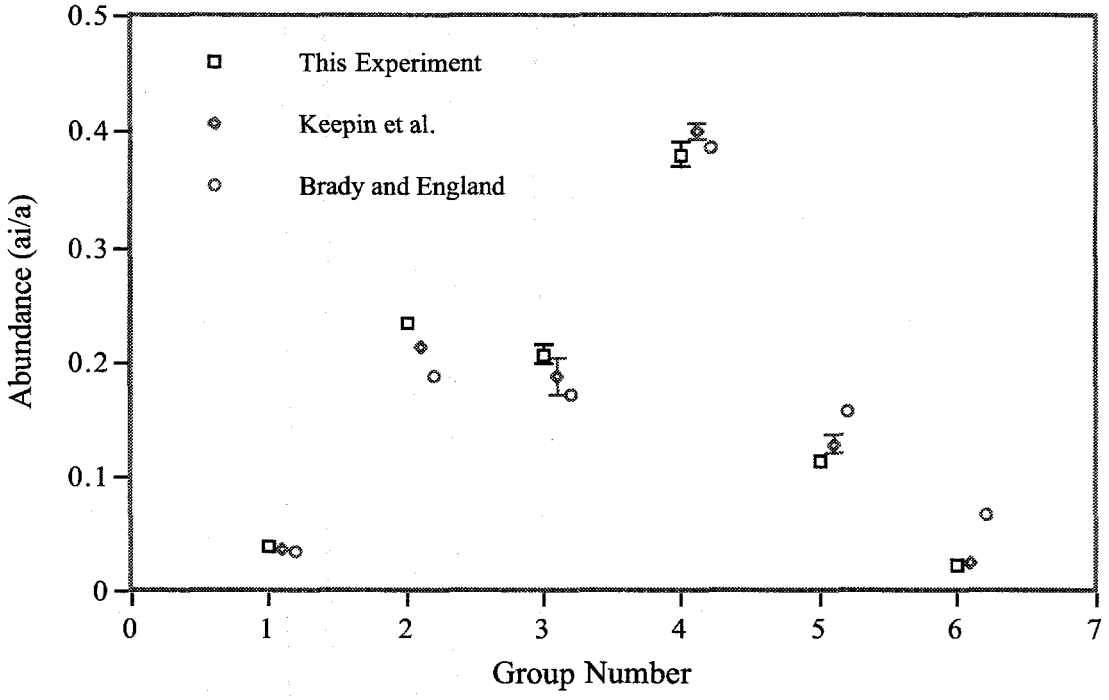

Figure 25. Graphical comparison of group abundances for U-235.

Figure 26 presents a comparison of the decay constants for ^{235}U. The parameters for all the references compared very well up to group 4. There is a considerable difference in values for groups 5 and 6 in Brady and England's data. Once again, data without error bars signifies that the error bar is smaller than the symbol. Brady and England's data do not have error bars reported. Group 6 in this experiment has smaller error bars than Keepin's. This is because delayed neutrons with the shortest half-lives also tend to have the highest energy. Since most detector systems are sensitive to energy, fewer counts will be observed for group 6. Because our detector system has a higher efficiency, the statistics for group six were better than Keepin and Wimett's.

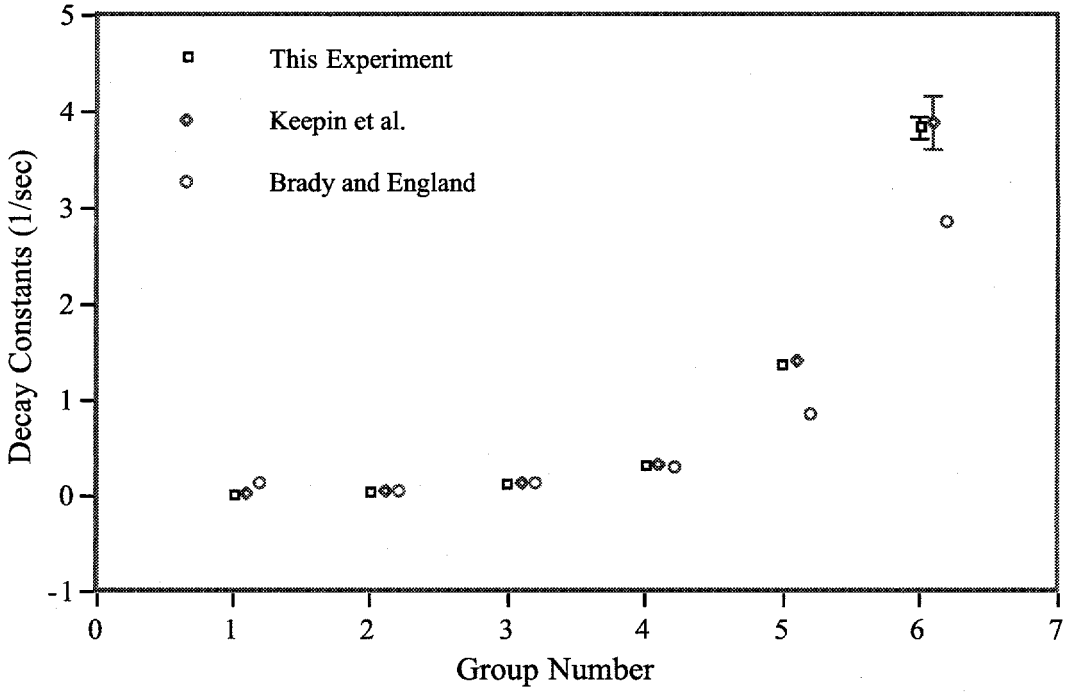

Figure 26. Graphical comparison of group decay constants for U-235.

5.2 ABSOLUTE YIELD MEASUREMENTS

There are two techniques to determine the total absolute yield from the measured data. One of the methods involves using data from the infinite irradiation while the second technique uses data from the instantaneous irradiation. The delayed neutron activity as function of time for an infinite irradiation can be expressed as

$$A(t) = F_s Y_{abs} \sum_i a_i e^{-\lambda_i t} \tag{5.8}$$

where F_s is the total number of fissions produced in the sample and Y_{abs} is the absolute yield. The number of counts, C_i, observed by a detector with a absolute efficiency, ε, over a counting interval ($t_1 \rightarrow t_2$) after an infinite irradiation is:

$$\sum C(t_1 \rightarrow t_2) = \varepsilon F_s Y_{abs} \int_{t_1}^{t_2} \sum_i a_i e^{-\lambda_i t} dt \tag{5.9}$$

Equation (5.9) assumes that the abundances and decay constants have already been measured and that ε and F_s are known. The measurement of the absolute efficiency was shown in Chapter 3. The determination of the number of fissions in the sample will be elaborated on later in this section. The absolute yield can be calculated from equation (5.9); however, this involves extrapolating the decay curve to the end of irradiation (t = 0), resulting in a less precise measurement. The most accurate technique to calculate the absolute yield is to observe the total number of counts following an instantaneous irradiation where the initial activity is proportional to $a_i \lambda_i$. However, in this method the values for the abundance and decay constant are not required because total counts are used.

$$\sum C_{tot} = \varepsilon F_s Y_{abs} \int_0^\infty a_i \lambda_i e^{-\lambda_i t} dt = \varepsilon F_s Y_{abs} \tag{5.10}$$

Therefore, the absolute yield is calculated directly as

$$Y_{abs} = \frac{\sum C_{tot}}{\varepsilon F_s} \tag{5.11}$$

As seen in equation (5.11) the instantaneous irradiation produces more accurate results, since the yield is determined from the total counts. While in the infinite irradiation, the absolute yield is determined only from extrapolation counting rate and from the measured delayed neutron parameters.

The total number of fissions, F_s, produced in a sample during a Godiva irradiation was measured by a standard foil-activation technique. For this experiment the activities of Ba-140, La-140, Ru-103, I-131, and Mo-99 were observed. These fission products were selected because their cumulative fission yields are well known (ENDF/B-VI), and also because they have long half-lives which permit the measurement of their activities in a clean gamma spectrum after the short-lived fission products have decayed.

In all, 7 U-235 foils with the same composition as the U-235 sample were used to measure the number of fissions induced in 14 U-235 irradiations. The procedure was to tape a foil to the outside of the transfer tube at the position adjacent to Godiva where sample was irradiated. Each of the 7 foils provided direct measure of the number of fissions induced in the pulse to which it was exposed. The foil was removed prior to the next irradiation. In cases in which the sample was subsequently subjected to pulses of the same size, as confirmed by period measurements, one foil provided an indication of the number of fissions in the consecutive, identical pulses.

Each foil was allowed to decay for about 13 days to allow short-lived fission products to decay. The number of fissions in the sample was then found by counting the La-140, 1596-keV gamma activity relative to a Godiva calibration foil. After 13 days, the activity of La-140 is in transient equilibrium with, and therefore proportional to, that of Ba-140 (half-life of 12.9 days). By comparing the La-140, 1596-keV gamma counts from the foil in question to these from a Godiva calibration foil, the number of fissions in the sample were calculated. The counting system that was employed for this study has been extensively used to provide reliable measurements of fissions in U-235, Np-237, and other nuclides for several years at Los Alamos National Laboratory.

The counting system consisted of a high-purity germanium detector with its associated electronics. The high-purity germanium detector was used to find the intensity of the 1596-keV photopeak. Elaborate analysis of the 1596-keV peak was unnecessary since the peak was well separated from any other peak. In some cases confirmatory information was obtained by measuring fission products other than Ba-140. The actual measurement of the number of fissions in the sample was carried out by a LACEF staff member. Table 6 compares the absolute yield calculated by this experiment to other values published. In all cases, the error associated with the measurement of counts under the La-140 photopeak was the dominant contributor to the error in the absolute yield.

5.3 THE PERIOD VERSUS REACTIVITY RELATIONSHIP

Perhaps the most stringent requirement for delayed neutron yield and decay data arises in their use, that is, via the relation between reactivity and reactor period. This relationship serves as an appropriate check for the data in Table 5.1. This relationship is better known as the inhour equation. The inhour equation is represented in terms of the dollar because of its particular adaptability to the reactivity region (difference between delayed and prompt critical is one dollar) of practical interest in fast systems. Figure 27 shows the inhour equation calculated using the parameters from this experiment, and measurements of period versus reactivity that have been made for Godiva. Keepin et al. (1956) performed measurements of period versus reactivity on the Godiva II assembly, which for this purpose was a geometrically clean assembly. This means that the assembly was not surrounded by equipment and electronics and could be lifted in free space. The parameters measured in this experiment compare well with Keepin's measurements. The agreement near prompt critical provides a sensitive check on the accuracy of short-period delayed neutron data. Figure 27 provides one more check of the accuracy and validity of data presented in Table 6.

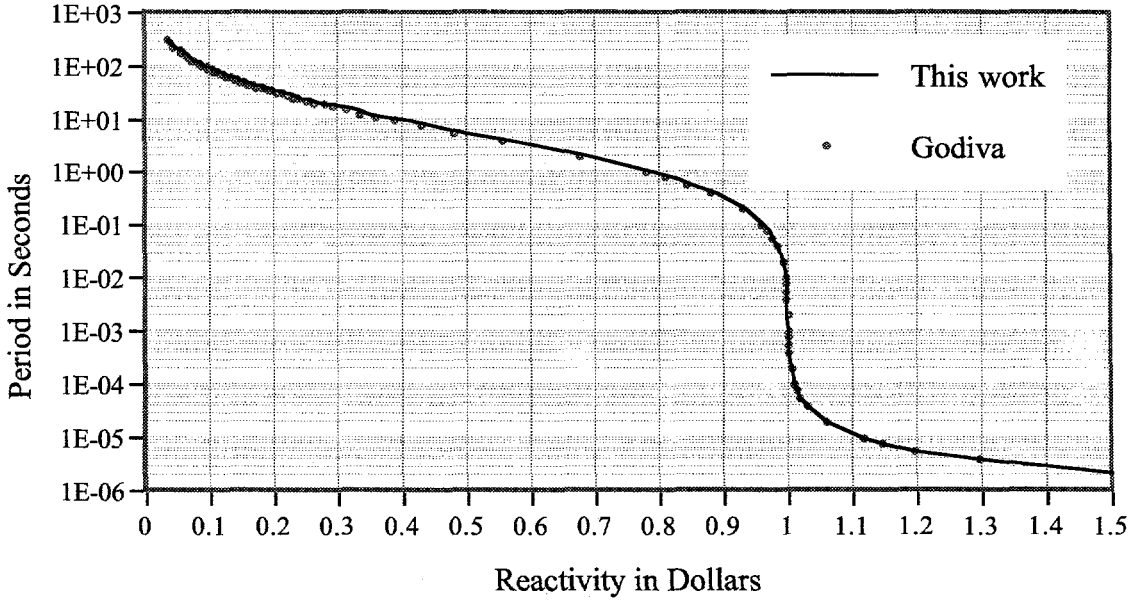

Figure 27. Inhour equation relationship for Godiva.

The period vs reactivity relationship used to plot Figure 27 is given by;

$$\rho(\$) = \frac{1}{\alpha \cdot T} + \sum_{i=1}^{6} \frac{a_i \frac{1}{\lambda_i}}{T + \frac{1}{\lambda_i}} \qquad (5.12)$$

where T is the reactor period in seconds; α is an experimentally measured value of 8.4×10^5 sec^{-1}; and a_i and λ_i are the abundance and decay constant, respectively, for the ith delayed neutron group. Equation (5.12) is valid because the reactor period is much greater than the prompt neutron lifetime.

The inhour equation results are also presented in tabular format in Table 8. The six-group representation from this experiment is compared to Keepin's parameters and to values from Brady and England to illustrate the differences. The time-dependent six-group representation of the delayed neutron emission from this experiment gives reactivities within 5% or less for periods smaller than 50 seconds when compared to the traditional Keepin values. The greatest difference is 6% for large periods. When this data is compared to Brady and England, values the greatest difference is 18% for long periods and about 11% near 0.4 $. Near prompt critical, the three sets of data agree relatively well. This is to be expected since prompt neutrons take over in this region, and delayed neutrons are not as important. Table 8 also demonstrates that the delayed neutron parameters from Brady and England tend to predict smaller reactivities in dollars for all periods compared to this experiment and Keepin's data. Other researchers have also noticed such a difference when using the delayed neutron parameters from Brady and England, which now are included in the ENDF/B-VI library (Hetrick, 1994 and Mihalczo et al., 1996). Mihalczo et al. showed that if the delayed neutron parameters from ENDF/B-VI are used to obtain reactivity from stable reactor periods measurements, then they would predict values 14% different from the traditional Keepin values. This means that what previously was called 0.4$ now will be 0.35$. So the entire reactivity scale will be different from what was conventional, and from calculations that agreed with measurements. Based on this experiment which confirms the

delayed neutron parameters measured by Keepin, there is little justification for abandoning the use of the time-honored Keepin data.

Table 8. Comparison of reactivity predictions from this experiment's parameters with recommended values for the Godiva assembly.

Period (sec)	Reactivity ($) using group constants from this experiment	Reactivity ($) using group constants from Brady's data.	Reactivity ($) using group constants from Keepin's data.	Relative* difference between this experiment and Brady's data.	Relative difference between this experiment and Keepin's data
300	0.04062	0.03327	0.03811	0.181	0.0618
200	0.05809	0.04771	0.05452	0.177	0.0614
100	0.1027	0.08497	0.09653	0.173	0.0601
50	0.1697	0.1422	0.16000	0.162	0.0571
20	0.2935	0.2522	0.2788	0.141	0.0501
10	0.4085	0.3602	0.3912	0.118	0.0424
1	0.7944	0.7633	0.7818	0.0391	0.0157
0.6	0.8529	0.8297	0.8430	0.0272	0.0116
0.2	0.9360	0.9254	0.9312	0.0113	0.00513
0.1	0.9645	0.9588	0.9619	0.00591	0.00260
0.06	0.9776	0.9741	0.9760	0.00358	0.00163
0.02	0.9919	0.9909	0.9916	0.001008	0.000301
0.01	0.9958	0.9955	0.9958	0.000301	0.000010

* Relative Error = (this experiment-Brady et al.)/this experiment

5.4 NEPTUNIUM-237 MEASUREMENTS

Neptunium is formed during irradiation of nuclear fuel. Of the higher-mass actinides produced, only the α particle emitting Np-237 has a long half-life (2 x 10^6 years). Np-237 is formed primarily from reactions of neutrons on uranium (either in fast neutron or thermal neutron fluxes) or as the daughter, by α decay, of Am-241.

$$^{238}U(n,2n)^{237}U \xrightarrow{\beta^-} {}^{237}Np \qquad \text{(fast neutron flux)}$$

$$^{235}U(n,\gamma)\,^{236}U(n,\gamma)\,^{237}U \xrightarrow{\beta^-} {}^{237}Np \qquad \text{(thermal neutron flux)}$$

$$^{241}Pu \xrightarrow[15\ years]{\beta^-} {}^{241}Am \xrightarrow[433\ years]{\alpha} {}^{237}Np$$

There are several reasons for the interest in Np-237. Those who evaluate the very long term risks associated with the disposal of radioactive wastes have been very concerned with Np-237. This concern is based on: (a) its presence in high-level waste from the nuclear fuel cycle, (b) its very long-half-life (2 x 10^6 years), (c) its purported relatively high gastrointestinal absorption factor, and (d) its critical mass.

Spent nuclear fuel is dominated by higher-mass actinides such as Np-237; the safe geological disposal of these isotopes, which have long lived decay chains, is difficult to prove. Neptunium-237 dominates the toxicity of highly active waste after 10,000 years. Alternatives have been proposed to dispose of these actinides. Under consideration is a neptunium burner (Seifritz, 1991). Neptunium could be separated during reprocessing and subsequently used as fuel in a sodium-cooled fast reactor that has a very hard neutron spectrum. Studies show that one reactor of this type could suffice to convert into fission products the neptunium produced by 125 light water reactors. To operate such a reactor, which would have large quantities of higher actinide isotopes in its core, a thorough knowledge and understanding of each actinide's delayed neutron parameters would be essential.

The amount of Np-237 produced depends on the type of reactor operated. Rees and Shipp, 1983 calculated the fission products and actinides for typical operating conditions of four reactor types: Magnox, AGR, LWR, and CDFR. The amounts of Np-237 produced for the generation of 1 GW(e)-year of electricity are shown in Table 9. For thermal reactors, the quantities shown refer to the time of reprocessing, which in this case is 5 years after removal of the fuel from the reactor.

Table 9. Amounts of Np-237 produced in various types of reactors.

Reactor	**Load factor (%)**	**Efficiency (%)**	**Amount of Np-237**	
			Bq	**Kg**
Magnox	80	25.4	2.9E+11	7.7
AGR	75	41	1.3E+11	5.1
LWR	74.5	32.2	2.1E+11	8.1
CDFR	72.2	38.8	9.7E+10	3.7

The analysis of the Np-237 delayed neutron parameters was performed in the same manner as for U-235. The Np-237 delayed neutron parameters in this experiment were computed from infinite and instantaneous irradiations. The data and error analyses reported in Table 10 for Np-237 follow the same strategy used for the U-235 calculation. The fast neutron-induced fission delayed neutron parameters for Np-237 results are presented in Table 10.

Table 10. Fast-fission delayed neutron data for Np-237.

Group	Decay Constant $(sec)^{-1}$	Relative Yield (a_i/a)	Absolute Yield, $(fissions)^{-1}$
1	0.0123 ± 0.0009	0.032 ± 0.003	0.000403
2	0.0284 ± 0.0005	0.238 ± 0.006	0.00299
3	0.0971 ± 0.007	0.175 ± 0.008	0.00221
4	0.296 ± 0.014	0.360 ± 0.017	0.00454
5	0.914 ± 0.058	0.150 ± 0.014	0.00189
6	3.2 ± 0.13	0.045 ± 0.006	0.000567
Absolute Yield (neutrons/fission)			
0.0126 ± 0.0007			

Table 10 shows the six-groups parameters for Np-237. Np-237 can be adequately represented by six-groups, since the dominant precursors for Np-237 are the same as U-235. The only difference is that these precursors are weighted differently in the mass yield curve due to the heavier mass of Np-237. However, they will decay with the same six dominant precursors. The absolute yield for Np-237 was calculated in the same manner as described for U-235. An Np-237 foil with identical isotopic composition was taped in the rabbit at the same position as the sample. A total of five foils were irradiated, which represented 15 instantaneous irradiations. The results measured in this experiment are compared to those recommend values from computational calculations (Brady and England, 1989), and to some recent experimental data (Saleh and Parish, 1997) in Table 11. Saleh and Parish reported the thermal neutron-induced fission of Np-237. However, their experiment was not able to measure a sixth group of delayed neutrons due to a long transfer time (440 msec). The reported efficiency and dead-time in this experiment were 1% and 9.27 μsec. There are some questions regarding thermally induced fission in ^{237}Np, since ^{237}Np is a threshold fissioner and the threshold is at 600 keV. Figure 28 shows the fission cross section for ^{237}Np (BNL, 1978). In the thermal range, the fission cross section is in the milli-barns range. From this figure, one can infer that ^{237}Np cannot go critical with thermal neutrons.

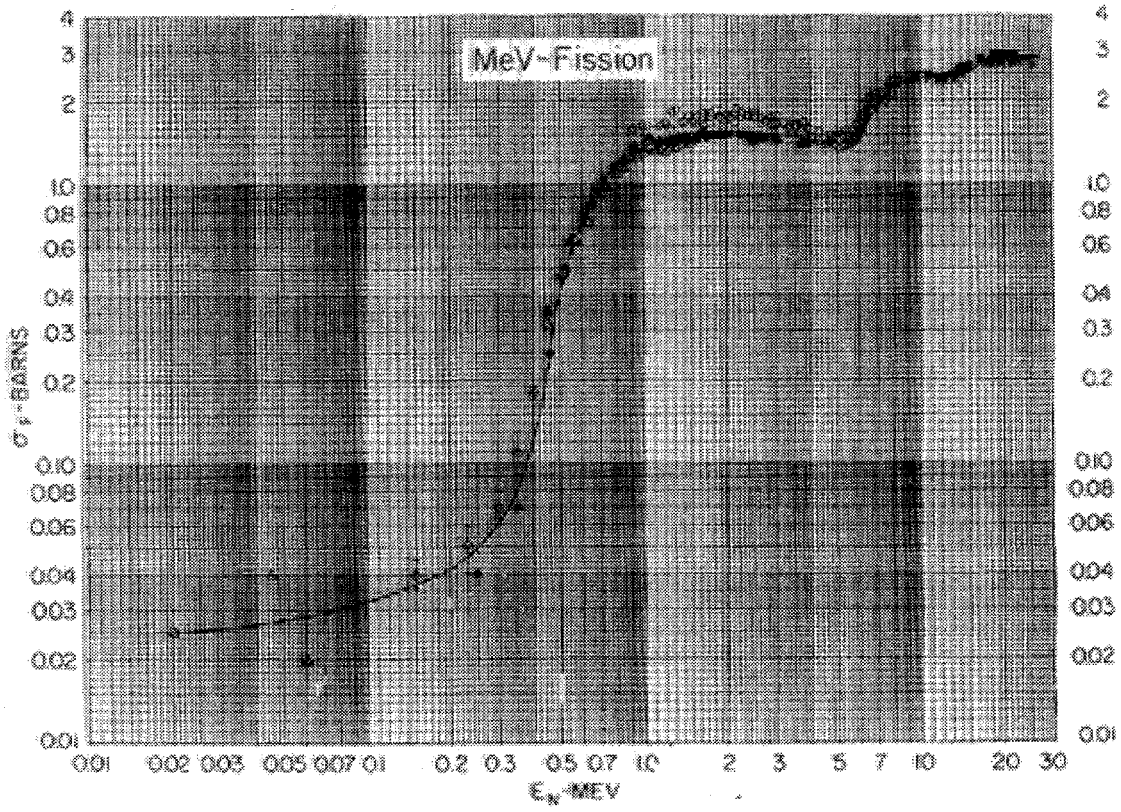

Figure 28. Fission cross sections for ^{237}Np.

Figure 29 was obtained to show the fission cross sections for Np-237 at thermal energies (this plot was obtained from the Theoretical-2 Division homepage at Los Alamos National Laboratory).

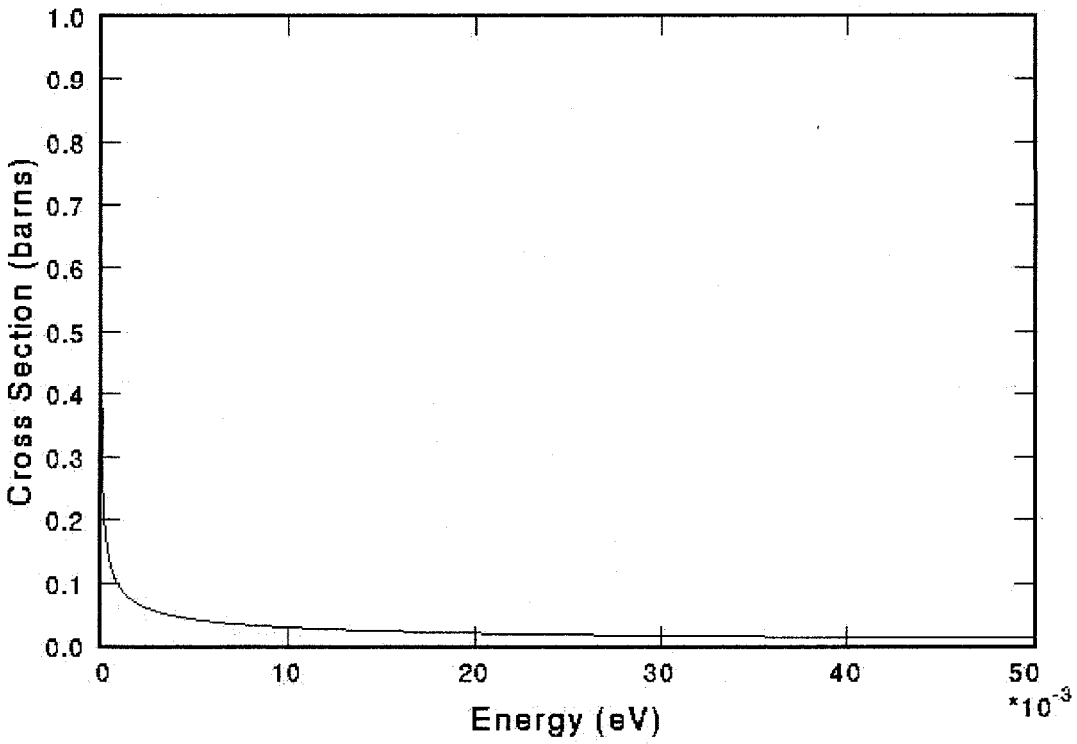

Figure 29. Thermal fission cross sections for Np-237.

As Figure 29 shows, the fission cross section at 0.0253 eV is too small to cause fission. The highest fission cross section in Figure 29 is 0.9 barns at 1E-5 eV, and then decreases rapidly to milli-barns by 0.01 eV. From this figure it can be inferred that the fissions caused in the Saleh experiment were induced by fast neutrons from the TRIGGA reactor.

Table 11. Comparison of Fast-fission delayed neutron data for ^{237}Np.

Group	Relative Yield, a_i/a			Decay Constant, λ_i (sec^{-1})		
	This Work	Saleh et al.	Brady et al.	This Work	Saleh et al.	Brady et al.
1	0.032±3E-3	0.040±0.002	0.0400	0.0123±9E-4	0.0129±6E-4	0.0133
2	0.238±6E-3	0.233±0.017	0.2162	0.0284±5E-4	0.0324±1E-3	0.0316
3	0.175±8E-3	0.19±0.01	0.1558	0.097±7E-3	0.105±0.002	0.1168
4	0.360±0.017	0.322±0.027	0.3633	0.296±0.014	0.341±0.013	0.3006
5	0.150±0.014	0.193±0.007	0.1659	0.91±0.058	0.85±0.06	0.8667
6	0.045±6E-3	0.021±0.004*	0.0589	3.2±0.13	---	2.7600

Absolute Yield, n/f		
This Work	Saleh et al.	Brady et al.
0.0126 ± 0.0007	0.0129 ± 0.0004	0.0114 ± 0.0012

*Calculated value

The delayed neutron parameters presented in Table 11 compare relatively well. The values in Table 11 are compared graphically to better observe the differences. Figure 30 shows a graphical representation for the relative yield.

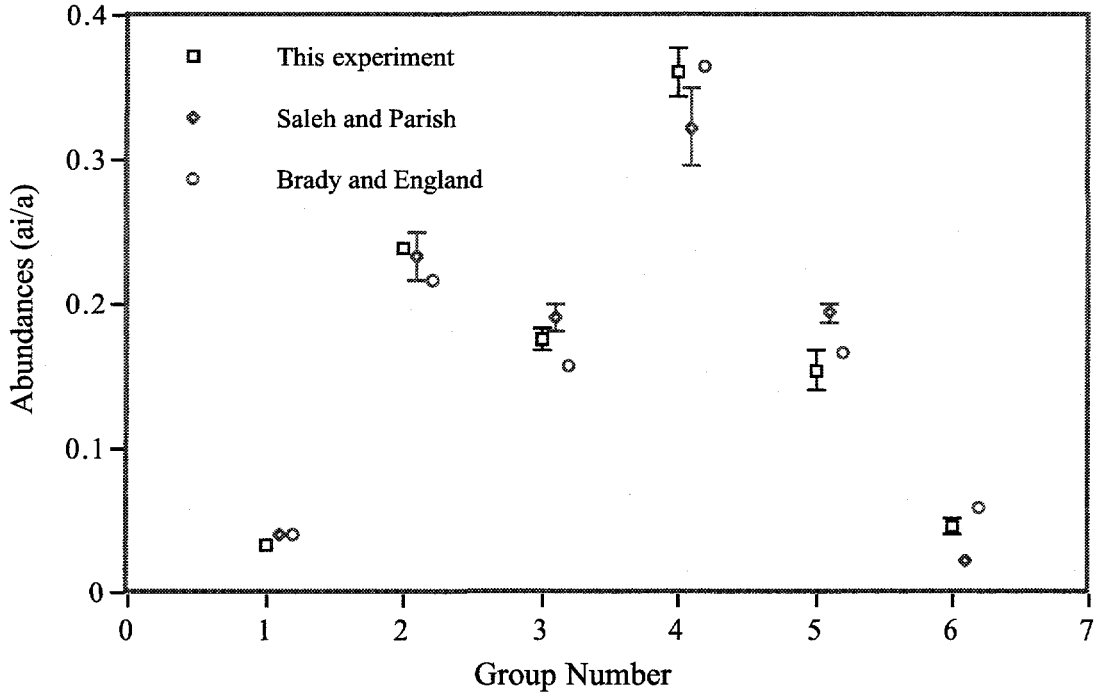

Figure 30. Graphical comparison of group abundances for Np-237.

Figure 30 illustrates the small differences in the relative yields with the reported error bars. The Brady and England values do not have error bars, as their values are based on computational methodologies. Figure 30 shows considerable differences for groups 5 and 6 in the reported values. The relative yield for group 6 in this experiment was measured while the relative yield in the other two references is calculated. It can be seen that the experimental value lies between the two calculated values.

Figure 31 shows the comparison of the group decay constants. The decay constants for groups 1 through 5 agree very well. This supports the notion that six 'main' periods groups exist, each consisting of a single main precursor or a combination of contributors with similar periods. The value for group six in this experiment is larger than the one predicted by Brady and England. Saleh and Parish were unable to measure the decay constant for group six as their travel time was too long.

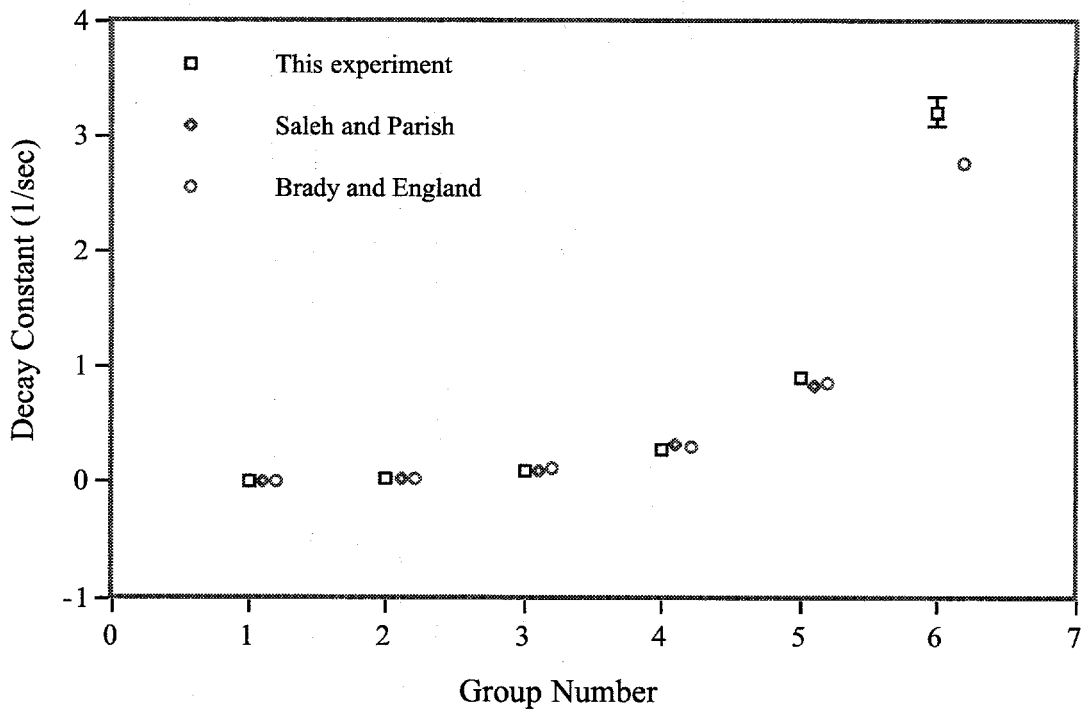

Figure 31. Graphical comparison of group decay constants for Np-237.

6. CONCLUSION

The primary emphasis in this dissertation was the experimental measurement of the delayed neutron parameters for Np-237. The delayed neutron parameters for U-235 were re-measured for two purposes. First, it was necessary to benchmark the experiment to validate the methodology used for Np-237. Second, work performed by Brady and England using computational methodologies raised some questions regarding Keepin and Wimett's delayed neutron parameters for U-235.

The measured values reported for the U-235 decay constants and abundances are in substantial agreement with the well-established Keepin data reported nearly 40 years ago. The absolute yield value measured for U-235 by this experiment is 0.0163 ± 0.0009 neutrons/fission. This value compares very well with the Keepin absolute yield of 0.0165 ± 0.0005. Some differences exist between the values from this experiment and values from Brady and England's work which are now included in the ENDF/B-VI library. The period reactivity relation arising from the yield was calculated using the parameters measured in this experiment and the six group parameters of Keepin and Wimett. It is believed that the present experiment confirms and validates the data measured by Keepin and Wimett. Based on the results obtained, there is little justification for abandoning the use of the time-honored Keepin data.

The measured group constants and yields for Np-237 are compared to recent experimental work by Saleh and Parish. Saleh and Parish were only able to measure five groups, but the parameters obtained for these groups compare well. As a result of these new data, Saleh and Parish conceded that their results are for the fast neutron induced fission, and not from the thermal neutron induced fission as they had previously reported. The values from this experiment are also compared to those obtained by the computational methodology of Brady and England. The Np-237 absolute yield value measured in this experiment is 0.0126 ± 0.0007, Brady and England computed a value of 0.0114 ± 0.0012, and Saleh and Parish reported a value of 0.0129 ± 0.0004.

The experimental uncertainties obtained in the measurement of the delayed neutron parameters are small. This is attributed to the high detector efficiency, sample size, and newly developed data acquisition system. The reported errors in the group parameters and the total yield values are mainly statistical. The good agreement between Keepin's data for U-235 and this experiment gives credibility for the analysis of the data and the experimental procedure.

In conclusion, the measured data for U-235 and Np-237 have been presented and compared to recent evaluations. In most cases the sets of experimental data compare well to each other. There are some differences when compared to computational methodologies. This experiment was able to measure the six-group delayed neutron parameters for Np-237, and for most parameters the standard deviations reported are smaller than recently published data. Therefore, it is recommended that the parameters from this experiment for Np-237 be included in new evaluations of the ENDF/B library. It is also recommend that Keepin's delayed neutron parameters for U-235 be reinstated in new versions of the ENDF/B library. There is no evidence for abandoning the use of the time-honored Keepin and Wimett data.

APPENDIX A

DELAYED NEUTRON PRECURSORS

Delayed neutrons have traditionally been divided into six groups since the early measurements performed by Keepin in 1965. A total of 271 delayed neutron precursors have been identified to date based on measurements and ($Q_\beta > B(n)$). The identified delayed neutron precursors, their half lives, and the temporal group in which the nuclide probably belongs are presented (England and Rider, 1994).

Nuclide	**Half-life (seconds)**	**Group Number**
Br-87	55.7	1
Rb-91	58.2	1
Br-88	16	2
Sb-134	10.2	2
Te-136	19	2
I-137	24.5	2
Cs-141	24.9	2
La-146	11	2
Cu-72	6.48	3
Cu-73	5.11	3
As-84	5.30	3
Se-87	5.60	3
Br-89	4.38	3
Rb-92	4.53	3
Rb-93	5.86	3
Y-97	3.70	3
Nb-104	4.80	3
Ru-114	8.14	3
Rh-115	8.32	3
Pd-120	3.91	3
In-127	3.76	3
Te-137	3.50	3
I-138	6.50	3

La-147	5.00	3
Ba-148	3.33	3
Pm-159	3.00	3
Ni-74	0.90	4
Cu-75	0.93	4
Zn-78	1.99	4
Ga-79	2.99	4
Ga-80	1.66	4
Ga-81	1.33	4
Ge-83	1.90	4
Ge-84	1.20	4
As-85	2.03	4
As-86	0.90	4
Se-88	1.50	4
Br-90	1.80	4
Kr-93	1.29	4
Rb-94	2.76	4
Sr-96	1.10	4
Y-97	1.11	4
Y-98	2.00	4
Y-99	1.40	4
Y-102	0.90	4
Zr-103	1.34	4
Nb-103	1.50	4
Zr-104	2.57	4
Nb-105	2.80	4
Zr-106	0.91	4
Nb-106	1.00	4
Mo-108	1.50	4
Mo-109	1.41	4
Tc-109	1.40	4
Mo-110	2.77	4
Tc-110	0.83	4
Tc-111	1.98	4
Mo-112	0.98	4
Ru-113	3.00	4

Rh-114	1.70	4
Ru-115	0.88	4
Ru-116	1.70	4
Rh-116	0.95	4
Rh-117	1.12	4
Pd-119	1.76	4
Ag-119	2.10	4
Ag-120	1.17	4
Pd-122	1.41	4
Ag-122	1.50	4
In-127	1.30	4
Cd-128	1.05	4
In-128	0.84	4
In-129	0.99	4
In-129m	2.50	4
Sn-133	1.47	4
Sn-134	1.04	4
Sb-135	1.82	4
Sb-136	0.82	4
Te-138	1.60	4
Te-140	0.80	4
I-140	0.86	4
Xe-141	1.72	4
Xe-142	1.22	4
Cs-142	1.69	4
Xe-143	0.96	4
Cs-143	1.78	4
Xe-144	1.10	4
Cs-144	1.00	4
Xe-145	0.90	4
Ba-146	2.00	4
Ba-147	1.76	4
La-148	1.30	4
La-149	2.41	4
Ba-150	0.96	4
Ce-153	1.47	4

Ce-154	2.02	4
Pr-154	1.06	4
Pr-155	1.12	4
Nd-158	2.69	4
Sn-164	1.39	4
Eu-164	1.53	4
Eu-165	1.35	4
Ni-73	0.49	5
Cu-74	0.65	5
Ni-76	0.330	5
Cu-77	0.31	5
Zn-79	0.31	5
Ga-82	0.60	5
Ga-83	0.31	5
Se-89	0.43	5
Se-90	0.56	5
Br-91	0.60	5
Br-92	0.36	5
Kr-92	0.36	5
Kr-95	0.78	5
Rb-95	0.38	5
Sr-97	0.40	5
Sr-98	0.65	5
Y-98	0.65	5
Sr-99	0.60	5
Sr-100	0.62	5
Y-100	0.80	5
Y-101	0.61	5
Zr-105	0.49	5
Nb-107	0.77	5
Zr-108	0.38	5
Nb-109	0.32	5
Mo-111	0.47	5
Tc-112	0.43	5
Tc-113	0.65	5
Ru-117	0.34	5

Ru-118	0.66	5
Rh-118	0.32	5
Rh-119	0.47	5
Ru-120	0.35	5
Pd-121	0.64	5
Ag-121	0.80	5
Pd-123	0.30	5
Ag-123	0.39	5
Pd-124	0.51	5
Ag-125	0.33	5
Cd-127	0.57	5
Cd-130	0.48	5
I-130	0.58	5
I-130m	0.51	5
Sn-135	0.42	5
Sn-136	0.72	5
Sb-137	0.48	5
Te-139	0.58	5
I-141	0.46	5
Te-142	0.59	5
I-143	0.40	5
Cs-145	0.59	5
Xe-146	0.56	5
Cs-146	0.34	5
Cs-147	0.55	5
Ba-149	0.70	5
La-150	0.61	5
Ba-151	0.33	5
La-151	0.72	5
Ba-152	0.42	5
La-153	0.33	5
Ce-155	0.53	5
Ce-156	0.60	5
Pr-156	0.38	5
Pr-157	0.38	5
Nd-159	0.61	5

Nd-160	0.79	5
Pm-160	0.73	5
Nd-161	0.31	5
Pm-161	0.79	5
Pm-162	0.32	5
Sm-165	0.45	5
Co-72	0.12	6
Co-73	0.13	6
Co-74	0.09	6
Co-75	0.08	6
Ni-75	0.23	6
Cu-76	0.26	6
Ni-77	0.10	6
Ni-78	0.13	6
Cu-78	0.12	6
Cu-79	0.13	6
Cu-80	0.09	6
Zn-80	0.49	6
Cu-81	0.07	6
Zn-81	0.12	6
Zn-82	0.13	6
Zn-83	0.08	6
Ga-84	0.10	6
Ga-85	0.09	6
Ge-85	0.25	6
Ge-86	0.25	6
Ge-87	0.13	6
As-87	0.30	6
Ge-88	0.13	6
As-88	0.13	6
As-89	0.12	6
As-90	0.09	6
Se-91	0.27	6
Se-92	0.17	6
Se-93	0.10	6
Br-93	0.18	6

Br-94	0.11	6
Kr-94	0.21	6
Br-95	0.11	6
Br-96	0.09	6
Kr-96	0.29	6
Rb-96	0.20	6
Kr-97	0.10	6
Rb-97	0.17	6
Kr-98	0.16	6
Rb-98	0.11	6
Rb-99	0.14	6
Rb-100	0.10	6
Rb-101	0.09	6
Sr-101	0.19	6
Sr-102	0.28	6
Y-103	0.26	6
Sr-104	0.16	6
Y-104	0.13	6
Y-105	0.15	6
Y-106	0.09	6
Y-107	0.09	6
Zr-107	0.24	6
Nb-108	0.24	6
Zr-109	0.13	6
Nb-110	0.13	6
Nb-111	0.17	6
Mo-113	0.23	6
Tc-114	0.20	6
Tc-115	0.27	6
Tc-116	0.11	6
Tc-117	0.15	6
Ru-119	0.19	6
Rh-120	0.17	6
Rh-121	0.25	6
Rh-122	0.11	6
Rh-123	0.13	6

Ag-124	0.25	6
Pd-125	0.17	6
Pd-126	0.25	6
Ag-126	0.14	6
Ag-127	0.17	6
Ag-128	0.09	6
Cd-129	0.29	6
Cd-131	0.11	6
In-131	0.28	6
In-131m	0.11	6
Cd-132	0.13	6
In-132	0.12	6
In-133	0.11	6
In-134	0.08	6
Sb-138	0.17	6
Sb-139	0.22	6
Te-141	0.27	6
I-142	0.20	6
I-144	0.15	6
I-145	0.19	6
Xe-147	0.20	6
Cs-148	0.20	6
Cs-149	0.24	6
Cs-150	0.12	6
La-152	0.28	6
La-154	0.15	6
La-155	0.15	6
Ce-157	0.21	6
Pr-158	0.17	6
Pr-159	0.18	6

APPENDIX B.

SAMPLE LIST FILES

This appendix shows sample list files, one for a burst and one for an infinite irradiation. The first section shows the list file for a burst irradiation. The first column is the bin number, second column is the content of the bin, third column shows the width of the bin, the fourth column shows the time after irradiation, and the fifth column shows the count rate for the irradiation.

Bin #	Content (cts)	Bin Size (sec)	Time (sec)	Count Rate
0	0	0.02	0.01	0
1	0	0.02	0.03	0
2	0	0.02	0.05	0
3	0	0.02	0.07	0
4	0	0.02	0.09	0
5	0	0.02	0.11	0
6	995	0.02	0.13	49780
7	993	0.02	0.15	49601
8	970	0.02	0.17	49567
9	981	0.02	0.19	49050
10	979	0.02	0.21	48950
11	990	0.02	0.23	49500
12	909	0.02	0.25	45450
13	876	0.02	0.27	43800
14	880	0.02	0.29	44000
15	919	0.02	0.31	45950
16	834	0.02	0.33	41700
17	831	0.02	0.35	41550
18	850	0.02	0.37	42500
19	843	0.02	0.39	42150
20	774	0.02	0.41	38700
21	803	0.02	0.43	40150
22	765	0.02	0.45	38250

23	750	0.02	0.47	37500
24	765	0.02	0.49	38250
25	752	0.02	0.51	37600
26	740	0.02	0.53	37000
27	731	0.02	0.55	36550
28	699	0.02	0.57	34950
29	689	0.02	0.59	34450
30	686	0.02	0.61	34300
31	693	0.02	0.63	34650
32	670	0.02	0.65	33500
33	673	0.02	0.67	33650
34	683	0.02	0.69	34150
35	619	0.02	0.71	30950
36	615	0.02	0.73	30750
37	603	0.02	0.75	30150
38	604	0.02	0.77	30200
39	628	0.02	0.79	31400
40	590	0.02	0.81	29500
41	573	0.02	0.83	28650
42	594	0.02	0.85	29700
43	560	0.02	0.87	28000
44	552	0.02	0.89	27600
45	556	0.02	0.91	27800
46	503	0.02	0.93	25150
47	548	0.02	0.95	27400
48	557	0.02	0.97	27850
49	548	0.02	0.99	27400
50	1039	0.04	1.02	25975
51	1011	0.04	1.06	25275
52	953	0.04	1.1	23825
53	938	0.04	1.14	23450
54	931	0.04	1.18	23275
55	975	0.04	1.22	24375
56	1006	0.04	1.26	25150
57	903	0.04	1.3	22575
58	926	0.04	1.34	23150

59	873	0.04	1.38	21825
60	902	0.04	1.42	22550
61	851	0.04	1.46	21275
62	885	0.04	1.5	22125
63	879	0.04	1.54	21975
64	840	0.04	1.58	21000
65	819	0.04	1.62	20475
66	805	0.04	1.66	20125
67	821	0.04	1.7	20525
68	772	0.04	1.74	19300
69	728	0.04	1.78	18200
70	718	0.04	1.82	17950
71	723	0.04	1.86	18075
72	708	0.04	1.9	17700
73	689	0.04	1.94	17225
74	667	0.04	1.98	16675
75	692	0.04	2.02	17300
76	664	0.04	2.06	16600
77	671	0.04	2.1	16775
78	683	0.04	2.14	17075
79	679	0.04	2.18	16975
80	654	0.04	2.22	16350
81	650	0.04	2.26	16250
82	616	0.04	2.3	15400
83	590	0.04	2.34	14750
84	616	0.04	2.38	15400
85	612	0.04	2.42	15300
86	579	0.04	2.46	14475
87	574	0.04	2.5	14350
88	577	0.04	2.54	14425
89	581	0.04	2.58	14525
90	559	0.04	2.62	13975
91	530	0.04	2.66	13250
92	540	0.04	2.7	13500
93	549	0.04	2.74	13725
94	489	0.04	2.78	12225

95	493	0.04	2.82	12325
96	562	0.04	2.86	14050
97	540	0.04	2.9	13500
98	519	0.04	2.94	12975
99	520	0.04	2.98	13000
100	1013	0.08	3.04	12662.5
101	963	0.08	3.12	12037.5
102	930	0.08	3.2	11625
103	975	0.08	3.28	12187.5
104	891	0.08	3.36	11137.5
105	851	0.08	3.44	10637.5
106	829	0.08	3.52	10362.5
107	878	0.08	3.6	10975
108	827	0.08	3.68	10337.5
109	817	0.08	3.76	10212.5
110	813	0.08	3.84	10162.5
111	799	0.08	3.92	9987.5
112	734	0.08	4	9175
113	767	0.08	4.08	9587.5
114	764	0.08	4.16	9550
115	728	0.08	4.24	9100
116	741	0.08	4.32	9262.5
117	692	0.08	4.4	8650
118	670	0.08	4.48	8375
119	686	0.08	4.56	8575
120	650	0.08	4.64	8125
121	664	0.08	4.72	8300
122	617	0.08	4.8	7712.5
123	618	0.08	4.88	7725
124	617	0.08	4.96	7712.5
125	637	0.08	5.04	7962.5
126	611	0.08	5.12	7637.5
127	626	0.08	5.2	7825
128	593	0.08	5.28	7412.5
129	568	0.08	5.36	7100
130	582	0.08	5.44	7275

131	498	0.08	5.52	6225
132	517	0.08	5.6	6462.5
133	550	0.08	5.68	6875
134	511	0.08	5.76	6387.5
135	527	0.08	5.84	6587.5
136	487	0.08	5.92	6087.5
137	502	0.08	6	6275
138	491	0.08	6.08	6137.5
139	475	0.08	6.16	5937.5
140	469	0.08	6.24	5862.5
141	457	0.08	6.32	5712.5
142	453	0.08	6.4	5662.5
143	470	0.08	6.48	5875
144	442	0.08	6.56	5525
145	453	0.08	6.64	5662.5
146	425	0.08	6.72	5312.5
147	456	0.08	6.8	5700
148	454	0.08	6.88	5675
149	395	0.08	6.96	4937.5
150	792	0.16	7.08	4950
151	801	0.16	7.24	5006.25
152	750	0.16	7.4	4687.5
153	736	0.16	7.56	4600
154	734	0.16	7.72	4587.5
155	687	0.16	7.88	4293.75
156	686	0.16	8.04	4287.5
157	690	0.16	8.2	4312.5
158	636	0.16	8.36	3975
159	653	0.16	8.52	4081.25
160	632	0.16	8.68	3950
161	606	0.16	8.84	3787.5
162	580	0.16	9	3625
163	545	0.16	9.16	3406.25
164	561	0.16	9.32	3506.25
165	484	0.16	9.48	3025
166	499	0.16	9.64	3118.75

167	486	0.16	9.8	3037.5
168	522	0.16	9.96	3262.5
169	456	0.16	10.12	2850
170	453	0.16	10.28	2831.25
171	441	0.16	10.44	2756.25
172	439	0.16	10.6	2743.75
173	447	0.16	10.76	2793.75
174	444	0.16	10.92	2775
175	404	0.16	11.08	2525
176	410	0.16	11.24	2562.5
177	393	0.16	11.4	2456.25
178	408	0.16	11.56	2550
179	422	0.16	11.72	2637.5
180	375	0.16	11.88	2343.75
181	387	0.16	12.04	2418.75
182	401	0.16	12.2	2506.25
183	386	0.16	12.36	2412.5
184	381	0.16	12.52	2381.25
185	346	0.16	12.68	2162.5
186	340	0.16	12.84	2125
187	347	0.16	13	2168.75
188	339	0.16	13.16	2118.75
189	334	0.16	13.32	2087.5
190	294	0.16	13.48	1837.5
191	302	0.16	13.64	1887.5
192	278	0.16	13.8	1737.5
193	302	0.16	13.96	1887.5
194	292	0.16	14.12	1825
195	280	0.16	14.28	1750
196	279	0.16	14.44	1743.75
197	291	0.16	14.6	1818.75
198	252	0.16	14.76	1575
199	278	0.16	14.92	1737.5
200	529	0.32	15.16	1653.125
201	507	0.32	15.48	1584.375
202	525	0.32	15.8	1640.625

203	460	0.32	16.12	1437.5
204	468	0.32	16.44	1462.5
205	476	0.32	16.76	1487.5
206	413	0.32	17.08	1290.625
207	470	0.32	17.4	1468.75
208	425	0.32	17.72	1328.125
209	454	0.32	18.04	1418.75
210	397	0.32	18.36	1240.625
211	415	0.32	18.68	1296.875
212	386	0.32	19	1206.25
213	369	0.32	19.32	1153.125
214	357	0.32	19.64	1115.625
215	358	0.32	19.96	1118.75
216	336	0.32	20.28	1050
217	340	0.32	20.6	1062.5
218	299	0.32	20.92	934.375
219	320	0.32	21.24	1000
220	316	0.32	21.56	987.5
221	303	0.32	21.88	946.875
222	333	0.32	22.2	1040.625
223	297	0.32	22.52	928.125
224	267	0.32	22.84	834.375
225	308	0.32	23.16	962.5
226	265	0.32	23.48	828.125
227	304	0.32	23.8	950
228	284	0.32	24.12	887.5
229	251	0.32	24.44	784.375
230	288	0.32	24.76	900
231	261	0.32	25.08	815.625
232	260	0.32	25.4	812.5
233	235	0.32	25.72	734.375
234	257	0.32	26.04	803.125
235	251	0.32	26.36	784.375
236	245	0.32	26.68	765.625
237	237	0.32	27	740.625
238	235	0.32	27.32	734.375

239	229	0.32	27.64	715.625
240	236	0.32	27.96	737.5
241	252	0.32	28.28	787.5
242	221	0.32	28.6	690.625
243	228	0.32	28.92	712.5
244	227	0.32	29.24	709.375
245	210	0.32	29.56	656.25
246	209	0.32	29.88	653.125
247	189	0.32	30.2	590.625
248	224	0.32	30.52	700
249	196	0.32	30.84	612.5
250	389	0.64	31.32	607.8125
251	370	0.64	31.96	578.125
252	365	0.64	32.6	570.3125
253	370	0.64	33.24	578.125
254	354	0.64	33.88	553.125
255	341	0.64	34.52	532.8125
256	324	0.64	35.16	506.25
257	316	0.64	35.8	493.75
258	293	0.64	36.44	457.8125
259	323	0.64	37.08	504.6875
260	270	0.64	37.72	421.875
261	307	0.64	38.36	479.6875
262	292	0.64	39	456.25
263	258	0.64	39.64	403.125
264	269	0.64	40.28	420.3125
265	253	0.64	40.92	395.3125
266	267	0.64	41.56	417.1875
267	263	0.64	42.2	410.9375
268	233	0.64	42.84	364.0625
269	245	0.64	43.48	382.8125
270	245	0.64	44.12	382.8125
271	233	0.64	44.76	364.0625
272	226	0.64	45.4	353.125
273	222	0.64	46.04	346.875
274	227	0.64	46.68	354.6875

275	200	0.64	47.32	312.5
276	213	0.64	47.96	332.8125
277	207	0.64	48.6	323.4375
278	225	0.64	49.24	351.5625
279	191	0.64	49.88	298.4375
280	219	0.64	50.52	342.1875
281	194	0.64	51.16	303.125
282	189	0.64	51.8	295.3125
283	204	0.64	52.44	318.75
284	177	0.64	53.08	276.5625
285	180	0.64	53.72	281.25
286	171	0.64	54.36	267.1875
287	158	0.64	55	246.875
288	164	0.64	55.64	256.25
289	167	0.64	56.28	260.9375
290	173	0.64	56.92	270.3125
291	148	0.64	57.56	231.25
292	148	0.64	58.2	231.25
293	150	0.64	58.84	234.375
294	153	0.64	59.48	239.0625
295	145	0.64	60.12	226.5625
296	120	0.64	60.76	187.5
297	131	0.64	61.4	204.6875
298	149	0.64	62.04	232.8125
299	150	0.64	62.68	234.375
300	266	1.28	63.64	207.8125
301	248	1.28	64.92	193.75
302	248	1.28	66.2	193.75
303	218	1.28	67.48	170.3125
304	232	1.28	68.76	181.25
305	204	1.28	70.04	159.375
306	219	1.28	71.32	171.0938
307	186	1.28	72.6	145.3125
308	187	1.28	73.88	146.0938
309	182	1.28	75.16	142.1875
310	177	1.28	76.44	138.2813

311	160	1.28	77.72	125
312	145	1.28	79	113.2813
313	159	1.28	80.28	124.2188
314	137	1.28	81.56	107.0313
315	162	1.28	82.84	126.5625
316	136	1.28	84.12	106.25
317	138	1.28	85.4	107.8125
318	120	1.28	86.68	93.75
319	151	1.28	87.96	117.9688
320	121	1.28	89.24	94.5313
321	128	1.28	90.52	100
322	114	1.28	91.8	89.0625
323	127	1.28	93.08	99.2188
324	115	1.28	94.36	89.8438
325	106	1.28	95.64	82.8125
326	105	1.28	96.92	82.0313
327	93	1.28	98.2	72.6563
328	107	1.28	99.48	83.5938
329	89	1.28	100.76	69.5313
330	85	1.28	102.04	66.4063
331	87	1.28	103.32	67.9688
332	95	1.28	104.6	74.2188
333	93	1.28	105.88	72.6563
334	76	1.28	107.16	59.375
335	68	1.28	108.44	53.125
336	64	1.28	109.72	50
337	60	1.28	111	46.875
338	66	1.28	112.28	51.5625
339	60	1.28	113.56	46.875
340	74	1.28	114.84	57.8125
341	68	1.28	116.12	53.125
342	63	1.28	117.4	49.2188
343	56	1.28	118.68	43.75
344	53	1.28	119.96	41.4063
345	60	1.28	121.24	46.875
346	57	1.28	122.52	44.5313

347	48	1.28	123.8	37.5
348	55	1.28	125.08	42.9688
349	46	1.28	126.36	35.9375
350	96	2.56	128.28	37.5
351	85	2.56	130.84	33.2031
352	72	2.56	133.4	28.125
353	78	2.56	135.96	30.4688
354	67	2.56	138.52	26.1719
355	90	2.56	141.08	35.1563
356	57	2.56	143.64	22.2656
357	56	2.56	146.2	21.875
358	55	2.56	148.76	21.4844
359	72	2.56	151.32	28.125
360	52	2.56	153.88	20.3125
361	49	2.56	156.44	19.1406
362	54	2.56	159	21.0938
363	45	2.56	161.56	17.5781
364	50	2.56	164.12	19.5313
365	41	2.56	166.68	16.0156
366	47	2.56	169.24	18.3594
367	39	2.56	171.8	15.2344
368	37	2.56	174.36	14.4531
369	33	2.56	176.92	12.8906
370	32	2.56	179.48	12.5
371	34	2.56	182.04	13.2813
372	37	2.56	184.6	14.4531
373	23	2.56	187.16	8.9844
374	27	2.56	189.72	10.5469
375	20	2.56	192.28	7.8125
376	29	2.56	194.84	11.3281
377	23	2.56	197.4	8.9844
378	19	2.56	199.96	7.4219
379	19	2.56	202.52	7.4219
380	25	2.56	205.08	9.7656
381	30	2.56	207.64	11.7188
382	25	2.56	210.2	9.7656

383	28	2.56	212.76	10.9375
384	17	2.56	215.32	6.6406
385	20	2.56	217.88	7.8125
386	16	2.56	220.44	6.25
387	15	2.56	223	5.8594
388	10	2.56	225.56	3.9063
389	14	2.56	228.12	5.4688
390	19	2.56	230.68	7.4219
391	15	2.56	233.24	5.8594
392	16	2.56	235.8	6.25
393	17	2.56	238.36	6.6406
394	17	2.56	240.92	6.6406
395	15	2.56	243.48	5.8594
396	16	2.56	246.04	6.25
397	9	2.56	248.6	3.5156
398	9	2.56	251.16	3.5156
399	10	2.56	253.72	3.9063
400	22	5.12	257.56	4.2969
401	20	5.12	262.68	3.9063
402	20	5.12	267.8	3.9063
403	16	5.12	272.92	3.125
404	14	5.12	278.04	2.7344
405	15	5.12	283.16	2.9297
406	16	5.12	288.28	3.125
407	13	5.12	293.4	2.5391
408	9	5.12	298.52	1.7578
409	6	5.12	303.64	1.1719
410	19	5.12	308.76	3.7109
411	11	5.12	313.88	2.1484
412	10	5.12	319	1.9531
413	9	5.12	324.12	1.7578
414	22	5.12	329.24	4.2969
415	12	5.12	334.36	2.3438
416	8	5.12	339.48	1.5625
417	8	5.12	344.6	1.5625
418	15	5.12	349.72	2.9297

419	13	5.12	354.84	2.5391

This section shows a sample list file obtained from an infinite irradiation. The first column is the bin number, second column is the content of the bin, third column shows the width of the bin, the fourth column shows the time after irradiation, and the fifth column shows the count rate for the irradiation.

Bin #	Content (cts)	Bin Size (sec)	Time (sec)	Count Rate
0	0	0.02	0.01	0
1	0	0.02	0.03	0
2	0	0.02	0.05	0
3	0	0.02	0.07	0
4	0	0.02	0.09	0
5	0	0.02	0.11	0
6	1480	0.02	0.13	7400
7	1436	0.02	0.15	71800
8	1503	0.02	0.17	75150
9	1493	0.02	0.19	74650
10	1568	0.02	0.21	78400
11	1430	0.02	0.23	71500
12	1386	0.02	0.25	69300
13	1319	0.02	0.27	65950
14	1285	0.02	0.29	64250
15	1248	0.02	0.31	62400
16	1293	0.02	0.33	64650
17	1286	0.02	0.35	64300
18	1204	0.02	0.37	60200
19	1246	0.02	0.39	62300
20	1281	0.02	0.41	64050
21	1171	0.02	0.43	58550
22	1224	0.02	0.45	61200
23	1229	0.02	0.47	61450
24	1201	0.02	0.49	60050
25	1156	0.02	0.51	57800
26	1151	0.02	0.53	57550
27	1178	0.02	0.55	58900
28	1174	0.02	0.57	58700

29	1126	0.02	0.59	56300
30	1084	0.02	0.61	54200
31	1142	0.02	0.63	57100
32	1130	0.02	0.65	56500
33	1112	0.02	0.67	55600
34	1112	0.02	0.69	55600
35	1107	0.02	0.71	55350
36	1125	0.02	0.73	56250
37	1109	0.02	0.75	55450
38	1074	0.02	0.77	53700
39	1079	0.02	0.79	53950
40	1117	0.02	0.81	55850
41	1106	0.02	0.83	55300
42	1131	0.02	0.85	56550
43	1091	0.02	0.87	54550
44	1022	0.02	0.89	51100
45	1069	0.02	0.91	53450
46	1058	0.02	0.93	52900
47	994	0.02	0.95	49700
48	1018	0.02	0.97	50900
49	1036	0.02	0.99	51800
50	2075	0.04	1.02	51875
51	2071	0.04	1.06	51775
52	1952	0.04	1.1	48800
53	2027	0.04	1.14	50675
54	1918	0.04	1.18	47950
55	1968	0.04	1.22	49200
56	2028	0.04	1.26	50700
57	1894	0.04	1.3	47350
58	1950	0.04	1.34	48750
59	1923	0.04	1.38	48075
60	1905	0.04	1.42	47625
61	1874	0.04	1.46	46850
62	1855	0.04	1.5	46375
63	1835	0.04	1.54	45875
64	1881	0.04	1.58	47025

65	1839	0.04	1.62	45975
66	1849	0.04	1.66	46225
67	1829	0.04	1.7	45725
68	1814	0.04	1.74	45350
69	1770	0.04	1.78	44250
70	1766	0.04	1.82	44150
71	1713	0.04	1.86	42825
72	1776	0.04	1.9	44400
73	1811	0.04	1.94	45275
74	1781	0.04	1.98	44525
75	1693	0.04	2.02	42325
76	1761	0.04	2.06	44025
77	1721	0.04	2.1	43025
78	1663	0.04	2.14	41575
79	1621	0.04	2.18	40525
80	1736	0.04	2.22	43400
81	1679	0.04	2.26	41975
82	1604	0.04	2.3	40100
83	1608	0.04	2.34	40200
84	1655	0.04	2.38	41375
85	1606	0.04	2.42	40150
86	1620	0.04	2.46	40500
87	1653	0.04	2.5	41325
88	1582	0.04	2.54	39550
89	1584	0.04	2.58	39600
90	1623	0.04	2.62	40575
91	1612	0.04	2.66	40300
92	1551	0.04	2.7	38775
93	1462	0.04	2.74	36550
94	1482	0.04	2.78	37050
95	1504	0.04	2.82	37600
96	1560	0.04	2.86	39000
97	1395	0.04	2.9	34875
98	1513	0.04	2.94	37825
99	1420	0.04	2.98	35500
100	2980	0.08	3.04	37250

101	2897	0.08	3.12	36212.5
102	2909	0.08	3.2	36362.5
103	2967	0.08	3.28	37087.5
104	2785	0.08	3.36	34812.5
105	2806	0.08	3.44	35075
106	2762	0.08	3.52	34525
107	2756	0.08	3.6	34450
108	2743	0.08	3.68	34287.5
109	2762	0.08	3.76	34525
110	2722	0.08	3.84	34025
111	2664	0.08	3.92	33300
112	2601	0.08	4	32512.5
113	2608	0.08	4.08	32600
114	2463	0.08	4.16	30787.5
115	2551	0.08	4.24	31887.5
116	2494	0.08	4.32	31175
117	2510	0.08	4.4	31375
118	2400	0.08	4.48	30000
119	2452	0.08	4.56	30650
120	2510	0.08	4.64	31375
121	2390	0.08	4.72	29875
122	2310	0.08	4.8	28875
123	2430	0.08	4.88	30375
124	2383	0.08	4.96	29787.5
125	2288	0.08	5.04	28600
126	2258	0.08	5.12	28225
127	2300	0.08	5.2	28750
128	2229	0.08	5.28	27862.5
129	2188	0.08	5.36	27350
130	2260	0.08	5.44	28250
131	2143	0.08	5.52	26787.5
132	2194	0.08	5.6	27425
133	2169	0.08	5.68	27112.5
134	2138	0.08	5.76	26725
135	2157	0.08	5.84	26962.5
136	2098	0.08	5.92	26225

137	2023	0.08	6	25287.5
138	2073	0.08	6.08	25912.5
139	2099	0.08	6.16	26237.5
140	2143	0.08	6.24	26787.5
141	2040	0.08	6.32	25500
142	1981	0.08	6.4	24762.5
143	2072	0.08	6.48	25900
144	2031	0.08	6.56	25387.5
145	1998	0.08	6.64	24975
146	2016	0.08	6.72	25200
147	1969	0.08	6.8	24612.5
148	1964	0.08	6.88	24550
149	1980	0.08	6.96	24750
150	3928	0.16	7.08	24550
151	3696	0.16	7.24	23100
152	3621	0.16	7.4	22631.25
153	3683	0.16	7.56	23018.75
154	3581	0.16	7.72	22381.25
155	3617	0.16	7.88	22606.25
156	3533	0.16	8.04	22081.25
157	3422	0.16	8.2	21387.5
158	3468	0.16	8.36	21675
159	3447	0.16	8.52	21543.75
160	3347	0.16	8.68	20918.75
161	3351	0.16	8.84	20943.75
162	3362	0.16	9	21012.5
163	3286	0.16	9.16	20537.5
164	3278	0.16	9.32	20487.5
165	3244	0.16	9.48	20275
166	3078	0.16	9.64	19237.5
167	3105	0.16	9.8	19406.25
168	3009	0.16	9.96	18806.25
169	2973	0.16	10.12	18581.25
170	2980	0.16	10.28	18625
171	2976	0.16	10.44	18600
172	2916	0.16	10.6	18225

173	2918	0.16	10.76	18237.5
174	2844	0.16	10.92	17775
175	2902	0.16	11.08	18137.5
176	2889	0.16	11.24	18056.25
177	2727	0.16	11.4	17043.75
178	2749	0.16	11.56	17181.25
179	2762	0.16	11.72	17262.5
180	2751	0.16	11.88	17193.75
181	2578	0.16	12.04	16112.5
182	2631	0.16	12.2	16443.75
183	2589	0.16	12.36	16181.25
184	2624	0.16	12.52	16400
185	2577	0.16	12.68	16106.25
186	2581	0.16	12.84	16131.25
187	2663	0.16	13	16643.75
188	2543	0.16	13.16	15893.75
189	2529	0.16	13.32	15806.25
190	2540	0.16	13.48	15875
191	2434	0.16	13.64	15212.5
192	2465	0.16	13.8	15406.25
193	2431	0.16	13.96	15193.75
194	2396	0.16	14.12	14975
195	2359	0.16	14.28	14743.75
196	2349	0.16	14.44	14681.25
197	2369	0.16	14.6	14806.25
198	2265	0.16	14.76	14156.25
199	2344	0.16	14.92	14650
200	4575	0.32	15.16	14296.875
201	4558	0.32	15.48	14243.75
202	4521	0.32	15.8	14128.125
203	4473	0.32	16.12	13978.125
204	4369	0.32	16.44	13653.125
205	4334	0.32	16.76	13543.75
206	4227	0.32	17.08	13209.375
207	4143	0.32	17.4	12946.875
208	4105	0.32	17.72	12828.125

209	4051	0.32	18.04	12659.375
210	3986	0.32	18.36	12456.25
211	3910	0.32	18.68	12218.75
212	3938	0.32	19	12306.25
213	3718	0.32	19.32	11618.75
214	3783	0.32	19.64	11821.875
215	3907	0.32	19.96	12209.375
216	3745	0.32	20.28	11703.125
217	3636	0.32	20.6	11362.5
218	3579	0.32	20.92	11184.375
219	3526	0.32	21.24	11018.75
220	3643	0.32	21.56	11384.375
221	3432	0.32	21.88	10725
222	3433	0.32	22.2	10728.125
223	3388	0.32	22.52	10587.5
224	3336	0.32	22.84	10425
225	3379	0.32	23.16	10559.375
226	3317	0.32	23.48	10365.625
227	3234	0.32	23.8	10106.25
228	3101	0.32	24.12	9690.625
229	3180	0.32	24.44	9937.5
230	3166	0.32	24.76	9893.75
231	3110	0.32	25.08	9718.75
232	3071	0.32	25.4	9596.875
233	3072	0.32	25.72	9600
234	2968	0.32	26.04	9275
235	2868	0.32	26.36	8962.5
236	2856	0.32	26.68	8925
237	2874	0.32	27	8981.25
238	2897	0.32	27.32	9053.125
239	2794	0.32	27.64	8731.25
240	2723	0.32	27.96	8509.375
241	2894	0.32	28.28	9043.75
242	2814	0.32	28.6	8793.75
243	2724	0.32	28.92	8512.5
244	2591	0.32	29.24	8096.875

245	2756	0.32	29.56	8612.5
246	2665	0.32	29.88	8328.125
247	2666	0.32	30.2	8331.25
248	2563	0.32	30.52	8009.375
249	2521	0.32	30.84	7878.125
250	4909	0.64	31.32	7670.3125
251	4934	0.64	31.96	7709.375
252	4901	0.64	32.6	7657.8125
253	4837	0.64	33.24	7557.8125
254	4613	0.64	33.88	7207.8125
255	4566	0.64	34.52	7134.375
256	4596	0.64	35.16	7181.25
257	4414	0.64	35.8	6896.875
258	4358	0.64	36.44	6809.375
259	4189	0.64	37.08	6545.3125
260	4210	0.64	37.72	6578.125
261	4043	0.64	38.36	6317.1875
262	3960	0.64	39	6187.5
263	3978	0.64	39.64	6215.625
264	3922	0.64	40.28	6128.125
265	3816	0.64	40.92	5962.5
266	3761	0.64	41.56	5876.5625
267	3726	0.64	42.2	5821.875
268	3692	0.64	42.84	5768.75
269	3547	0.64	43.48	5542.1875
270	3451	0.64	44.12	5392.1875
271	3463	0.64	44.76	5410.9375
272	3380	0.64	45.4	5281.25
273	3307	0.64	46.04	5167.1875
274	3284	0.64	46.68	5131.25
275	3211	0.64	47.32	5017.1875
276	3101	0.64	47.96	4845.3125
277	3080	0.64	48.6	4812.5
278	2949	0.64	49.24	4607.8125
279	2972	0.64	49.88	4643.75
280	2984	0.64	50.52	4662.5

281	2813	0.64	51.16	4395.3125
282	2780	0.64	51.8	4343.75
283	2696	0.64	52.44	4212.5
284	2818	0.64	53.08	4403.125
285	2649	0.64	53.72	4139.0625
286	2654	0.64	54.36	4146.875
287	2569	0.64	55	4014.0625
288	2452	0.64	55.64	3831.25
289	2482	0.64	56.28	3878.125
290	2436	0.64	56.92	3806.25
291	2472	0.64	57.56	3862.5
292	2399	0.64	58.2	3748.4375
293	2329	0.64	58.84	3639.0625
294	2355	0.64	59.48	3679.6875
295	2276	0.64	60.12	3556.25
296	2210	0.64	60.76	3453.125
297	2221	0.64	61.4	3470.3125
298	2245	0.64	62.04	3507.8125
299	2105	0.64	62.68	3289.0625
300	4161	1.28	63.64	3250.7813
301	4080	1.28	64.92	3187.5
302	3870	1.28	66.2	3023.4375
303	3778	1.28	67.48	2951.5625
304	3657	1.28	68.76	2857.0313
305	3583	1.28	70.04	2799.2188
306	3430	1.28	71.32	2679.6875
307	3427	1.28	72.6	2677.3438
308	3164	1.28	73.88	2471.875
309	3210	1.28	75.16	2507.8125
310	3003	1.28	76.44	2346.0938
311	3037	1.28	77.72	2372.6563
312	2867	1.28	79	2239.8438
313	2802	1.28	80.28	2189.0625
314	2715	1.28	81.56	2121.0938
315	2614	1.28	82.84	2042.1875
316	2497	1.28	84.12	1950.7813

317	2399	1.28	85.4	1874.2188
318	2441	1.28	86.68	1907.0313
319	2372	1.28	87.96	1853.125
320	2300	1.28	89.24	1796.875
321	2256	1.28	90.52	1762.5
322	2124	1.28	91.8	1659.375
323	2021	1.28	93.08	1578.9063
324	1954	1.28	94.36	1526.5625
325	1998	1.28	95.64	1560.9375
326	1885	1.28	96.92	1472.6563
327	1786	1.28	98.2	1395.3125
328	1747	1.28	99.48	1364.8438
329	1741	1.28	100.76	1360.1563
330	1649	1.28	102.04	1288.2813
331	1659	1.28	103.32	1296.0938
332	1584	1.28	104.6	1237.5
333	1521	1.28	105.88	1188.2813
334	1510	1.28	107.16	1179.6875
335	1405	1.28	108.44	1097.6563
336	1408	1.28	109.72	1100
337	1394	1.28	111	1089.0625
338	1294	1.28	112.28	1010.9375
339	1268	1.28	113.56	990.625
340	1337	1.28	114.84	1044.5313
341	1294	1.28	116.12	1010.9375
342	1199	1.28	117.4	936.7188
343	1171	1.28	118.68	914.8438
344	1149	1.28	119.96	897.6563
345	1176	1.28	121.24	918.75
346	1123	1.28	122.52	877.3438
347	1082	1.28	123.8	845.3125
348	943	1.28	125.08	736.7188
349	1025	1.28	126.36	800.7813
350	2079	2.56	128.28	812.1094
351	1836	2.56	130.84	717.1875
352	1721	2.56	133.4	672.2656

353	1673	2.56	135.96	653.5156
354	1673	2.56	138.52	653.5156
355	1514	2.56	141.08	591.4063
356	1435	2.56	143.64	560.5469
357	1385	2.56	146.2	541.0156
358	1351	2.56	148.76	527.7344
359	1281	2.56	151.32	500.3906
360	1214	2.56	153.88	474.2188
361	1180	2.56	156.44	460.9375
362	1178	2.56	159	460.1563
363	1082	2.56	161.56	422.6563
364	1037	2.56	164.12	405.0781
365	972	2.56	166.68	379.6875
366	951	2.56	169.24	371.4844
367	910	2.56	171.8	355.4688
368	884	2.56	174.36	345.3125
369	892	2.56	176.92	348.4375
370	816	2.56	179.48	318.75
371	756	2.56	182.04	295.3125
372	729	2.56	184.6	284.7656
373	711	2.56	187.16	277.7344
374	711	2.56	189.72	277.7344
375	645	2.56	192.28	251.9531
376	630	2.56	194.84	246.0938
377	634	2.56	197.4	247.6563
378	586	2.56	199.96	228.9063
379	589	2.56	202.52	230.0781
380	565	2.56	205.08	220.7031
381	502	2.56	207.64	196.0938
382	452	2.56	210.2	176.5625
383	503	2.56	212.76	196.4844
384	479	2.56	215.32	187.1094
385	455	2.56	217.88	177.7344
386	450	2.56	220.44	175.7813
387	451	2.56	223	176.1719
388	365	2.56	225.56	142.5781

389	395	2.56	228.12	154.2969
390	369	2.56	230.68	144.1406
391	353	2.56	233.24	137.8906
392	355	2.56	235.8	138.6719
393	368	2.56	238.36	143.75
394	320	2.56	240.92	125
395	285	2.56	243.48	111.3281
396	282	2.56	246.04	110.1563
397	307	2.56	248.6	119.9219
398	283	2.56	251.16	110.5469
399	263	2.56	253.72	102.7344
400	518	5.12	257.56	101.1719
401	460	5.12	262.68	89.8438
402	468	5.12	267.8	91.4063
403	404	5.12	272.92	78.9063
404	388	5.12	278.04	75.7813
405	340	5.12	283.16	66.4063
406	350	5.12	288.28	68.3594
407	323	5.12	293.4	63.0859
408	292	5.12	298.52	57.0313
409	265	5.12	303.64	51.7578
410	277	5.12	308.76	54.1016
411	259	5.12	313.88	50.5859
412	223	5.12	319	43.5547
413	197	5.12	324.12	38.4766
414	203	5.12	329.24	39.6484
415	198	5.12	334.36	38.6719
416	161	5.12	339.48	31.4453
417	181	5.12	344.6	35.3516
418	149	5.12	349.72	29.1016
419	169	5.12	354.84	33.0078

APPENDIX C

TESTING AND SIMULATION OF DELAYED NEUTRON DATA

Appendix C documents the method used to analyze the delayed neutron data, and the testing of the nonlinear least squares Levenberg-Marquardt method. As mentioned in Chapter 5 the method and program for the analysis was tested for accuracy and reliability using a set of simulated data. Keepin's original delayed neutron parameters were used to simulate the delayed neutron decay. Statistical noise was introduced into the data to simulate a 'real' irradiation. The simulations and the calculations were performed using Mathcad 6+. A description of the input file and the theory is provided in this appendix as it appears in the input file.

First, the delayed neutron parameters for the fast fission of U-235 are introduced in vector form. These parameters are used to calculate the smooth (no statistical noise) delayed neutron decay.

$$u = (0.038, 0.0127, 0.213, 0.0317, 0.188, 0.115, 0.407, 0.311, 0.128, 1.4, 0.026, 3.87)^T$$

The vector **u** defines the abundances and decay constants in the following format: a_1, λ_1, a_2, λ_2, and so on.

An array called time, t, is created to set the time bins for the data. The first 25 bins in t have a width of 100 msec. The binwidth is doubled every 25 bins. The time mark in each bin is at the mid-point of the bin. Thus,

del = 0.1 sp = 25 k = 0..7sp-1 kk = 0..sp-1

$$t_{kk} = (kk + 0.5)\,del$$

$$t_{kk+sp} = sp \cdot del + (kk + 0.5) \cdot 2 \cdot del$$

$$t_{kk+2 \cdot sp} = 3 \cdot sp \cdot del + (kk + 0.5) \cdot 4 \cdot del$$

$$t_{kk+3 \cdot sp} = 7 \cdot sp \cdot del + (kk + 0.5) \cdot 8 \cdot del$$

$$t_{kk+4 \cdot sp} = 15 \cdot sp \cdot del + (kk + 0.5) \cdot 16 \cdot del$$

$$t_{kk+5 \cdot sp} = 31 \cdot sp \cdot del + (kk + 0.5) \cdot 32 \cdot del$$

$$t_{kk+2 \cdot sp} = 63 \cdot sp \cdot del + (kk + 0.5) \cdot 64 \cdot del$$

where t is the time array given at each stage of the change in binwidth, k is the total number of data points, kk is index of group of 25 times, and sp is the index at which the bin size is doubled.

The equations to calculate the smooth function for the simulated infinite and instantaneous irradiations are defined as:

$$sat0(t) = RA \cdot \left(\sum_{i=0}^{5} u_{2 \cdot i} \exp\left(-u_{2 \cdot i+1} \cdot t\right) \right) \cdot del \qquad \text{(c.1)}$$

RA is the size of the irradiation during a delayed critical operation. The instantaneous (burst) irradiation is defined as:

$$bur0(t) = B \cdot \left(\sum_{i=0}^{5} u_{2 \cdot i} \cdot u_{2 \cdot i+1} \exp\left(-u_{2 \cdot i+1} \cdot t\right) \right) \cdot del \qquad \text{(c.2)}$$

B is the size of the burst.

Equations (c.1) and (c.2) are a function of, t, the time bin interval.

$$sat1_k = sat0(t_k) \qquad bur1_k = bur0(t_k) \qquad \text{(c.3)}$$

The random number generator function in Mathcad is used to simulate statistical noise in the data. The number generator function samples a Gaussian distribution.

$$R = rnorm(14 \cdot sp, 0, 1) \qquad \text{(c.4)}$$

The random numbers generated in equation (c.4) are used as statistical noise in equations (c.1) and (c.2). Equation (c.1) now becomes:

a = 0..6 b = 0..sp-1

$$sat2_{25\cdot a+b} = sat1_{25\cdot a+b}\cdot\left[1+\frac{R_{25\cdot a+b}}{\sqrt{2^a\cdot sat1_{25\cdot a+b}}}\right] \qquad (c.5)$$

Applying the same process to the infinite delayed neutron decay.

$$bur2_{25\cdot a+b} = bur1_{25\cdot a+b}\cdot\left[1+\frac{R_{25\cdot a+b}}{\sqrt{2^a\cdot bur_{25\cdot a+b}}}\right] \qquad (c.6)$$

Figure C-1 shows the infinite and instantaneous curves computed with equations (c.5) and (c.6).

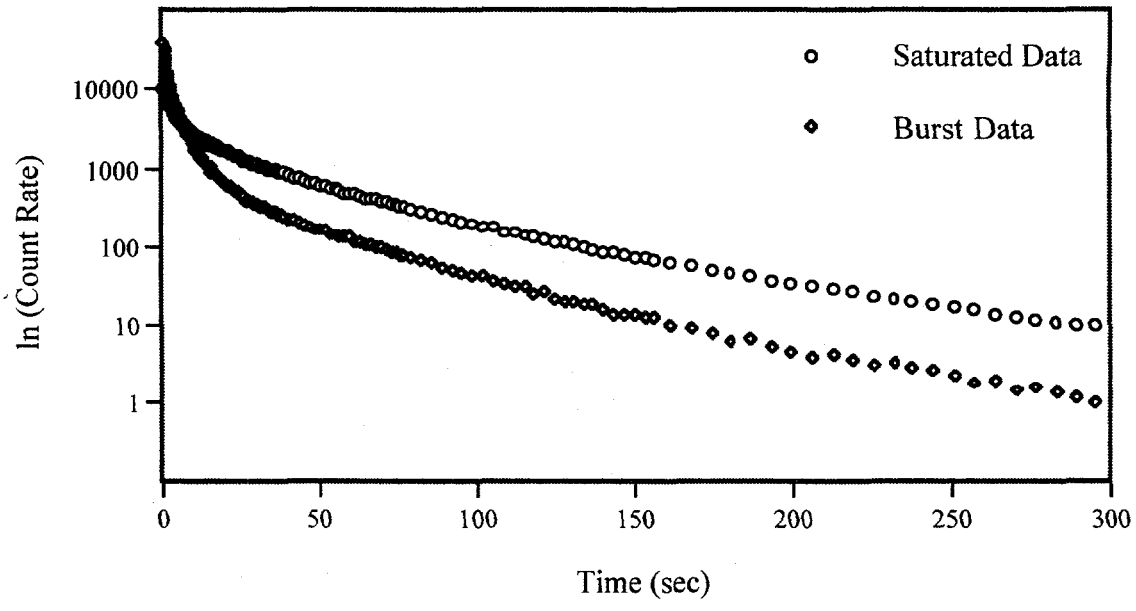

Figure C-1. U-235 data with noise for saturation and burst simulation.

Initial guesses for the minimization are given to fit the infinite irradiation. The initial guesses depend on the size of the irradiation.

g1 = RA u_0 del g2 = RA u_2 del
g3 = RA u_4 del g4 = RA u_6 del
g5 = RA u_8 del g6 = RA u_{10} del

A standard deviation is calculated for the infinite irradiation:

$$s_{25\cdot a+b} = \sqrt{sat2_{25\cdot a+b} \cdot 2^a} \qquad \text{(c.7)}$$

Next, define the sum of exponential functions that fit the delayed neutron decay data. This function has the partial derivatives with respect to each of the parameters to be fit for the minimization process.

$$F(z,w) := \begin{bmatrix} \sum_{ib=0}^{5} w_{2\cdot ib}\cdot\exp\left(-w_{2\,ib+1}\cdot z\right) \\ \exp\left(-w_1\cdot z\right) \\ w_0\cdot\exp\left(-w_1\cdot z\right)\cdot(-z) \\ \exp\left(-w_3\cdot z\right) \\ w_2\cdot\exp\left(-w_3\cdot z\right)\cdot(-z) \\ \exp\left(-w_5\cdot z\right) \\ w_4\cdot\exp\left(-w_5\cdot z\right)\cdot(-z) \\ \exp\left(-w_7\cdot z\right) \\ w_6\cdot\exp\left(-w_7\cdot z\right)\cdot(-z) \\ \exp\left(-w_9\cdot z\right) \\ w_8\cdot\exp\left(-w_9\cdot z\right)\cdot(-z) \\ \exp\left(-w_{11}\cdot z\right) \\ w_{10}\cdot\exp\left(-w_{11}\cdot z\right)\cdot(-z) \end{bmatrix} \qquad ia := \begin{bmatrix} 1 \\ 1 \\ 1 \\ 1 \\ 1 \\ 1 \\ 1 \\ 1 \\ 0 \\ 1 \\ 0 \end{bmatrix} \qquad a := \begin{bmatrix} g1 \\ 0.0127 \\ g2 \\ 0.0317 \\ g3 \\ 0.115 \\ g4 \\ 0.311 \\ g5 \\ 1.4 \\ g6 \\ 3.87 \end{bmatrix}$$

The vector **ia** indicates which parameters are to be fit and which are to be held constant. The vector **a** is the initial guess to be used in fitting the data. At this point, the Levenberg-Marquardt nonlinear least square routine is called to compute the delayed neutron parameters.

Satcal = Mrqmin (t,sat2,s,a,ia,F) (c.8)

The calculated parameters are shown in the output table generated by Mathcad.

Satcal =

	0	1
0	384.184	21.921
1	0.013	0
2	$2.163 \cdot 10^{3}$	0
3	0.032	0
4	$2.838 \cdot 10^{3}$	0
5	0.14	0
6	$3.403 \cdot 10^{3}$	0
7	0.398	0
8	847.179	0
9	1.4	0
10	255.389	0
11	3.87	0

The abundances need to be normalized. Compute a new array with the calculated delayed neuron parameters for the saturation case.

$$sn = Satcal^{\langle 0 \rangle}$$

$$satn_k = \sum_{i=0}^{5} sn_{2 \cdot i} \exp\left(-sn_{2 \cdot i+1} \cdot t_k\right) \quad \text{(c.9)}$$

Figure C-2 shows the original simulated data and the curve fit for the saturation case. Figure C-2 is broken down into small time intervals to present the results in more detail.

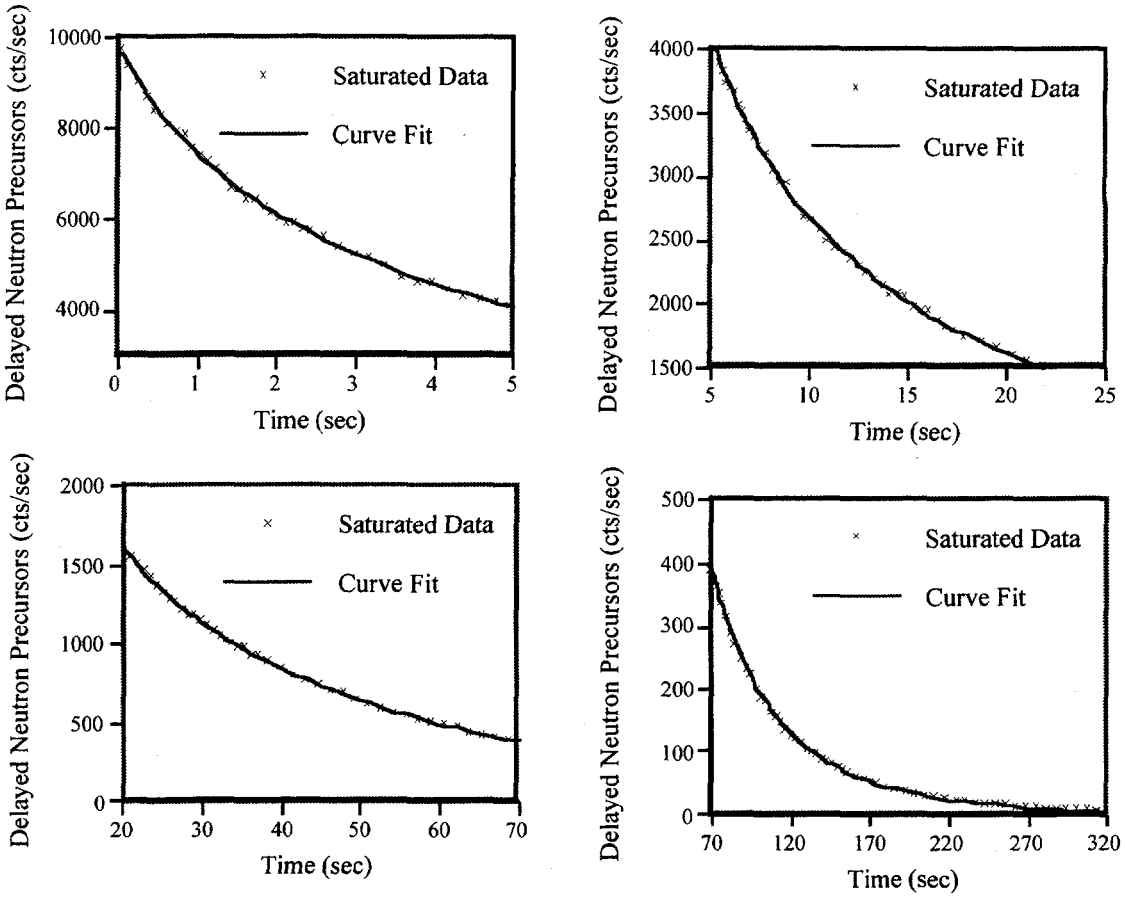

Figure C-2. Original data curve fits for the saturation simulation.

Performed a similar process for the instantaneous irradiation. The initial guesses depend on the size of the burst.

b1 = B u_0 del b2 = B u_2 del
b3 = B u_4 del b4 = B u_6 del
b5 = B u_8 del b6 = B u_{10} del

The FF function contains the sum of exponential, and partial derivatives of the instantaneous relationship with respect to each of the parameters to be fit.

$$FF(z,w) := \begin{bmatrix} \sum_{ib=0}^{5} w_{2\cdot ib}\cdot w_{2\cdot ib+1}\cdot \exp\left(-w_{2\cdot ib+1}\cdot z\right) \\ w_1\cdot \exp\left(-w_1\cdot z\right) \\ w_1\cdot\left(w_0\cdot\exp\left(-w_1\cdot z\right)\right)\cdot(-z) + w_0\cdot\exp\left(-w_1\cdot z\right) \\ w_3\cdot \exp\left(-w_3\cdot z\right) \\ w_3\cdot\left(w_2\cdot\exp\left(-w_3\cdot z\right)\right)\cdot(-z) + w_2\cdot\exp\left(-w_3\cdot z\right) \\ w_5\cdot \exp\left(-w_5\cdot z\right) \\ w_5\cdot\left(w_4\cdot\exp\left(-w_5\cdot z\right)\right)\cdot(-z) + w_4\cdot\exp\left(-w_5\cdot z\right) \\ w_7\cdot \exp\left(-w_7\cdot z\right) \\ w_7\cdot\left(w_6\cdot\exp\left(-w_7\cdot z\right)\right)\cdot(-z) + w_6\cdot\exp\left(-w_7\cdot z\right) \\ w_9\cdot \exp\left(-w_9\cdot z\right) \\ w_9\cdot\left(w_8\cdot\exp\left(-w_9\cdot z\right)\right)\cdot(-z) + w_8\cdot\exp\left(-w_9\cdot z\right) \\ w_{11}\cdot \exp\left(-w_{11}\cdot z\right) \\ w_{11}\cdot\left(w_{10}\cdot\exp\left(-w_{11}\cdot z\right)\right)\cdot(-z) + w_{10}\cdot\exp\left(-w_{11}\cdot z\right) \end{bmatrix} \qquad ia := \begin{bmatrix} 1 \\ 1 \\ 1 \\ 1 \\ 1 \\ 1 \\ 1 \\ 1 \\ 1 \\ 1 \\ 1 \\ 1 \end{bmatrix} \qquad a := \begin{bmatrix} b1 \\ .013 \\ b2 \\ .03 \\ b3 \\ .11 \\ b4 \\ .3 \\ b5 \\ 1.4 \\ b6 \\ 4 \end{bmatrix}.$$

The calculated output table for the instantaneous irradiation is:

Burcal =

	0	1
0	$3.219\cdot10^{3}$	44.045
1	0.012	0
2	$2.112\cdot10^{4}$	0
3	0.031	0
4	$1.897\cdot10^{4}$	0
5	0.112	0
6	$4.1\cdot10^{4}$	0
7	0.309	0
8	$1.318\cdot10^{4}$	0
9	1.389	0
10	$2.41\cdot10^{3}$	0
11	4.34	0

Compute a new instantaneous curve.

$$bn = Burcal^{<0>}$$

$$burn_k = \sum_{i=0}^{5} bn_{2\cdot i} \cdot bn_{2\cdot i+1} \exp\left(-bn_{2\cdot i+1} \cdot t_k\right) \qquad \text{(c.10)}$$

Figure C-3 shows the original data and the curve fit for the instantaneous irradiation. Figure C-3 is shown in segments to observe the decay in more detail.

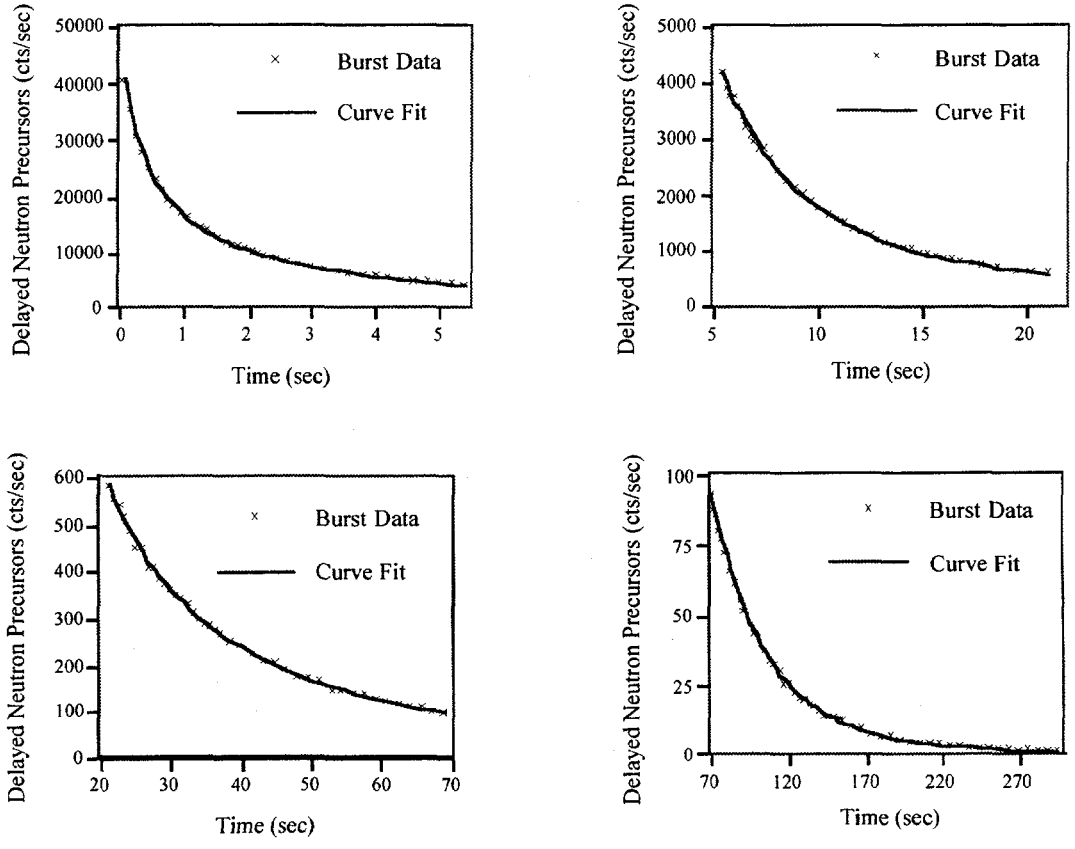

Figure C-3. Original data curve fits for the instantaneous simulation.

Table C-1 shows Keepin's delayed neutron parameters and the simulated parameters obtained with the Levenberg-Marquardt method. The simulated constants were obtained from 15 simulated burst irradiations and 15 simulated saturation irradiations.

Table C-1. Data simulation to test the Levenberg-Marquardt method.

	Keepin' s Constants		Calculated Constants	
Group	Abundance	Decay Constant	Abundance	Decay Constant
1	0.038 ± 0.003	0.0127 ± 0.0002	0.037 ± 0.005	0.012 4± 0.0007
2	0.213 ± 0.005	0.0317 ± 0.0008	0.218 ± 0.002	0.0310 ± 0.0007
3	0.188 ± 0.016	0.1150 ± 0.0030	0.184 ± 0.021	0.115 ± 0.008
4	0.407 ± 0.007	0.3110 ± 0.0030	0.400 ± 0.010	0.312 ±0.006
5	0.128 ± 0.008	1.4 ± 0.081	0.123 ± 0.003	1.386 ± 0.030
6	0.026 ± 0.003	3.87 ± 0.369	0.023 ± 0.006	3.901 ± 0.350

Figures C-4 and C-5 show a graphical representation for the data listed in Table C-1. Figure C-4 shows the abundance vs group number for Keepin's data and for the simulated data.

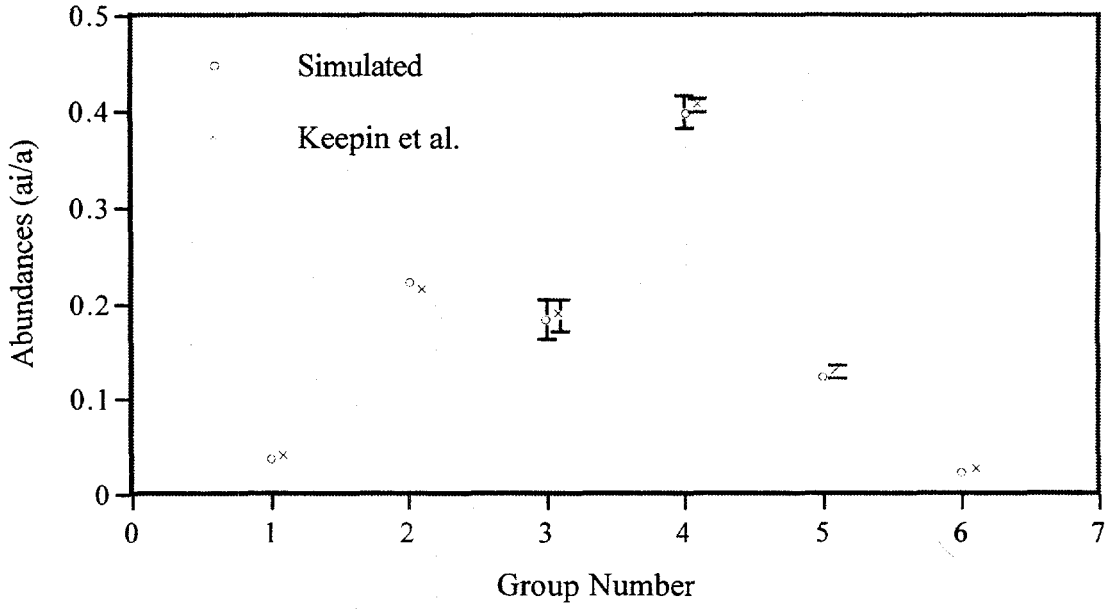

Figure C.4. Graphical representation of abundaces.

This figure illustrates that most of the simulated parameters lie within the standard error in Keepin's data. Note that the standard error bars for groups one, two, and six are smaller than the symbol, for that reason they

do not show in the graph. Figure C-5 present the decay constants vs group number for the simulated data and Keepin's parameters. All the parameters in the simulated data lie within the standard error. Once again some of the error bars are not shown because they are smaller than the symbols.

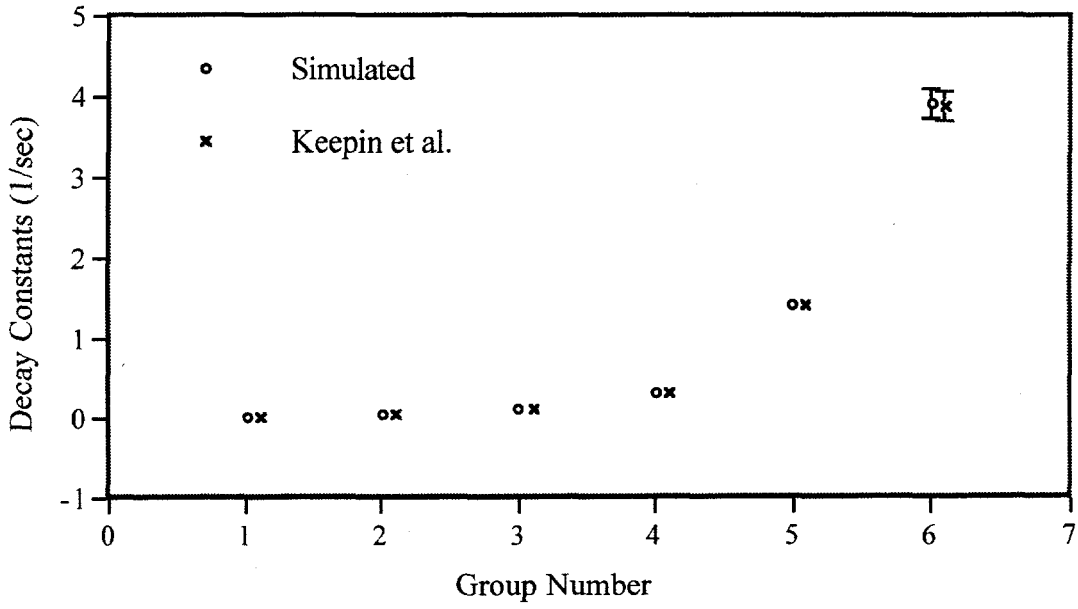

Figure C-5. Graphical representation of decay constants.

REFERENCES

H. Anderson, E. Fermi, A. Wattenburg, and W. Zinn, "Method for Measuring Neutron Absorption Cross Sections by the Effect on the Reactivity of a Chain Reaction," *Physical Review* **72**, 16 (1947).

R. Anderson, A. Robba, D. Seale, K. Butterfield, and G. Brunson, "*Intrinsic Neutron Source Strengths in Uranium Solutions*," Los Alamos National Laboratory, LA-UR-91-2081 (1991).

A. Aniel and H. Feldstein, "A Semi-empirical Treatment of Neutron Emission Probabilities from Delayed Neutron Precursors," *Phys. Lett.* **31B**(2), 59-60 (1970).

G. Arnone, G. Brunson, and K. Coop, "*A Pulse Arrival-Time Recording Module for Analyzing Neutron Multiplicities*," Los Alamos National Laboratory, LA-UR-91-8231 (1991).

R. Batchelor, and H. Mck Hyder, "The Energy of delayed Neutrons from Fission," *J. Nuclear Energy* **3**, 7 (1956).

P. J. Bendt and F. R. Scott, "Delayed Neutrons from Short-lived Precursors," *Physics Review* **97**, 744 (1955).

E. F. Bennett, "*The Am-Li Neutron Spectrum*," Argonne National Laboratory Report ANL-7017 (1965).

P. R. Bevington, *Data Reduction and Error Analysis for the Physical Sciences*, New York, McGraw-Hill (1969).

N. Bohr and J. A. Wheeler, "The Mechanism of Nuclear Fission," *Physical Review* **56**, 426 (1939).

M. C. Brady, "Evaluation and Application of Delayed Neutron Precursor Data," PhD Dissertation, Texas A&M University (1989).

Brookhaven National Laboratory, "Neutron Cross Section Library," BNL-325 (1978).

G. Brunson, E. Pettitt, and R. McCurdy, "*Measurements of Delayed Neutron Yields in Plutonium-239, Uranium-238 and Thorium-232 Relative to the Yield in Uranium-235*," Argonne National Laboratory report ANL 5480 (1955).

G. Brunson, Los Alamos Critical Experiments Facility, Private Communication (August, 1996).

R. Clement, "*Neutron Source Calibration Report*," Los Alamos National Laboratory (1996).

D. A. Clifford, U.K. Atomic Weapons Research Establishment, Aldermaston (1972).

S. Cox, T. Fields, L. Friedman, R. Sjoblom, and L. Smith, "Delayed Neutrons from Spontaneous Fission of Cf-252," *Physical Review* **112**, 960 (1958).

ENDF/B: Evaluate Nuclear Data Files, available from and maintained by the National Nuclear Data Center, Brookhaven National Laboratory, Upton, New York. Version VI.

T. England, and B. Rider, "*Evaluation and Compilation of Fission Product Yields, 1993*," LA-UR-94-3106, Los Alamos National Laboratory (1994).

A. Evans and M. Krick, "Equilibrium Delayed Neutron Spectra from Fast Fissions of U-235, U-238 and Pu-239," *Trans. Am. Nucl. Soc.* **23**, 496 (1976).

G. Fiegs, "Measurements of Delayed Fission Neutron Spectra of U-235, U-238 and Pu-239 with Proton Recoil Proportional Counters," *J. Nuclear Energy* **26**, 585 (1972).

D. Hetrick, "*The Effect of Fast Fissions on the Inhour Equation for SHEBA*," Eagle Report NIS6-94:0478DLH (1994).

F. Hoffman, B. Field, and P. Stein, "Delayed Neutrons for U-235 After Short Irradiation," *Physical Review* **74**, 1330 (1948).

D. Hughes, J. Dabbs, and A. Cahn, "Delayed Neutrons from Fission of U-235," *Physical Review* **73**, 111 (1948).

J. L. Jaech, "Statistical Methods in Nuclear Material Control," TID-26298, US Atomic Energy Commission (1973).

G. R. Keepin, *Progress in Nuclear Energy* Series I Vol. I (1956).

G. R. Keepin, *Physics of Nuclear Kinetics*, Addison Wesley Publishing Co., Reading, Massachusetts (1965).

G. R. Keepin, T. Wimett, and R. Zeigler, "Delayed Neutrons from fissionable Isotopes Of Uranium, Plutonium, and Thorium," *J. Nuclear Energy* **6**, 1-21 (1957).

G. R. Keepin, "*Nuclear Safeguards Research and Development Program Status Report April-June 1969*," Los Alamos National Laboratory report, LA-4227-MS (1969).

G. Knoll, *Radiation Detection Measurements*, John Wiley and Sons Publishing Co., Michigan (1989).

K. Kratz, and G. Herrmann, "Systematic of Neutron Emission Probablities from Delayed Neutron Precursors," *Nucl. Sci. and Eng.* **87**, 418-431 (1984).

M. Krick and A. Evans, "Delayed Neutron Yield from U-235 as a function of the Neutron Energy Inducing Fission," *Bull. Am. Phys. Soc.* **15**, 87 (1970).

M. Krick, and A. Evans, "The measurement of the total-delayed neutron yields as a function of the energy inducing fission," *Nuclear Science and Engineering* **47**, 311 (1972).

J. W. Kunstadter, J. J. Floyd, and L. B. Borst, "Delayed Neutrons from U-235," *Physics Review* **91**, 594 (1953).

LACEF, *"Los Alamos Critical Experiment Facility Training Reference Manual,"* Los Alamos National Laboratory, LA-CP-92-235 (1994).

K. Levenberg, "A Method for the Solution of Certain Nonlinear Problems in Least-Square," *Quart. Applied Mathematics* **2**, 164-168 (1944).

Y. Lyutostanskii, I. Panov, and V. Sirotkin, "The possibility of Emission of Two Neutrons in Beta Decay of Nuclei with $A \geq 50$," *Soviet J. Nuclear Physics* **37**, 163-164 (1983).

B. Maksiutenko, "Relative Yields of Delayed Neutrons in the Fission of U-238, U-235, and Th-232 by Fast Neutrons," *Journal of Experimental and Theoretical Physics* **35**, 815 (1958).

D. W. Marquardt, "An Algorithm for Least-Squares Estimation of Nonlinar Parameters," *J. of the Society for Applied Mathematics* **11**, 431-441 (1963).

J. T. Mihalczo, J. Lynn, and J. Taylor, "The Central Void Reactivity in the Oak Ridge Enriched Uranium (93.2) Metal Sphere," Oak Ridge National Laboratory report, ORNL/TM-13349.

G. Moscati and J. Goldemberg, "Delayed Neutron Yields in the Photo Fission of U-238 and Th-232," *Physics Review* **126**, 1098 (1962).

J. More, B. Garbow, and K. Hillstrom, "*User's Guide to Minpack I*" Argonne National Laboratory, ANL-80-74 (1980).

P. Nikotin and K. Petrzhak, "Delayed Neutrons in the Photo Fission of Heavy Nuclei," *Soviet Atomic Energy* **20**, 268 (1966).

A. Pappas and G. Rudstam, "An Approach to the Systematics of Delayed Nuetron Precursors," *Nuclear Physics* **21**, 353-366 (1960).

S. Pearlestein and R. Kinsey, "National Data Center," Brookhaven National Laboratory. Upton, NY (1976).

W. H. Press, S. Teukolsky, and W. Vetterling, *Numerical Recipes, The Art of Scientific Computing*, Cambridge University Press (1992).

W. C. Redman and D. Saxon, "Delayed Neutron Measurements for U-235 and Pu-239," *Physical Review* **72**, 567 (1947).

J. H. Rees and C. M. Shipp, "Chemical Aspects of the Management of Neptunium in Nuclear Wastes: A Review," *Nuclear Energy* **22**, 423-432 (1983).

R. Roberts, R. Meyer, and P. Wang, "Further Observations on the Splitting of Uranium and Thorium," *Physical Review* **55**, 510 (1939).

G. Rudstam, and S. Shalev, "Energy Spectra of Delayed Neutrons from Separated Fission Products," *Nucl. Phys.* **235**, 397-409 (1974).

D. Rutherford, "*Forecast of Criticality Experiments and Experimental Programs Needed to Support Nuclear Operations in the United States of America*," Los Alamos National Laboratory report, LA-12683-MS (1994).

H. Saleh, and T. Parish, "Measurements of Delayed Neutron Decay Constants and Fission Yields from U-235, Np-237, Am-241, and Am-243," *Nucl. Sci. and Eng.* **125**, 51-60 (1997).

R. Sanchez, "Critical Mass of Np-237," Transactions of the Criticality Safety Group Meeting, Albuquerque, NM (1995).

W. Seifritz, "Preliminary Design of a Future Neptunium Burner," *Kerntechnik* **51**, 167-173 (1991).

S. Shalev and J. Cuttler, "The Energy Distribution of Delayed Fission Neutrons," *Nucl. Sci. and Eng.* **51**, 52-66 (1973).

N. Shpakov, K. Petrzhak, S. Bark, and O. Kostochkin, "Delayed Neutron Investigations," *Soviet Atomic Energy* **11**, 1190 (1962).

R. Smith, T. MacVicar, and D. Thorne, "Delayed Neutron Investigation with the Zephyr Fast Reactor," *Journal of Nuclear Energy* I **4**, 133 (1957).

A. Snell, J. Levinger, and E. Meiners, "Studies of the Delayed Neutrons," *Physical Review* **72**, 545 (1947).

K. H. Sun, R. A. Charpie, and F. Pecjack, "Measurements of Delayed Neutron Yields," *Physics Review* **79**, 3 (1950).

S. Synetos and J. Williams, "Delayed Neutron Yield and Decay Constants for Thermal Neutron Induced Fission of U-235," *Nuclear Energy* **22**, 267 (1983).

L. Szilard and W. Zinn, "Instantaneous Emission of Fast Neutrons in the Interaction of Slow Neutrons with Uranium," *Physical Review* **55**, 799 (1939).

R. Tanczyn, Q. Sharfuddin, W. Schier, and M. Pullen, "Composite Delayed Neutron Energy Spectra for Thermal Fission of U-235," *Nucl. Sci. and Eng.* **94**, 353-364 (1986).

N. Tsoulfanidis, *Measurement and Detection of Radiation*, Hemisphere Publishing Corp., New York (1983).

R. Tuttle, "Delayed Neutron data for reactor physics analysis," *Nucl. Sci. and Eng.* **56**, 37 (1975).

R. Tuttle, "Review of Delayed Neutron Yields in Nuclear Fission," Proc. Consultants' Mtg. on Delayed Neutron Properties, Vienna, Austria, March 26-30 (1979).